ABSTRACT

Title of Dissertation: MEASURING AND MAPPING FOREST WILDLIFE HABITAT CHARACTERISTICS USING LIDAR REMOTE SENSING AND MULTI-SENSOR FUSION

Peter Hyde, Doctor of Philosophy, 2005

Dissertation Directed By: Professor Ralph Dubayah
Department of Geography

Managing forests for multiple, often competing uses is challenging; managing Sierra National Forest's fire regime and California spotted owl habitat is difficult and compounded by lack of information about habitat quality. Consistent and accurate measurements of forest structure will reduce uncertainties regarding the amount of habitat reduction or alteration that spotted owls can tolerate. Current methods of measuring spotted owl habitat are mostly field-based and emphasize the important of canopy cover. However, this is more because of convenience than because canopy cover is a definitive predictor of owl presence or fecundity. Canopy cover is consistently and accurately measured in the field using a moosehorn densitometer; comparable measurements can be made using airphoto interpretation or from examining satellite imagery, but the results are not consistent. LiDAR remote sensing can produce consistent and accurate measurements of canopy cover, as well as other aspects of forest structure (such as canopy height and biomass) that are known or thought to be at least as predictive as canopy cover. Moreover, LiDAR can be used to produce maps of forest

structure rather than the point samples available from field measurements. However, LiDAR data sets are expensive and not available everywhere. Combining LiDAR with other, remote sensing data sets with less expensive, wall-to-wall coverage will result in broader scale maps of forest structure than have heretofore been possible; these maps can then be used to analyze spotted owl habitat. My work consists of three parts: comparison of LiDAR estimates of forest structure with field measurements, statistical fusion of LiDAR and other remote sensing data sets to produce broad scale maps of forest structure, and analysis of California spotted owl presence and fecundity as a function of LiDAR-derived canopy structure. I found that LiDAR was able to replicate field measurements accurately. Additionally, I was able to statistically combine LiDAR with passive optical and RaDAR (SAR backscatter and InSAR range) data to produce broad scale maps of forest structure that are consistent and accurate relative to field data and LiDAR data alone. Finally, I was able to demonstrate that these forest structural attributes predict spotted owl presence and absence as well as productivity.

MEASURING AND MAPPING FOREST WILDLIFE HABITAT CHARACTERISTICS USING LIDAR REMOTE SENSING AND MULTI-SENSOR FUSION.

By

Peter Hyde

Dissertation submitted to the Faculty of the Graduate School of the
University of Maryland, College Park, in partial fulfillment
of the requirements for the degree of
Doctor of Philosophy
2005

Advisory Committee:
Professor Ralph Dubayah, Chair
Professor James Dietz
Doctor Scott Goetz
Professor Christopher Justice
Professor Axel Kleidon

Acknowledgements

I thank Michelle West, Steve Wilcox, Brian Boroski, Meghan Salmon, Ryan Wilson, Aviva Pearlman, Sharon Pronchik, John Williams, Brian Emmett, and Josh Rhoads for assistance with field data collection; Carolyn Hunsaker, Bob Knox, Craig Dobson, Leland Pierce, Malcolm North, and Jo Ann Fites-Kaufman for assistance developing the field protocol, planning, and direction; Bryan Blair, Jason Drake, Birgit Peterson, and Michelle Hofton for assistance with LIDAR data processing; and Wayne Walker for field planning and supervision of crews, data collection, reviews of manuscripts, and generating ideas. I thank my committee, Professor James Dietz, Doctor Scott Goetz, Professor Christopher Justice, Professor Axel Kleidon, and especially the Chair, Professor Ralph Dubayah. I also thank Gabrielle Canonico and William P. Hyde for editing portions of this document.

Table of Contents

List of Tables

List of Figures

Chapter 1: Introduction

Forest wildlife habitat characteristics

Forests contain approximately 50% of Earth's terrestrial, macroscopic species (Wilson 1999). The implications for converting forest to agriculture or other uses would then seem clear; deforestation reduces the amount of available habitat for forest species. In addition, the remaining habitat is often subjected to fragmentation, or the additional losses of species due to alterations in the spatial arrangement of forest patches above and beyond those lost due to reductions in area. For example, placing a road through the center of a forest may only reduce the total area of a forest by a small fraction, while the remaining patches might be too small to support species that require a larger, continuous forest interior. Remote sensing has proven to be a very effective means of measuring these types of changes, i.e., the reductions in area and increases in fragmentation associated with deforestation (Skole and Tucker 1993, Steininger 1996, Cohen et al. 2002).

However, area and fragmentation are strictly measurements of the horizontal component of forest structure. Forests also have a vertical structure which is alterable in ways that are not as obvious from satellite imagery (Weishampel et al. 1996). Because of the practical difficulties in measuring the vertical structure of forests beneath the top of the forest canopy relatively less is known about the impact of certain silvicultural practices, such as selective logging or prescribed burns (Weishampel et al. 1996). Changes in structure are not always apparent from above, or even from below, forest canopies (Weishampel et al. 1996).

Ecological theory suggests that there is a causal link between the structural complexity of a landscape and its compositional (species) diversity. The search for correlates to, and causes of, diversity has a long history in ecology, e.g., Darwin, Wallace, Clements, Hutchinson, May, Volterra, Lotka, Gause, Lack, and Merriam (Morrison et al. 1998). Many factors have been considered and some remain controversial: several have been entirely or partially rejected by some while partially or wholly accepted by others. The major theories explaining global patterns of diversity include (Recher 1971):

- Historical- communities gain diversity over time. Undoubtedly history plays a role, but its influence is difficult to quantify
- Biological- increased competition causes greater niche partitioning, or, conversely, predation reduces competition allowing more species to coexist. However, biological interactions are difficult to quantify and this set of hypotheses are nearly impossible to falsify.
- Environmental- environmental conditions, especially climate (or climatic stability) relate to productivity, which in turn allow for longer and more complex food webs. Climate does seem to account for broad scale gradients of diversity. However, there are critical exceptions. Estuaries and wetlands are highly productive yet do not have high levels of diversity. Tropical ocean systems receive more solar radiation than temperate ocean systems yet have lower levels of diversity.

While all of these theories have some empirical support at global scales, they do not fully explain patterns at finer scales, such as regions, landscapes, and patches (Recher 1971).

At scales finer that the globe or continent, the variability of environmental conditions rather than the environment *per se* may influence the number of ecological niches available for species (Recher 1971). This variation is often described as heterogeneity when referring to the horizontal dimension and complexity when referring to the vertical dimension together, heterogeneity and complexity are hereafter referred to as patchiness (August 1983).

Both natural and anthropogenic processes influence patchiness in forests (Fahrig and Merriam 1985). At broad spatial and temporal scales, this patchiness is primarily influenced by climate and geology (Fahrig and Merriam 1985). At finer scales, patchiness is primarily driven by competition and disturbance (Fahrig and Merriam 1985). Anthropogenic disturbance causes not only reductions in forest area but also alterations in the spatial pattern of the remaining forest patches, a process often termed habitat fragmentation (Fahrig and Merriam 1985). Many organisms use forest patches as habitat and the structure of forest patches, particularly the forest canopy, provides niche space. Thus, changes in forest canopy structure may alter the suitability of forests for other organisms (August 1983).

The process of habitat alteration and its consequences for forest species has been an active area of research in ecology and biogeography for decades. Most of these studies consider the alterations of habitat in the horizontal dimension, such as the composition and configuration of patches (Rotenberry and Wiens 1980).

However, forest canopies are three-dimensional elements, i.e., they have length, width, and depth. Therefore, to fully understand the relationship between structural and compositional diversity, one must describe forest canopies as three-dimensional surfaces (Rotenberry and Wiens 1980). Recent evidence suggests that measures of the horizontal structure alone are inadequate to characterize the impacts of land cover change on biodiversity (Trzcinski et al. 1999). Consideration of both dimensions simultaneously is currently lacking (Rotenberry and Wiens 1980)

There are three types of measurements that will be used here to describe forest structure: canopy height, canopy cover, and biomass distribution. The height of forest canopy is a surrogate for age, although their relationship is curvilinear. Canopy cover, or the fraction of sky obscured by vegetation, is an important predictor biodiversity (Trzcinski et al. 1999). Biomass (and similar metrics, such as tree density) is positively correlated with bird species distributions (Beier and Drennan 1997).

The importance of forest wildlife habitat characteristics

Forests remain an important source of natural resources. There is a pressing need to manage forests for multiple (economic, ecological, recreational, hydrological) resources in sustainable manner (Hunsaker et al 2002). Silvicultural practices, particularly on National Forests, have come under close scrutiny in recent decades (Lee and Irwin 2005). While the detrimental effects of clear-cutting are well documented, the effects of selective logging are less well known (King and DeGraaf 2000). Ample evidence exists that silviculture affects bird communities by altering vegetation structure (King and DeGraaf 2000). Exactly how much selective logging a

species or a community can tolerate is an active area of research (Beier and Drennan 1997). It is, therefore, important to determine critical thresholds in forest structural attributes. It also critical to determine error budgets associated with measurement of critical structural characteristics. For example, if it is found that a species requires a minimum of 40% forest cover to persist, and the standard error of the estimation procedure is +/- 10%, then the target must be adjusted (to 50% cover) to provide an error margin.

The distribution and abundance of many species, including California spotted owls, martens, and goshawks, are dependent on forest structure. For example, the association between spotted owls and old growth forests is well documented (North et al. 1999). It is not known, however, how to evaluate the habitat potential of forests because old-growth forests are highly variable structurally (North et al. 1999). High canopy closure, numbers of large trees, abundance of coarse woody debris, and the presence of multiple vegetation strata are thought to be among the most important components of spotted owl habitat (Call and Gutierrez 1992), while Bias and Gutierrez (1992) conclude that broad scale, coarse grain structure maps are unsuitable for spotted owl research; the obvious conclusion is that sensors or techniques that can measure the former are far more preferable than those that produce the latter.

The development of measurement techniques that accurately and consistently describe the structural complexity of forests is a necessary first step towards building habitat models for forest species. The identification of environmental conditions that promote or maintain compositional diversity could augment or even obviate the need for costly species inventories. An improved understanding of the relationship

between species and their habitats will reduce the uncertainty associated with resource management (Hunsaker et al 2002, Lee and Irwin 2005).

The focus of this effort is on several structural measurements, i.e., canopy height, canopy cover and biomass. These are not the only measurements of structure, nor are they necessarily the most efficacious vis-à-vis wildlife habitat analysis. They do have several advantages. First, there is clear biophysical understanding of the underlying structure of forests that they intend to represent. Second, there is a reasonably clear mechanism by which the structure being measured would be diagnostic of habitat suitability. Third, each of these can be measured in the field and directly compared with remote sensing data sets.

Canopy height refers to the distance from the highest point of canopy-forming trees to the ground. Although canopy height is a component of vertical structure, most often it has been used as a surrogate for age, or as a "site index": the overall capacity of a site to produce timber. However, the relationship between canopy height and forest age is often curvilinear, not linear (Koike and Syahbuddin 1993) (Figure 1).

Figure 1. The curvilinear relationship between tree height and age (shaded circles). Adapted from Aber, 1979.

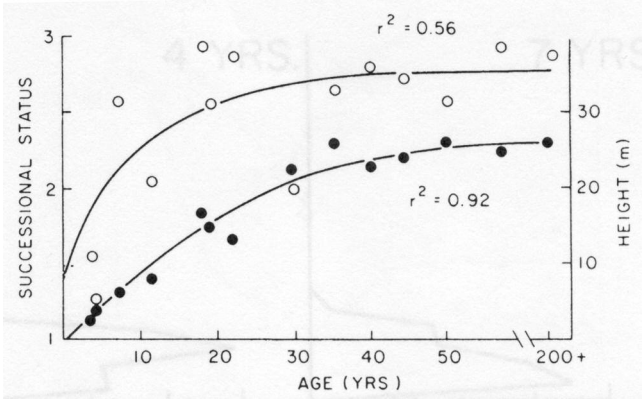

Tree height diversity may be viewed as surrogate for stratification and old-growth conditions (North et al. 1999); areas in high tree height diversity may provide a multitude of perching areas for spotted owls and yet be open enough to allow diving flights for prey capture.

Canopy cover refers to the fraction of sky obscured by vegetation. Many forest species, particularly birds, are associated with forests with high canopy cover. Spotted owls are likely to nest in areas with greater canopy cover (>=70%) or basal area of snags, medium-, and old-growth trees (Blakesley et al. 1992), although the California subspecies may tolerate lower amounts of cover, ca. 50% (Hunsaker et al. 2002). Northern goshawks are likely to be found in areas of high canopy cover (>=40%), areas with large trees or high tree density, and show strong (habitat) selection for areas with >80% cover (Beier and Drennan 1997).

Heterogeneity may increase the amount of ecological or niche space (August 1983, Downes et el 1998). Vertical structure may also provide new substrates, which in turn support more food resources. One of the first observations that species perceive and exploit very small variations in vertical canopy space was made by MacArthur (1958). He found that warbler species similar in size and shape fed and nested in different portions of the canopy (Figures 2 and 3).

Figure 2. The nesting height of some warbler species. Adapted from MacArthur, 1958.

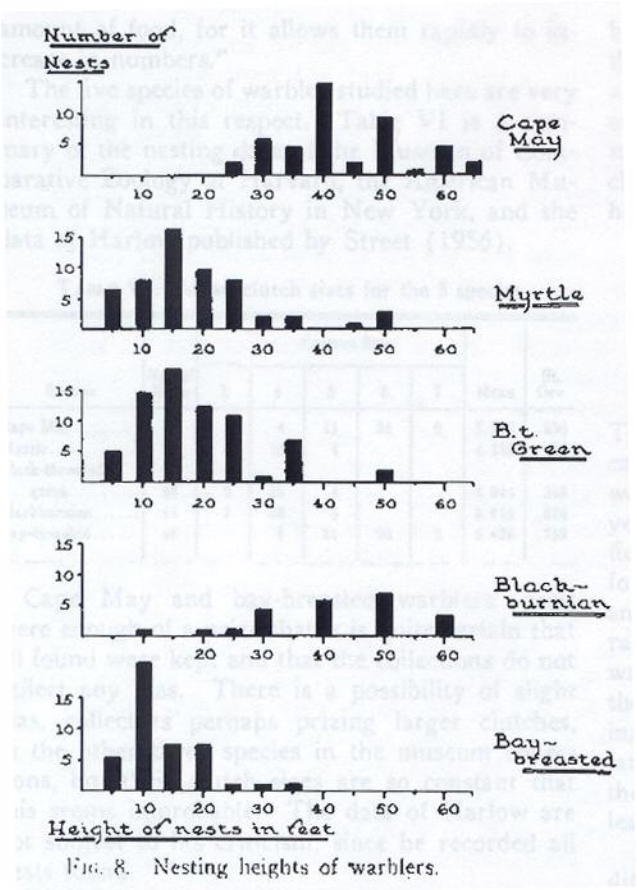

Fig. 8. Nesting heights of warblers.

Figure 3. Composition of warbler populations and their relationship to canopy volume. Adapted from MacArthur, 1958

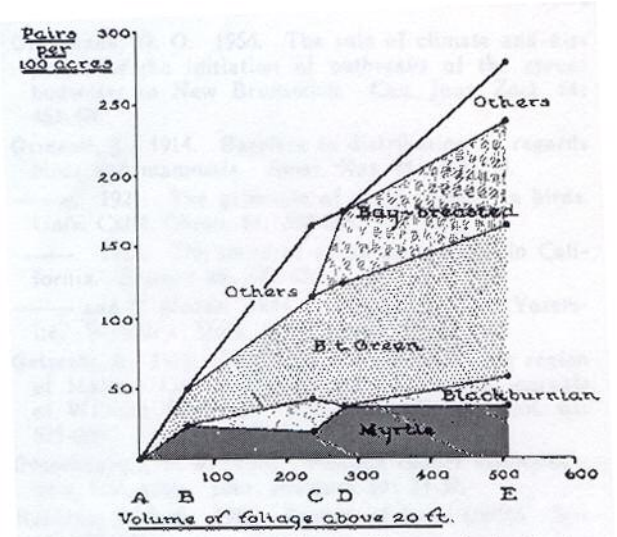

Fig. 10. Composition of the warbler population in plots A, B, C, D, and E. "Others" refers to other warbler species which feed at greater heights than 20 feet above the ground. The units of volume measurement are only proportional to the volume, but each unit roughly equals 1500 cubic feet per acre.

Methods used to measure forest wildlife habitat characteristics

The methods used to measure forest wildlife habitat characteristics fall into three main classes: *in situ* observations, passive remote sensing, and active remote sensing. All three have been used with some measure of success; however, they do not provide maps of sufficient quality to serve the needs of biological diversity research. Wildlife habitat characteristics are typically measured in the field on small (< 1 ha) plots and are intended to assess fine scale processes. Broad scale measurement and mapping of these characteristics from field surveys is generally cost prohibitive. Remote sensing provides the only cost effective means of measuring forest wildlife habitat characteristics in a spatially and temporally continuous manner. Measurements of

forest canopy structure are generally made by developing empirical relationships between field-derived measurements of the biophysical variable and the intensity of the return signal from the remote sensing system.

However, many remote sensing techniques are not ideally suited for measuring forest canopy structure in the vertical dimension. This is especially true of forests that are older, structurally complex, or have closed canopies. The signal from passive sensors is dominated by the upper layers of forest canopies; very little solar radiation reaches the ground and is returned to the sensor. Canopy height has been measured using interferometric synthetic aperture radar (InSAR) with a modest degree of accuracy in structurally simple forests (Treuhaft and Siqueira 2000), but not as of yet in mature secondary or primary growth forests. Canopy cover has been recovered via passive remote sensing from forests up to about 80% cover, but the return signal tends to saturate at higher levels, making it difficult for this technique to distinguish primary from mature secondary growth (Steininger 1996). Canopy heights can be measured via photogrammetry, but are difficult to produce in closed forests because the entire tree cannot be seen and because canopy elements of individual trees are often interlocked (Bebi et al. 2001).

Light detecting and ranging (LIDAR) remote sensing may provide a means through which forest canopy structure, particularly in the vertical dimension, may be measured (Nelson et al. 1984, Nelson et al. 1988, Nilsson 1996, Lefsky 1997, Lefsky et al. 1999a, Lefsky et al. 1999b, Lefsky et al. 2001, Dubayah and Drake 2000, Drake 2001, Drake et al. 2002). Unlike passive sensors, the LIDAR signal penetrates through the entire canopy. Unlike radar, LIDAR signals do not saturate in forests that

are structurally complex (Weishampel et al. 2000). Therefore, LIDAR offers the promise of measuring forest canopy structure in all forest types and uniquely has the capacity to provide measurements of vertical structure.

In situ observations

The traditional technique for measuring tree height is through the use of an inclinometer; the angles from an observer to the base and top of a tree, as well as the horizontal distance from the observer to the base of the tree are used to calculate tree height. However, this method is very sensitive to the angle used by the observer. At large angles, small measurement errors or imprecision in the instrument will lead to large errors in height estimation. More recently, electronic rangefinder using sound or light have been used. Often, the method that a researcher uses for height estimation is unreported (Rosenzweig and Winakur 1969). Also, allometric relationships, such as diameter at breast height (dbh)-to-height regression equations (or the use of dbh instead of height as an indicator of age, e.g., Bias and Gutierrez 1992) are used.

Canopy cover is measured in the field in a variety of ways. The point-quadrat method involves the observation of the frequency of occurrence of a particular vegetation type (Rotenberry and Wiens 1980). Sighting tubes (e.g., moosehorn densiometer) instead of rods or poles are sometimes used to ensure vertical orientation (Beier and Drennan 1997). Spherical densiometers, which capture the fraction of sky obscured by vegetation, are also used (DeGraaf et al. 1998). Hemispherical photography has been used (Danson and Curran 1993) but there are problems associated with using such a wide field of view; the technique tends to

overestimate cover due to occlusion of canopy gaps. Often, the method used to estimate canopy cover is unreported (Pianka 1966, Bias and Gutierrez 1992).

An early method of measuring vertical structure involved the use of boards (MacArthur and MacArthur 1961, Rosenzweig and Winakur 1969). One investigator holds a board at a specified height and moves away from a second observer until the board is half obscured by foliage. The distance between the investigators is inversely proportional to the density of foliage at the specified height. The measurement is repeated at various heights. The board method was sometimes used in a more systematic fashion, with perhaps less subjective height intervals that did not assume stratification (Rosenzweig and Winakur 1969). Both methods are indirect; they measure something that is presumably correlated with foliar height diversity.

An alternate method, a type of point-quadrat method, involves the recording of the number of contacts of vegetation within specified height intervals marked on a vertical rod or pole (Wilson 1965, Rotenberry and Wiens 1980). With a similar method, an optical point-quadrat method, the height of first contact is measured with a calibrated telephoto lens (MacArthur and Horn 1969, Aber 1979).

If multiple layers are present, these methods tend to overestimate foliage in lower layers and underestimate foliage in upper layers unless a very large number of samples are taken (Fukushima et al. 1998). The accuracy of height measurement declines with distance, making these methods unsuitable in canopies over approximately 25 m (MacArthur and Horn 1969). Destructive sampling, e.g. clipping or stratified clipping has also been used, but is impractical at scales broader than a single tree (Fukushima et al. 1998). Photo methods of the two dimensional

distributions of foliage density have also been attempted, but are laborious and only provide coarse resolution (Tanaka et al. 1998).

The MacArthur-Horn and Aber methods assume a random distribution of foliage (Poisson model) and that foliage density is horizontally uniform (Koike 1985). However, leaf angle often changes as a function of height; leaves in the upper portion of canopies tend to be plagiophile (midway between horizontal and vertical), while leaves in the lower portion of canopies tend to be planophile (horizontal) (Hutchison et al. 1986). The assumption of leaf orientation has implications for rate at which light transmitted through canopies is extinguished (Meir et al. 2000), (Table 2), and thus bears on the appropriateness of MacArthur's technique as it is sometimes used a justification for a light extinction correction (e.g., Lefsky et al. 1999a).

Table 1. The effect of leaf orientation on light extinction coefficients. Adapted from Meir, et al, 2000.

Height (m)	A	B	C
4	0.5	0.8	0.5
8	0.5	0.8	0.5
16	0.5	0.7	0.6
24	0.5	0.6	0.7
32	0.5	0.5	0.8
40	0.5	0.5	0.8

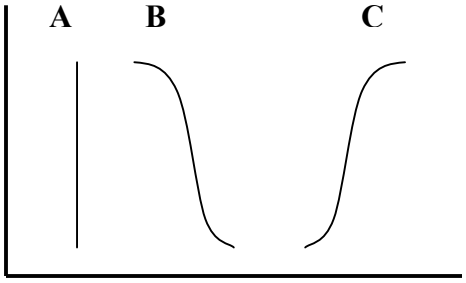

A = Spherical distribution
B = Varying from spherical at top of canopy to planophile at bottom
C = Varying from planophile at top of canopy to spherical at bottom

Randomly distributed foliage has a higher light extinction coefficient than non-randomly distributed (clumped) foliage (Monsi et al. 1973). Trees with needleleaves are typically more clumped than are broadleaves, and thus needleleaf canopies likely have smaller light extinction rates, making a MacArthur-Horn transform less appropriate in coniferous than deciduous forests. The use of

hemispherical photography to estimate vertical structure also relies on similar assumptions regarding the distribution of leaf inclination angles.

All of these techniques are based on subjective estimates of vegetation density in *subjectively defined* canopy layers, and presume continuity of the foliage in the vertical direction (August 1983). More objective methods include balloon-lofted rafts, cranes, scaffolding towers, tree climbing techniques, and lifting devices used by the construction industry ("cherry pickers"); however, measuring canopies in these ways is dangerous, time-consuming and expensive, limiting the number of samples that can be collected for most studies (Bassow and Bazzaz 1997).

Passive remote sensing

At some point in the aging process, forest successional stages become so similar in density, structure and optical properties that one is unable to discriminate between them with passive sensors (Kimes et al. 1999). The return signal from passive optical sensors return is a function of vegetation structure and their optical properties, which are influenced by slope, aspect, elevation (Kimes et al. 1996), as well as sun-target-sensor geometry and atmospheric effects.

Airphoto interpretation of tree heights from stereopairs works well in sparse canopies, but is limited when canopy cover is dense due to problems discriminating individual crowns (Bebi et al. 2001). Airphoto interpretation is also problematic due to very large errors in height estimates on steep slopes (Tanaka and Nakashizuka 1997). Coarser resolution satellite imagery suffers from the same problems; however, the use of multiple view angles, e.g., Multi-angle Imaging Spectroradiometer (MISR) (Diner et al 1999) may lead to improvements in height estimation.

The delimiting of tree and non-tree features from imagery suffers from some of the same problems associated with canopy height. High spatial resolution imagery is required to separate canopies and canopy elements and thus is limited to small spatial extents. These methods are also labor intensive and the manual delineation of forest patches is highly subjective. The spectral mixing of scene elements (crown, shadow, ground, non-forest vegetation) in medium to coarse resolution imagery limits their utility for measuring vertical structure. Cover measurements are very sensitive to angle of the field of view, or view angle. When view angles are large (>30 degrees from the ground), cover measurements are biased high because gaps in the canopy are obscured by foliage near to the observer. Hunsaker et al. (2002) found that Landsat Thematic Mapper (TM) overestimates cover relative to aerial photography.

Air photo interpretation or photogrammetry suffers from high rates of misclassification with respect to metrics of vertical structure due to the difficulties in distinguishing multilayered from uniform canopies and distinguishing intermediate tree size classes (Bebi et al. 2001). It is possible to assess vertical structure using shadow lengths, and this method could be improved with the use of digital terrain and solar radiation models. Metrics of stand complexity derived from field measurements show a high correlation to texture images derived from SPOT HRV data and to "wetness" images derived from Landsat TM data (Cohen and Spies 1992).

Active remote sensing

Radar sensors operate on the principle that microwave radiation received by the sensor, or backscatter, is proportional to the amount and organization of canopy elements. Shorter wavelengths are more sensitive to smaller canopy elements

(foliage, twigs) while longer wavelengths are more sensitive to large canopy elements (trunk). However, radar backscatter saturates in closed forests (Kasischke et al. 1997). The use of multiple channels (wavelengths and polarizations) may improve the accuracy of such measurements. Also, coupling radar backscatter to ecosystem models may provide measurements of forest structural attributes (Castel et al. 2001, Ranson et al. 2001).

Traditional radar (SAR) remote sensing has been used to measure canopy height in boreal forests (Dobson et al. 1995). Polarimetric interferometric SAR, which should be more effect than traditional SARs, has also been used to measure canopy height, but again in relatively structurally simple (boreal) ecosystems (Treuhaft and Siqueira 2000). Interferometric SAR has been used to assess biomass in structurally simple forests (Treuhaft and Siqueira 2000), but this technique is in the exploratory stage.

Light detecting and ranging (LIDAR) sensors also operate on principle that radiation received by the sensor, or backscatter, is proportional to the amount and organization of canopy elements. Unlike RaDAR, the radiation emitted by the sensor is typically in the shorter wavelength bands (ultraviolet, visible, or near infrared). LIDAR systems range from very narrow beams (small footprint, ca. 0.3 – 1 m diameter (Naesset 1997, Nelson et al. 1988) to relatively broad beams (large footprint, 10-30 m diameter (Blair et al. 1999). Typically, small footprint systems record the first or last return (and sometimes both), while large footprint systems typically record the entire return signal; the latter systems produce a nearly continuous three dimensional portrait of forest canopy structure.

The heights of forest canopies have been measured in a variety of ecosystem types using LiDAR, ranging from the structurally simple (Naesset 1997, Nelson et al. 1984, Nelson et al. 1988) to the complex (Nelson et al. 1997, Lefsky et al. 1999a, Peterson 2000). However, the validation sites in structurally complex ecosystems may not be statistically representative vis-à-vis slope; these sites are often in flat areas.

Canopy cover has been derived from LIDAR (Nelson et al. 1984, Nelson et al. 1988, Nilsson 1996, Lefsky 1997, Lefsky et al. 1999a, Lefsky et al. 1999b, Lefsky et al. 2001, Dubayah and Drake 2000, Drake 2001, Drake et al. 2002). However, some of the assumptions regarding the distribution of foliage and the degree to which occlusion affects signal are questionable. Lefsky (1997) and Lefsky et al. (1999a, 1999b) attempts to correct for overestimation of abundance of canopy elements in upper layers due to occlusion or blocking of lower layers ; however, this correction overestimates canopy elements in the lower layers. The assumptions underpinning Lefsky's method are more valid in broadleaf deciduous forests than in needleleaf evergreen, because, as noted, needleleaves tend to be more clumped than broadleaves. The vertical distribution of intercepted surfaces (VDIS) derived from a LIDAR signal is similar in principle to foliar height diversity, but includes the distribution of non-foliar canopy elements (e.g., twigs and trunk). For habitat assessment purposes, VDIS may be a more accurate predictor of suitability than foliar height diversity, given that niche space is not limited solely to foliar elements.

Summary

Forests provide habitat for a variety of species, accounting for about half of all terrestrial, macroscopic species. The National Forest system in the United States has traditionally managed these forests for multiple uses, including timber extraction, recreation, and water quality. In recent decades, these forests have also been managed explicitly for the benefit of wildlife species. The importance of natural fire regimes, and conversely the negative impacts of fire suppression, has also become an important management concern. However, it is unknown how the effects of these disparate and sometimes competing uses will interact. This is particularly true with regard to fire and habitat management, although selective logging is still an important consideration.

Fire and selective logging have the potential to change both the floristics and the physiognomy or structure of the forest; some of the changes are easier to detect and quantify than others. Remote sensing can improve the cost effectiveness of monitoring land cover change by providing continuous or nearly continuous measurements in both space and time. In contrast, measuring structural characteristics is difficult, and no single method provides an adequate solution. It is almost axiomatic in the literature that field methods are superior to other methods; however, field methods have biases and inconsistencies, are sometimes crude estimators of actual structure, and are limited in scale.

LIDAR may be the most promising in terms of delivering the required measurements, but is not widely available and is very expensive in terms of cost per unit area (Table 2).

Table 2. Representative examples of costs for several remote sensing image acquisitions. Prices do not include pre-flight (e.g., transportation or GPS) costs or post-flight processing. Prices for large footprint systems were not available.

Sensor (spatial resolution)	Acquisition Cost ($ per square kilometer)	Source
LiDAR (< 1 m)	386	Airborne 1 Corporation, El Segundo, CA, USA
High resolution passive optical (1 – 5 m)	116-386	UNESCO
Moderate resolution passive optical (10 – 30 m)	0.04	U.S. Geological Survey
Low resolution passive optical (500 – 1000 m)	0	NASA
RaDAR (8 - 50 m)	0.01 – 1.16	RADARSAT International, Richmond, BC, Canada

Radio detecting and ranging (RaDAR) is relatively inexpensive, as is multi-temporal, multi-spectral imagery; however, these sensors do not provide the requisite measurements of structure in the vertical dimension. Combining information from multiple sensors (multi-sensor fusion) may be useful in bridging the gap between availability and accuracy. Remote sensing data sets, validated with field observations, together will likely improve these measurements- a hypothesis that will be tested as part of this effort.

The following chapters will investigate the use of remote sensing to provide maps of forest structure for habitat analysis (Figure 4). The first chapter focuses on LIDAR techniques and how these compare with traditional field observations. The

second chapter fuses structural information from several remote sensing data sets in the attempt to create synergy in characterizing forest structure. The penultimate chapter applies the results of the previous chapters to the creation of habitat models for California spotted owls in the Sierra Nevada of California. The final chapter summarizes the results of the research chapters and discusses the implications for future biodiversity studies.

Figure 4. Flowchart depicting the relationship between the chapters of this document.

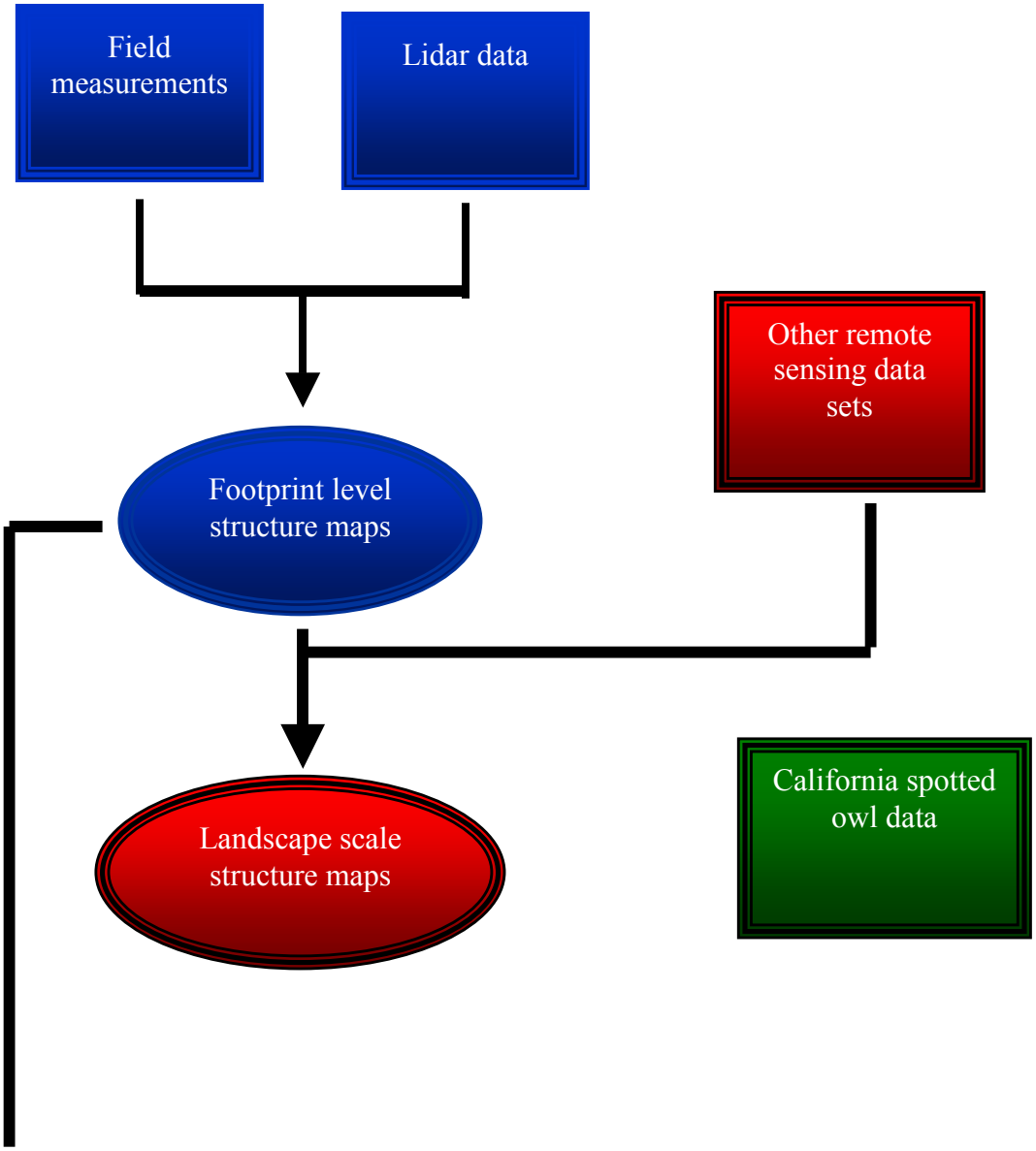

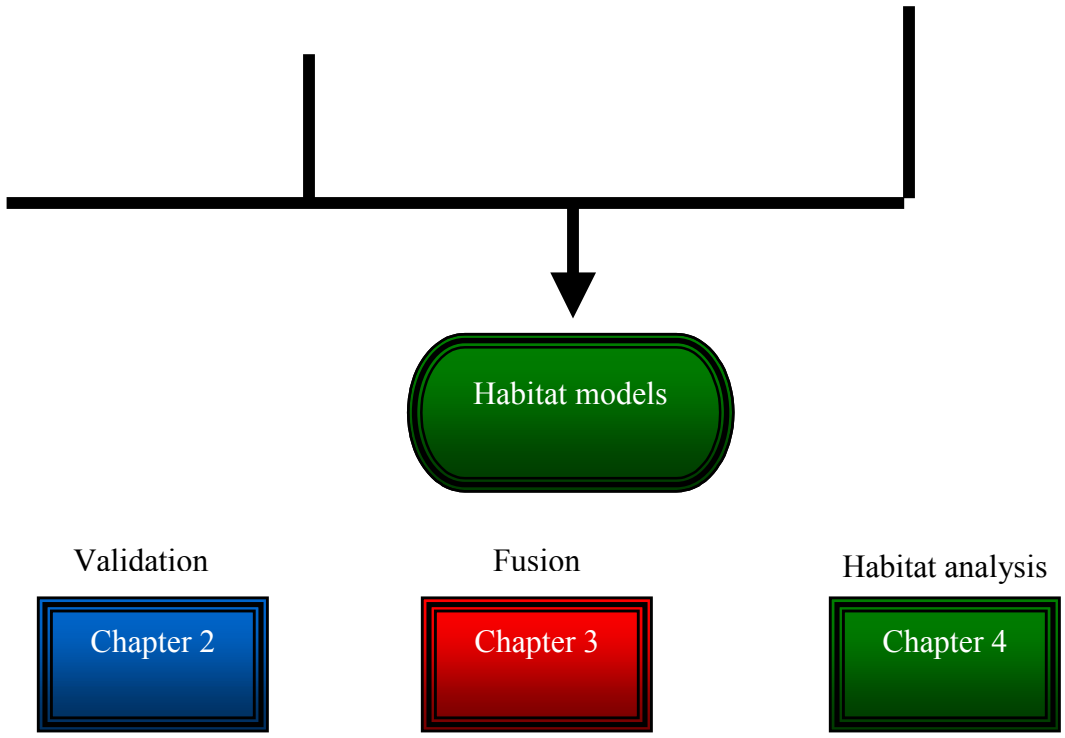

Chapter 2: Mapping forest structure for habitat analysis using waveform LIDAR: validation of montane ecosystems

Introduction

Management of forests for multiple uses, such as timber harvesting and protection of biological diversity, is challenging. Effective management often requires either information about the presence and abundance of organisms – which is not available for many species- or the development of indicators of habitat quality that correlate with species distributions. At the landscape scale, the structure of forests can be quantified and used to predict the occurrence of some species. These structural attributes include the height of the forest canopy, the amount of canopy cover, and biomass.

Field measurements of canopy height and canopy cover are conceptually simple. Direct measurements of biomass are somewhat more problematic because they require destructive sampling, although indirect methods, e.g., allometric equations relating dbh and/or height to biomass, suffice for most applications. However, *in situ* observations of forest structure, particularly in montane settings, are time-consuming and are often limited by accessibility, resulting in relatively small (ca. < 1 ha) field studies. Measurement and mapping of these characteristics from field surveys are generally cost prohibitive at fine spatial scales, across large areas.

Remote sensing methods, primarily multi-spectral (Hyppa et al. 1998) and more recently hyperspectral (Pu and Gong 2004) have been explored as cost effective means of measuring forest structural characteristics in a spatially and temporally continuous manner. However, these techniques are poorly suited for measuring vertical forest canopy structure (Weishampel et al. 2000). Radar methods, such as interferometric synthetic aperture radar (InSAR) are better at characterizing structure in forests, especially those that are structurally simple or have open canopies (Treuhaft and Cloude 1999, Treuhaft and Siqueira 2000), but as is the case with multi-spectral methods, these are primarily by correlation.

In contrast, LIDAR remote sensing directly measures important vertical and spatial forest structure. Numerous studies using both small footprint (< 0.5 m radius) and large footprint, waveform digitization airborne LIDAR, have demonstrated its ability to recover structure such as canopy height, canopy cover, canopy height profile, canopy volume, biomass and basal area at unprecedented accuracies (Nelson et al. 1984, Nelson et al. 1988, Nilsson 1996, Lefsky 1997, Lefsky et al. 1999a,

Lefsky et al. 1999b, Lefsky et al. 2001, Dubayah and Drake 2000, Drake 2001, Drake et al. 2002) but these relationships have not been tested in all ecosystem types. These studies developed relationships between *in situ* observations of forest structure and airborne laser data. The field samples in these studies were typically small in number, of limited spatial extent, or were located on relatively flat terrain. Because the application of LIDAR remote sensing to land surface characterization is relatively new, the accuracies achievable under a variety of environmental conditions is not yet well known, especially for large-footprint LIDAR. Factors such as topographic slope, canopy vertical structure and forest spatial structure (such as clumping of trees) are all hypothesized to affect the accuracies of retrieved structures. This is especially true of montane regions where there is a large range of slopes, elevation, soils and climate, all of which affect species composition and canopy architecture, such as height and cover. Yet it is in these difficult montane conditions where much forest management takes place. Thus, developing a better understanding of the effects of these factors on LIDAR retrievals is important.

For example, topographic slope can cause the LIDAR ground return (the last Gaussian return from the surface) to spread, leading to inaccurate ground determination, and consequently, canopy heights (Hofton et al. 2000). Slopes can also cause heights retrieved from LIDAR to be shorter or taller than their actual heights if the stem is located away from the center of the footprint (Rocchio 2000, Hofton et al 2002). The reason for this is that heights are determined relative to the mean ground elevation within a footprint, so that a stem which is upslope of the footprint center will appear taller and one which is downslope will appear shorter than the actual

height (Rocchio 2000, Hofton et al 2002). Also, the returns from short trees on steep slopes can be convolved or blurred with the surrounding topography. The architecture or shape of individual crowns can impact the accuracy of canopy height retrieval; some amount of canopy penetration can occur with more pointed, typically coniferous, crowns leading to underestimates of canopy height. Aspect and elevation relative to the flight of the aircraft can influence sensor-target geometric relationships and thus the actual size of the LIDAR footprint, leading to uncertainty about the actual area mapped by a footprint. The spatial distribution of canopy materials within the footprint affects the amount of signal returned to the sensor because of the non-uniform (Gaussian) illumination of the footprint by the LIDAR pulse; i.e. there is less energy at the edge of the footprint which may cause canopy materials at the edge to go undetected or be underestimated.

Developing a thorough understanding of the effects and interactions of these factors will require many studies. However, as part of the Vegetation Canopy LIDAR (VCL) mission (Dubayah et al. 1997), airborne, large footprint LIDAR data were acquired by the LVIS (Laser Vegetation Imaging Sensor) over Sierra National Forest in California in 1999. The goal of this experiment was to provide calibration and validation data to help define algorithms and subsequent accuracies of forest structure retrievals over montane regions under a wide range of slopes, canopy closures and environmental conditions.

Objectives

The primary objective of this chapter is to assess the ability of a large footprint LIDAR to retrieve canopy structure over the diverse montane forests of the Sierra

Nevada. My ultimate goal is to provide spatially continuous maps of forest structure at the landscape scale as a prerequisite for forest management. In the research presented here I compare spatially explicit field measurements of structure to metrics derived from LIDAR data collected by LVIS. My field plots cover a large range of slope, aspect, elevation, canopy cover, canopy shape and arrangement, and thus provide a rigorous assessment of LIDAR retrieval in montane conditions.

The remainder of this chapter is organized as follows. First I describe my collection of field plot data, and give details of the LVIS data acquisition over the Sierra Nevada. Next I present methods for data processing and analysis of both LIDAR and field data, including the derivation of canopy height, canopy cover and biomass. I then give the results of statistical comparisons between field-derived and LIDAR-derived forest structure. Finally, I discuss the significance of my results relative to the retrieval of forests characteristics in montane regions, and the implications of these for mapping forest structure.

Data Collection

Study area

The study area is located in Sierra National Forest in the Western slope of the Central Sierra Nevada of California (USA). This site is approximately 60,000 ha, with elevation ranging from 853 to 2,743 m (for a complete description, see (Hunsaker et al. 2002). Vegetation types include white fir (*Abies concolor*), red fir (*Abies magnifica*), Sierran mixed-conifer, ponderosa pine (*Pinus ponderosa*), and montane hardwood-conifer. Climate is heavily dependent upon elevation. Temperature ranges from below freezing (0 degrees centigrade) to over 38 degrees centigrade;

precipitation falls mainly between October and April. The area is subject to wildfires or wildland fires, either naturally-occurring (typically caused by lightning strikes), accidentally set by humans, or by prescribed burns in order to reduce the accumulation of understory and standing biomass. Selective logging also occurs on the forest but is severely restricted and occurs mostly as part of experimental treatments.

The study area is open to the public and may be subject to a variety of recreational activities, including hiking, fishing, hunting, shooting, boating, camping, cycling, picnicking, rafting, "four wheeling" or the use of off-road vehicles, skiing, and horseback riding. However, many U.S.D.A. Forest Service roads are gated and locked, preventing access by vehicle and thus limiting the exposure of all field plots as well as a majority of the study area to outside activity. Approximately one-third of the study area is located within the Teakettle Experimental Area, where access is very tightly controlled and almost exclusively restricted to U.S.D.A. Forest Service employees and collaborating researchers. The study area was chosen for several reasons: because it is spotted owl habitat, because of the availability of spotted owl demography data and remote sensing data sets, and because the location was deemed suitable as a test-bed for LiDAR remote sensing calibration-validation activities in steep-sloped terrain.

LiDAR data

LIDAR data was collected by the Laser Vegetation Imaging Sensor (Blair et al. 1999) during October 1999 while deciduous trees were in leaf-on condition. LVIS is an airborne laser altimeter that records the time and amplitude of a laser pulse reflected

off target surfaces. LVIS is a full waveform-digitizing system and records the vertical distribution of nadir-intercepted surfaces at 30 cm vertical resolution. The LVIS instrument flew aboard the NASA C-130H aircraft at about 7 km above ground level. LVIS is an imaging LIDAR, recording spots or "footprints" illuminated within a 7-degree potential field of view. For the Sierra Nevada flights these footprints had a nominal radius of 12.5 m, nominally separated by 12.5 m across track and continuous along track. Because of variations in altitude of the plane above the varying topography of the Sierra, actual footprint radii vary between 9-11 m. An area of about 175 square kilometers was mapped. The fundamental observation of LVIS is a waveform that gives the vertical distribution of intercepted surfaces. The amplitude of the waveform at any height is proportional to the amount of reflective material intercepted at a particular height, the orientation of that material, and its reflectance (ignoring such effects as multiple scattering within the footprint). Initial processing of the data is required to remove various biases to permit accurate geolocation. The data are then further processed to find ground and canopy returns, to derive various waveform metrics, such as the height of median energy and canopy top height, using automated methods.

Field plot data

One hundred twenty-four (124) plots centered on laser footprints were distributed throughout the study area using a modified stratified random sampling scheme; the data from 13 plots were excluded because of no discernable ground return existed in the waveform (likely due to saturation in very dense forests), leaving 112 suitable for analysis. Although the plots were located on laser footprints, the actual waveforms

were not examined before the stratification (to prevent bias), and therefore there was no attempt to retain only waveforms that showed a strong ground return. The number of plots placed within each land cover type (Table 3) were proportional to their actual distribution within Sierra National Forest, with the exception of the red fir class; this vegetation type was oversampled because of its importance as remnant old-growth. Field plot data were collected by field crews from the University of Michigan, the U.S.D.A. Forest Service and University of Maryland; the names of the individuals are listed in the Acknowledgement section (above).

Table 3. Field plots by vegetation class (Meyer & Laudenslayer, 1988).

Vegetation class	# plots
Red fir	36
White fir	19
Ponderosa pine	7
Other pine	4
Sierra mixed conifer	22
Montane hardwood	2
Montane hardwood-conifer	6
Wet meadow	10
Barren	6

Concentric circular plots were established, with an inner plot of 0.07 ha (15 m radius) and an outer plot of 1 ha (56.4 m radius). The 0.07 ha ("footprint") plots were designed to allow direct comparison of field measurements with individual LIDAR

footprints; the plot size was slightly larger than the nominal footprint to compensate for geolocation errors, if needed. The 1 ha ("stand") plots were designed to be commensurate with existing Forest Service field plots. It is assumed that no changes in hardwoods occurred between the field and remote sensing data collections.

Field plot data were collected during the summers of 2000 and 2001 and error-checked in 2002. Within the 0.07 ha plots, all live stems with a diameter at breast height (dbh) >= 10 cm were inventoried and species type was recorded. The dbh of the stem was measured with fiberglass tapes. The height of the stem, the height of the full crown, and the height of the partial crown (if present) were measured with an Impulse LR laser range finder (Laser Technology, Inc., Englewood, CO). The sweep of the partial crown, if present, was estimated to the nearest 30 degrees. The shape of the crown was characterized as elliptical, umbrella-shaped, conical, or cylindrical. Four crown radii (two each along and across slope) were measured with fiberglass tapes. The bearing of each stem with respect to the plot center was measured with a digital flux gate compass (Laser Technology, Inc., Englewood, CO) and the distance of each stem to the plot center was measured with the laser range finder.

Canopy cover was measured every 5 m along four transects and at the plot center with a moosehorn densiometer (Moosehorn CoverScopes, Medford, OR), following an established Forest Service field protocol. Due to time constraints, on only a subset of plots (n = 40), canopy cover was measured every 3 m on twelve 15 m transects (spaced every 30 degrees for a total of 60 observations) and at the plot center with a moosehorn densiometer and a LAI2000 plant canopy analyzer (Li-Cor,

Lincoln, NE). This more intensive sampling was performed to help assess the effects of under/over sampling as it is notoriously difficult to achieve consistent field-sample estimates of canopy cover.

Within the 1 ha plots, all live stems >= 76 cm dbh were inventoried. The species, the height of the stem, and dbh were also recorded.

Data Analysis

LIDAR data

The focus of this study is the derivation of three structural measurements, canopy height, canopy cover and aboveground biomass. Canopy height and canopy cover are directly retrieved from waveform data using algorithms described below. Both of these require identification of a ground return in the waveform, and associated with this, the identification of the canopy portion of the waveform. Biomass is not directly measured by LVIS; rather, metrics derived from LIDAR waveforms, such as canopy height, and height of median energy (HOME), are correlated with canopy structure.

Ground and Canopy height

Past studies e.g. Lefsky (1997), Lefsky (2000b) have relied on mainly manual methods for finding ground returns, especially where the returns are weak relative to the background noise level. While appropriate for validation studies with small numbers of waveforms, manual methods are impossible for the large numbers of LVIS waveforms used here (about 1 million). Because canopy height is determined relative to the ground, accurately retrieving ground elevation is critical. Thus, an automated algorithm for finding both ground and canopy height was employed.

The algorithm involves: 1) removing noise and resampling the waveform to improve sensitivity and resolution, 2) re-estimating noise statistics, 3) finding the center or mode of the last pulse, i.e., the ground, and 4) detection of the highest surface return above the noise level, i.e., the top of the canopy. The difference between the height of the ground and the top of the canopy is equal to the maximum height of the canopy, often referred to simply as canopy height. (Figure 5)

In cases where no ground return could be identified by the algorithm, the data were not used (thus leading to the elimination of some of the field validation waveforms above).

Figure 5. Diagram of an LVIS waveform. Home refers to the Height of the Median Energy Return, or the height of mid-point of the cumulative energy distribution within each waveform.

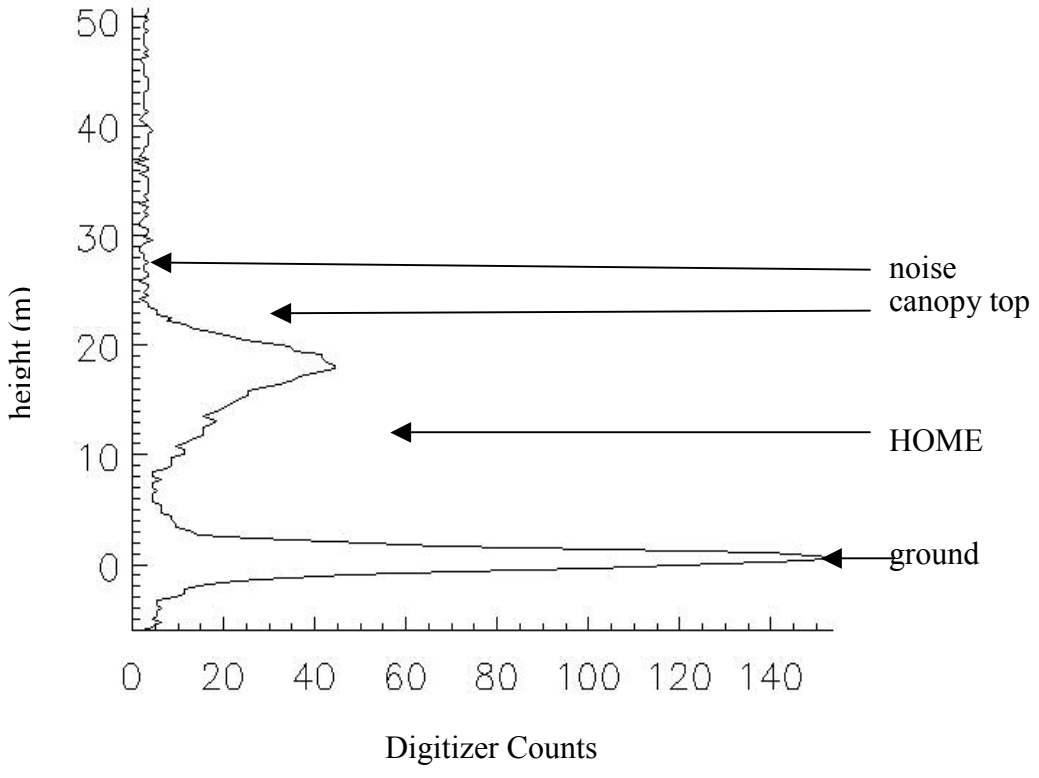

Canopy cover

An algorithm was used to extract canopy cover from LVIS waveforms that uses canopy height as derived in the previous step to define the top of the canopy. The bottom of the canopy is defined as the second to last return above a noise threshold (Figure 5). Once the ground and canopy portions of the waveform are thus separated, canopy cover is calculated by dividing the canopy portion of the waveform by the total energy in the waveform (canopy return plus ground return).

Differences in reflectivity in the near infra-red portion of the spectrum between canopy and ground must be accounted for. For example, if the canopy is very bright relative to the ground, the amount of energy reflected by the canopy portion will be incorrectly attributed to high closures in the canopy (i.e. the weak reflectance from the ground will be inferred to be because of weak incoming energy rather than weak reflectance). Thus, the ratio of canopy to ground reflectance must be known (Lefsky 1997). Others, e.g., Lefsky et al (1999a) and Drake et al (2002) have assumed a ratio of 2 for a variety of areas. I empirically estimated this ratio through examination of high spatial resolution passive optical (Quickbird, Satellite Imaging Corp., Houston, TX) imagery. Representative samples of forest and non-forested areas were delineated; NIR reflectance was averaged across samples and then ratioed. The resulting correction factor of 1.6 differs significantly from these previous studies.

Biomass

While LIDAR does not measure biomass directly, metrics derived from LIDAR have proven effective in estimating forest biomass (Nelson et al. 1984, Nelson et al. 1988, Nilsson 1996, Lefsky 1997, Lefsky et al. 1999a, Lefsky et al. 1999b, Drake 2001, Lefsky et al. 2001). Canopy height by itself is sufficient in some, more structurally simple, biomes (Lefsky et al 1999b). In more structurally complex biomes, such as tropical and old-growth Western coniferous forests, some indication of the depth of the canopy is also useful for predicting biomass (Lefsky et al 1999a, Drake et al 2002). Additional metrics used in as proxies for biomass include canopy height squared and canopy reflectance. All metrics were calculated from waveforms at both the plot and stand levels.

Field data

Field measurements at the footprint and stand levels include maximum canopy height, i.e., the height of the tallest stem within the plot. Field height data were also pooled according to vegetation type (Table 3), which was used as a proxy for crown shape, e.g., stands of pure red fir tended to be conical or pointed, while deciduous crowns tended to be more rounded. Elevation for each plot was acquired from a 7.5' USGS Digital Elevation Model, which was also used to calculate slope. Allometric equations relating stem biomass to height and dbh were obtained from the USDA Forest Service (Waddell and Hiserote 2003). These equations were applied to the field data to calculate total standing (aboveground) biomass for each stem; the biomass of all stems within the plot was added to provide totals at the footprint and stand levels.

LIDAR and field canopy height and canopy cover were compared through regression analysis at the footprint and stand levels using linear regression techniques; results are summarized in Table 4.

Table 4. Accuracy of predictive models derived through regression analysis.

Field measurement	Scale	Root mean square difference (m)	Coefficient of determination (r^2)	Model*	n	p
height (m)	footprint	8.9	0.75	Y= 0.83 * LHT + 7.85	112	< 0.000
height (m)	stand	6.4	0.75	Y= 0.59 * LHT – 0.07	112	< 0.000
cover (%)	footprint	13.4	0.81	Y= 0.82 (CE / (CE + GE)) + 1.4	40	< 0.000
biomass (Mg ha^{-1})	footprint	73.5	0.83	Y= 54.1 * HOME + 5.6 * LHT^2 – 15.1	112	< 0.000
Biomass (Mg ha^{-1})	stand	54.8	0.86	Y= 4.6* mean LHT – 6.7 * min LHT + 39.2* mean HOME – 16.5 * median HOME – 41.7 * min HOME – 1.5 * max HOME – 45.3	112	< 0.000

*LHT = LVIS canopy height HOME = height of the median energy return
GE= ground energy CE = canopy energy

The residuals of the regression between field and LIDAR height measurements were compared to slope, aspect, and cover to quantify the effects of these factors on height retrieval. Plots were then grouped together by land cover types and separate regression models were fit for each group to quantify the effects of crown shape. Field estimates of biomass were compared to LIDAR metrics using stepwise multiple linear regression techniques**.**

Results

Canopy height

Field and LIDAR canopy heights showed good agreement ($r^2 = 0.75$, RMSD = 8.2 m, n=112, $p < 0.00$; Figure 6) at the footprint level, comparable to other results using large footprint LIDAR e.g., Lefsky et al (1999b).

Figure 6. Scatterplot of LVIS canopy heights vs. field canopy heights. Outliers are likely caused by the overestimate of LiDAR canopy height due to the existence of large tree crowns at the edge of waveforms.

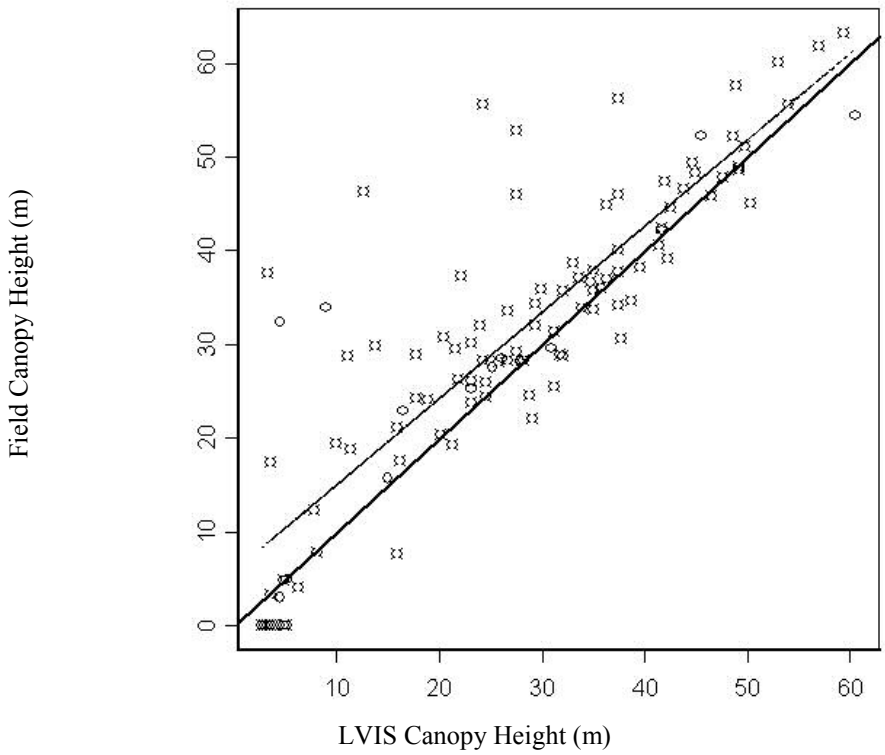

Bare plots were included in the comparison. Note that for some plots, field estimates are much larger than LIDAR estimates, by tens of meters, which weakens the relationship (analyzed further below).

Contrary to expectations that slope is the major source of error in montane systems, examination of the residuals of the regression showed a weak, and statistically insignificant correlation with slope ($r^2 = 0.19$, SE = 11.8 m, n=112, p = 0.25; Table 5).

Table 5. Potential sources of error in LIDAR vs. field canopy height measurements at the footprint level.

Potential error source	Coefficient of determination (r^2)	Standard error	n	p
slope	0.19	11.8 m	112	0.25
aspect	0.01	13.1 m	112	0.08
elevation	0.00	13.1 m	112	0.75
cover	0.00	5.9 %	40	0.08

There was no systematic relationship between differences in field vs. LIDAR measurements and aspect ($r^2 = 0.01$, SE = 13.1 m, n=112, p=0.08), elevation ($r^2 = 0.00$, SE = 13.1 m, n=112, p=0.75), or canopy cover ($r^2 = 0.01$, RMSD = 5.9 m, n=40, p =0.08) (Table 5). There were some differences among vegetation classes (Table 6), a rough proxy for crown shape; the plots containing hardwoods were far more accurate ($r^2 = 0.88$, SE = 4.0 m, n=8, p = 0.04) than those containing exclusively conifers (with a high $r^2 = 0.72$ and a low of 0.35).

Table 6. Accuracy of canopy height measurement (at the footprint scale) as a function of landcover class. Only the Montane hardwood & Montane hardwood-conifer contains deciduous trees; the remaining land cover classes (except for wet meadow and barren) contain only conifers.

Vegetation class	Root mean square difference (m)	Coefficient of determination	n	p	Residuals fit to distance	Residuals fit to slope
Red fir	8.8	0.72	36	0.00	0.10	< 0.00
White fir	8.9	0.60	19	0.00	0.05	0.06
Ponderosa & Jeffrey pine	11.1	0.43	11	0.03	0.06	0.03
Sierra mixed conifer	10.0	0.35	22	0.00	0.18	< 0.00
Montane hardwood & Montane hardwood-conifer	4.0	0.88	8	0.00	0.00	0.04

Wet meadow	9.5	0.54	10	0.02	0.10	0.10
Barren	3.6	0.85	6	0.00	0.29	0.07

Field measurements of canopy height from the two montane hardwood plots were pooled with measurements from montane hardwood-conifers, the only other landcover class that contained some deciduous trees. Field and LIDAR canopy height were in closest agreement in the montane hardwood-conifer ($r^2 = 0.88$, RMSD = 5.4 m, n=6, $p < 0.00$) and combined montane hardwood & montane hardwood-conifer plots ($r^2 = 0.88$, RMSD = 4.5 m, n=8, $p < 0.00$) and lowest in the Ponderosa pine ($r^2 = 0.25$, RMSD = 8.4 m, n=7, p=0.25) and other pine ($r^2 = 0.58$, RMSD = 11.0 m, n=4, p=0.24) plots. Analysis of variance revealed no significant difference among the coefficients of determination ($p = 0.06$, df =2, 9) or RMSD (p=0.47, df=2, 9).

The above analyses were performed assuming a nominal footprint size of 12.5 m. Although efforts were made by the aircraft to follow the terrain, variations in footprint size because of changes in elevation were inevitable. I modeled the expected footprint size for each footprint based on the sensor/target geometry which yielded a range of footprint radius sizes from 9-11 m. If the largest stem in field data was beyond 11 m, this would lead to some of the large errors noted above (because the stem would not be in the imaged footprint). For example, a stem map of Plot 18 (Figure 7) shows the tallest tree occurs at a distance of 12.1 m, whereas the calculated footprint size is 10.5 m.

Figure 7. Example of a large underestimate of tree height caused by edge location of the tallest tree. The radii of the concentric circles are 9, 12.5, and 15 meters in length. The very small black circles are the centers of LIDAR footprints; the text beneath them is the canopy height

value at that location. The small gray circles are stems; the radius of the circle is the average of four crown radii measurements taken in the field. The italicized text inside the stem locations is the field measurement of tree height. These measurements are possible because the location of each stem was measured in the field.

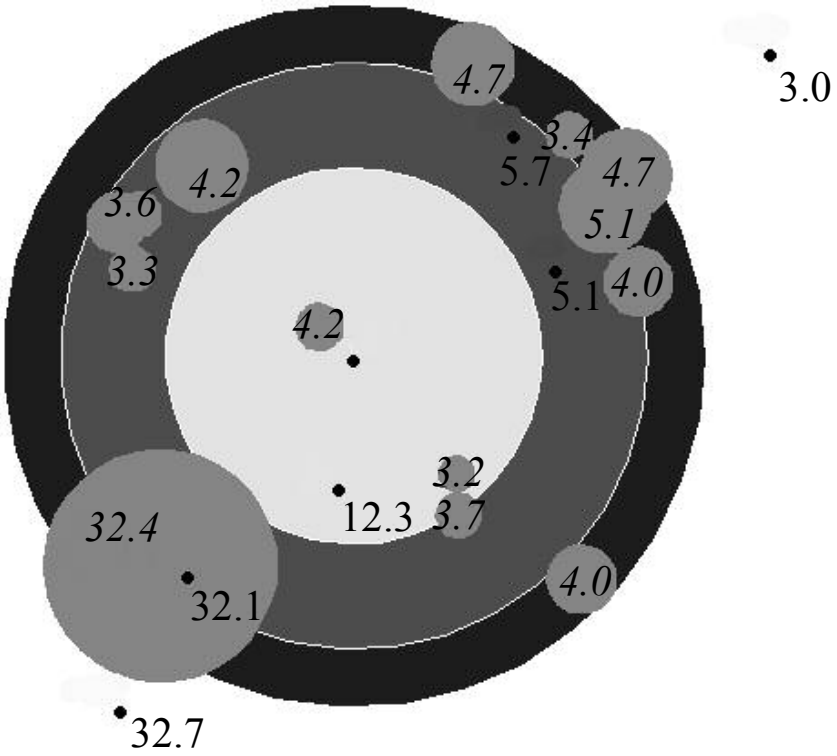

I then compared LIDAR height with the tallest stem within the calculated footprint radius. The result was an r-squared value of 0.72, RMSD of 7.6 and did not significantly improve the results. However, when separate regressions were performed as a function of footprint size, r-squared values increased from 0.76 for 11 m radius footprint up to 0.88 for 9 m radius. One reason for this increase is that the larger fooprint sizes coincidentally include those plots where the largest tree is near the edge of the footprint; there is no systematic, physical reason for why this is so. This then suggests an issue with sensitivity.

As discussed earlier, the incident energy pattern within an LVIS footprint is not uniform, but rather drops off as a Gaussian, so that errors may increase as the tallest stem moves from the center of footprint to the edges, especially for pointed crowns. I recalculated my height comparisons, this time by grouping plots together as a function tallest stem distance, from 3-12.5 m, and assuming a nominal footprint size of 12.5 m (and set this as an upper boundary for the analysis). I also excluded barren plots to isolate the effect stem distance. Results are shown in Table 7 and Figure 8.

Table 7. Canopy height retrieval accuracy as a function of distance.

i	n	RSE	RMSD	Coefficient of determination	st dev	Bias (field – LIDAR)	slope Coefficient of determination*
3	5	3.74	4.01	0.97	4.33	-0.26	0.18
4	9	3.99	3.87	0.94	4.01	0.58	0.32
5	15	3.44	3.45	0.96	3.52	0.51	0.19
6	24	4.14	4.21	0.95	4.1	1.27	0
7	32	4	4.07	0.94	3.95	1.18	0.01
8	45	4.88	5.26	0.9	4.85	2.16	0.01
9	55	6.38	6.75	0.82	6.38	2.36	0
10	64	7.09	7.69	0.77	7.09	3.1	0
11	77	7.52	8.45	0.74	7.61	3.78	0.02
12	91	7.37	8.43	0.73	7.5	3.93	0
13	101	7.87	9.33	0.69	8.19	4.55	0.01

*None of the slope r^2s are significant above 0.10 level

Figure 8. Canopy height retrieval accuracy and bias as a function of distance.

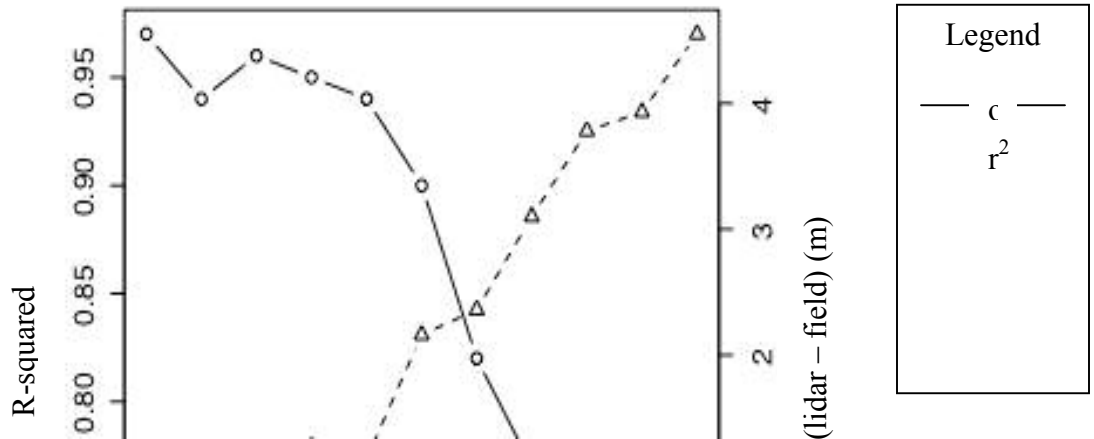

$\overline{\Delta}$
bias

The location of the tallest stem relative to the center of the footprint makes a dramatic difference in the results. If the stem is within 8 m of the center, my r-squared values are above 0.90, with rmsd below 5 m. After about 9 m, my r-squared values drop quickly to a low of 0.69. The bias is always positive (field – height) and increases near linearly with distance of the stem. This suggests that LVIS underestimates tree heights as the crown moves to the edge of the footprint (perhaps because of energy drop off).

Given this large effect on the height accuracy, I reassessed the effects of slope by looking for correlation of the height residuals with slope within distance classes (shown in Table 6) (and thus isolating the effect of stem distance). As before, there were no significant correlations of residual error with slope, i.e. none of the remaining variability could be explained by slope, regardless of distance class.

Field and LIDAR canopy heights also were in good agreement ($r^2 = 0.75$, RMSD = 6.0 m, n = 122, $p < 0.00$) at the stand level. In all cases, there are across-

track gaps between footprints due to pitch and roll of the aircraft. Therefore none of the 1ha plots were completely mapped, although some plots were more thoroughly mapped than others. Differences in field versus LIDAR canopy height were minimized when >40% of the plot area was mapped (about 35 LIDAR observations per ha; Figure 9).

Figure 9. Field vs. LIDAR measurements at the stand level. The left pane, marked 'A' is a scatterplot of plots that were mapped poorly (less 40% of the area mapped) while the right pane 'B' is a scatterplots of plots that were mapped well.

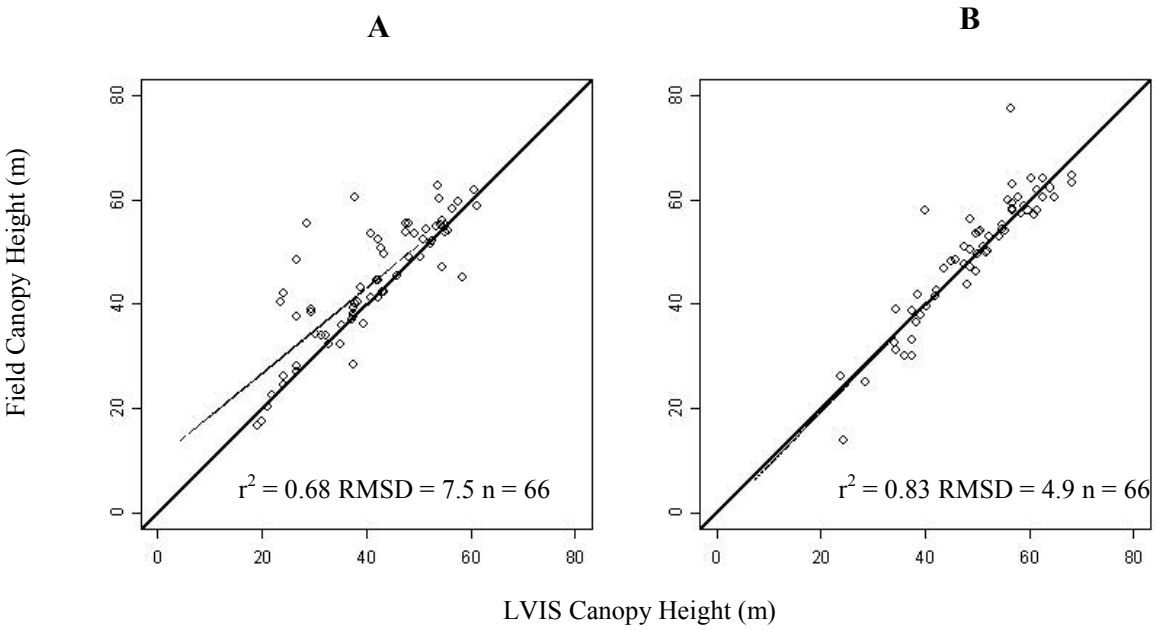

Canopy cover

The agreement between field and LIDAR measurements of canopy cover was only somewhat poor (r^2=0.54, RMSD=19.6%, p<0.00) for those plots (n=112) where the limited sampling protocol was used. In contrast, at the 40 plots that were more intensively field sampled, field and LIDAR estimates were in good agreement (r^2=0.81, RMSD=9.4%, n=40, p <0.00; Figure 10)

Figure 10. Field vs. LIDAR measurements of canopy cover at the footprint level. P < 0.00.

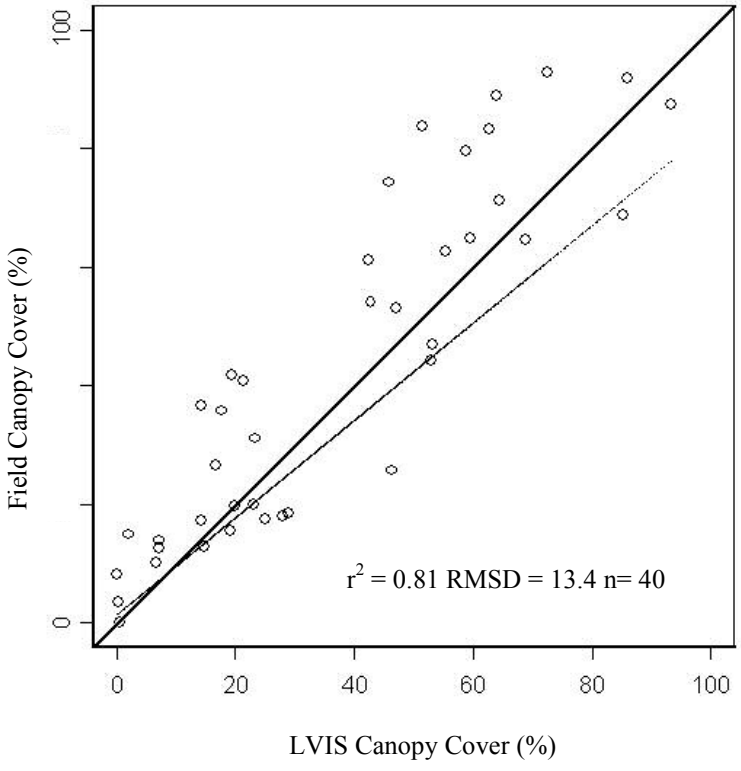

The best results occurred when the moosehorn observations were limited to those within 9 m of the plot center. To highlight the importance of using the correct ground to canopy reflectance, I compared results using a ratio of 2 for these 40 plots. In this case, the strength of the relationship decreased significantly (r^2=0.49, RMSD=22.0%, n= 40, $p < 0.00$). I do not expect that height or distance would influence canopy cover retrieval accuracy and the residuals of the regression were not related to either of these factors.

Biomass

LIDAR-derived biomass agreed well with field-estimated biomass at the footprint (r^2 = 0.83, RMSD = 73.5 Mg ha^{-1}, $p < 0.00$) and stand levels (r^2 = 0.86, RMSD = 54.8 Mg ha^{-1}; $p < 0.00$; Figure 11).

Figure 11. Results of step-wise multiple linear regression models between LIDAR metrics and field-measured biomass at the footprint (left panel) and stand (right panel) levels.

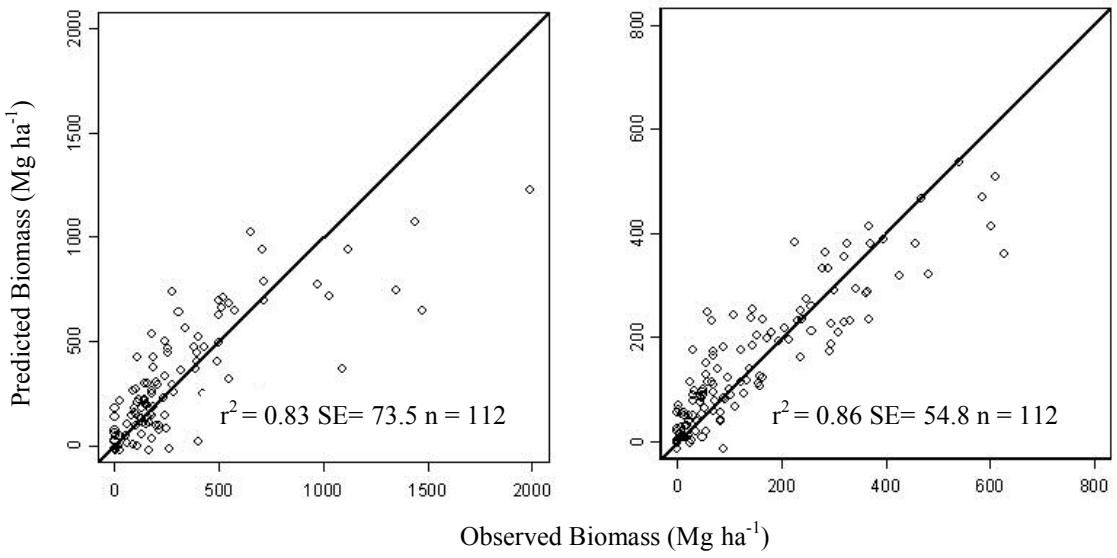

Laser height squared and HOME were significant predictors of biomass at the footprint level, while mean and minimum laser height, mean, minimum, median, and maximum HOME were significant predictors of biomass at the stand level.

Discussion

Results suggest that for my study site, the accuracy of canopy height retrieval at the footprint level was not clearly related to topography (slope, aspect and elevation) or canopy cover, but rather was strongly influenced by the spatial arrangement (more precisely the distance from footprint center) of the largest trees (at least for those

plots that had an identifiable ground return, i.e., those plots that were not excluded because of signal saturation). I hypothesize that this could be the result of two factors: footprint size errors (i.e. assuming the footprint to be 12.5 m in radius when it is actually smaller); or the Gaussian drop off in power across the footprint, resulting in a lack of sensitivity to canopy material progressively towards the edges of the footprint.

The results seem to suggest that it is the latter which is more important, because there is little improvement in variance explained or reduction in RMSD by using the exact footprint size vs. a nominal footprint size of 12.5 m. However, my results are somewhat confounded by the fact that the plots with the largest errors are the ones that have their tallest stem at the edge of the footprint, and these coincidentally are the largest radius footprints. Nonetheless, the dramatic increase in accuracy as the tallest stem is located towards the center of the plot strongly suggests that there is a drop in sensitivity as a result of the drop in power near the edge of the footprint. This effect should be most pronounced with crowns that are pointed, where the increase in intercepted leaf area is slow as a function of distance from the top of the stem. The linear increase in positive bias with stem distance also supports this contention. Finding more general conclusions about the interaction of footprint size, footprint energy pattern, crown shape, and stem location will require further studies. For example, I achieved very good results when the actual footprint radius was 9 m, suggesting perhaps that a smaller footprint size is appropriate for coniferous forests that show large variations in stem height over short distances.

Based on previous research (Rocchio 2000, Hofton et al 2002), I expected slope to be the major source of error. The maximum expected height error for a typical Sierra location is estimated with the following equation:

Error = tan S * D/2

where S is the slope and D is the footprint diameter

This gives a predicted error of about 3 – 4 m, assuming the average slope of my study site, 18%, and footprint radius range of 9 – 12.5 m. Slope effects should show up not as biases, as it is equally likely that the tallest stem would be above the center of the footprint or below, but rather as an added scatter to the relationship (i.e. increase the RMSD). I observed no relationship of my residual errors with slope (or the tangent of slope). The lowest RMSD observed was 3.45 m (considering only stems less than 5 m from center in Table 5). The magnitude of this error is about right for slope induced error, but again residuals from my linear regression are uncorrelated with slope. One possible explanation is that there are a set of factors such as uneven energy distribution across the slope, spatial arrangement effects, etc that are masking slope effects or interacting with slope in a non-linear fashion.

Crown shape, using land cover as a proxy, would seem to have an influence on height retrieval accuracy: the more rounded crowns of deciduous trees appear as a discernable feature in the waveform more quickly than more pointed coniferous crowns. However, the small number of plots containing deciduous trees limits my confidence in making generalizations about crown shape. Differences in canopy height measurements are likely to be a function of several convolved factors: crown

shape, canopy cover or crown density, and slope, as well as the spatial arrangement of the canopy with respect to the laser footprint.

My retrievals of canopy cover were encouraging; however my experience in the Sierra Nevada suggests a few cautionary notes. First, when following a standard USFS field sampling protocol, results were poor, with an r-squared value of just over 0.50. It was only at the intensively sampled plots where there was strong agreement between LIDAR and field estimates. Secondly, LIDAR underestimated canopy cover relative to field estimates. I would have expected the opposite given the slightly off-nadir collection angle of many LVIS footprints (caused by scanning). This is probably an artifact of the collection process on the ground; human observers are not as likely to observe very small gaps within canopies as does LiDAR; humans tend to note the larger gaps between canopies. These two together highlight the difficulties in "ground-truthing" canopy cover and the great care that must be taken in designing and implementing a field protocol. Lastly, note the importance of knowing the correct ratio of ground to canopy reflectance. It is not clear to us how stationary (in a spatial statistics sense) this ratio is, and therefore I cannot say how often it needs to be re-estimated. The requirement of needing a priori or ancillary data to correctly retrieve canopy cover pushes its estimation somewhat farther away from a "direct" retrieval. It may be possible to estimate this ratio directly from the LIDAR data if there is some confidence that the outgoing pulse energies leaving the system are about the same, or if different, that they are recorded, as should also be the case with systems that employ a variable gain (to avoid saturation in the recorded return pulse). In theory

then, the total NIR energy in vegetated and unvegetated waveforms could be used to estimate the ratio.

Biomass again proved to be reliably estimated by LIDAR. Forest structural characteristics, such as canopy height, canopy cover, and biomass are correlated but curvilinear, not linear, and saturate with age and site conditions (Aber 1979). There are tall stands with high biomass and tall stands with moderate biomass. Distinguishing between the two requires other information besides height. In the tropics, height of the median energy (mean HOME at the stand level) return does just this (Drake et al 2001). However, in the less dense, coniferous canopies of the Sierras, stand level mean HOME was not as useful because of strong ground returns that skew HOME towards the ground. Minimum height and minimum HOME helped distinguish stands that contained some shorter-stature trees or bare patches from stands with uniformly tall trees.

Recall that the ultimate goal of my research is to provide spatially continuous maps of forest structure at the landscape scale as a prerequisite for habitat suitability studies. Using the direct retrieval of canopy height and cover, and the statistical relationship developed between field and LIDAR data for biomass, I created maps of each of these over the domain of my LIDAR data (Figures 12-14). The accuracies observed using my extensive set of field plots gives me some confidence in the accuracy of the final derived map products. It is this mapping of forest structural characteristics at the landscape scale which I believe will be so useful for future habitat studies.

Figure 12. LIDAR-derived canopy height in Sierra National Forest. Note the linear discontinuities in canopy height; these are caused by differing management practices between U.S.D.A. Forest Service lands and private inholdings. A power line right-of-way is also clearly visible in the image. The canopy height values are calibrated to the field data.

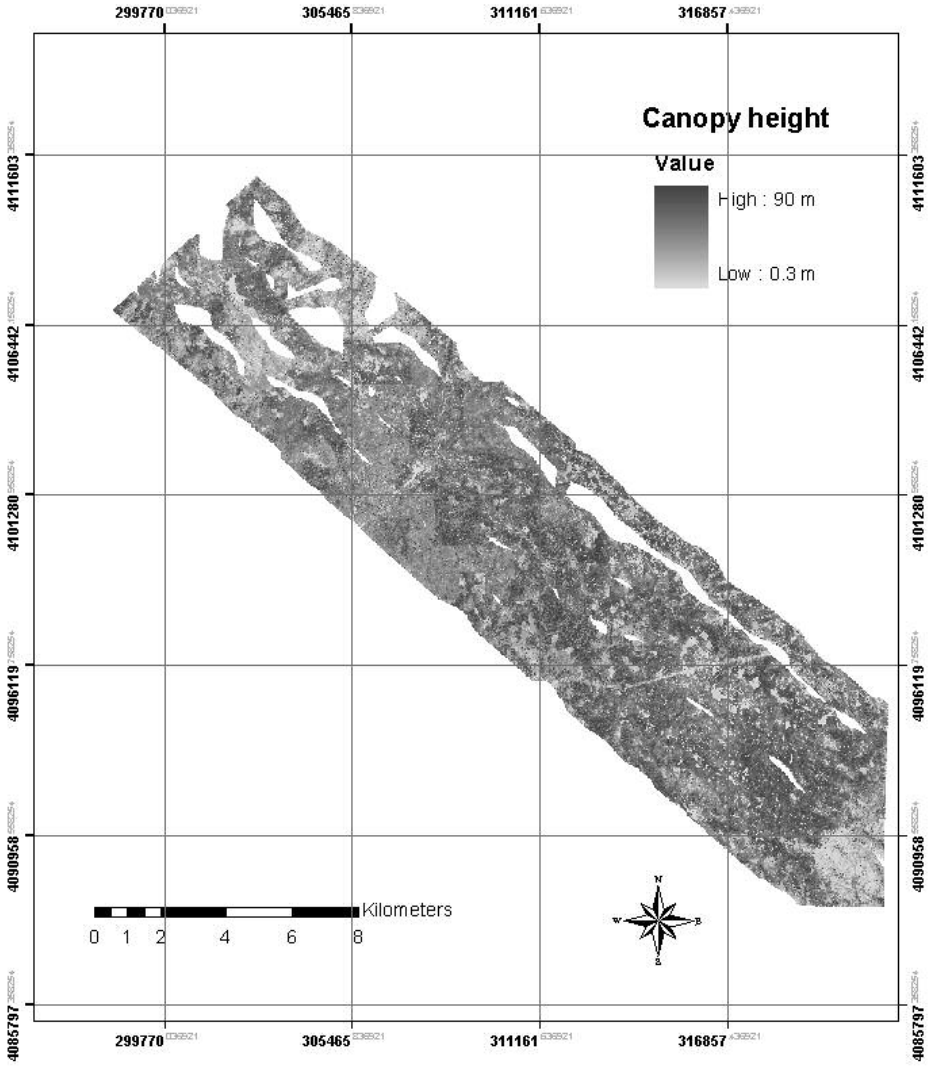

Figure 13. LIDAR-derived canopy cover in Sierra National Forest.

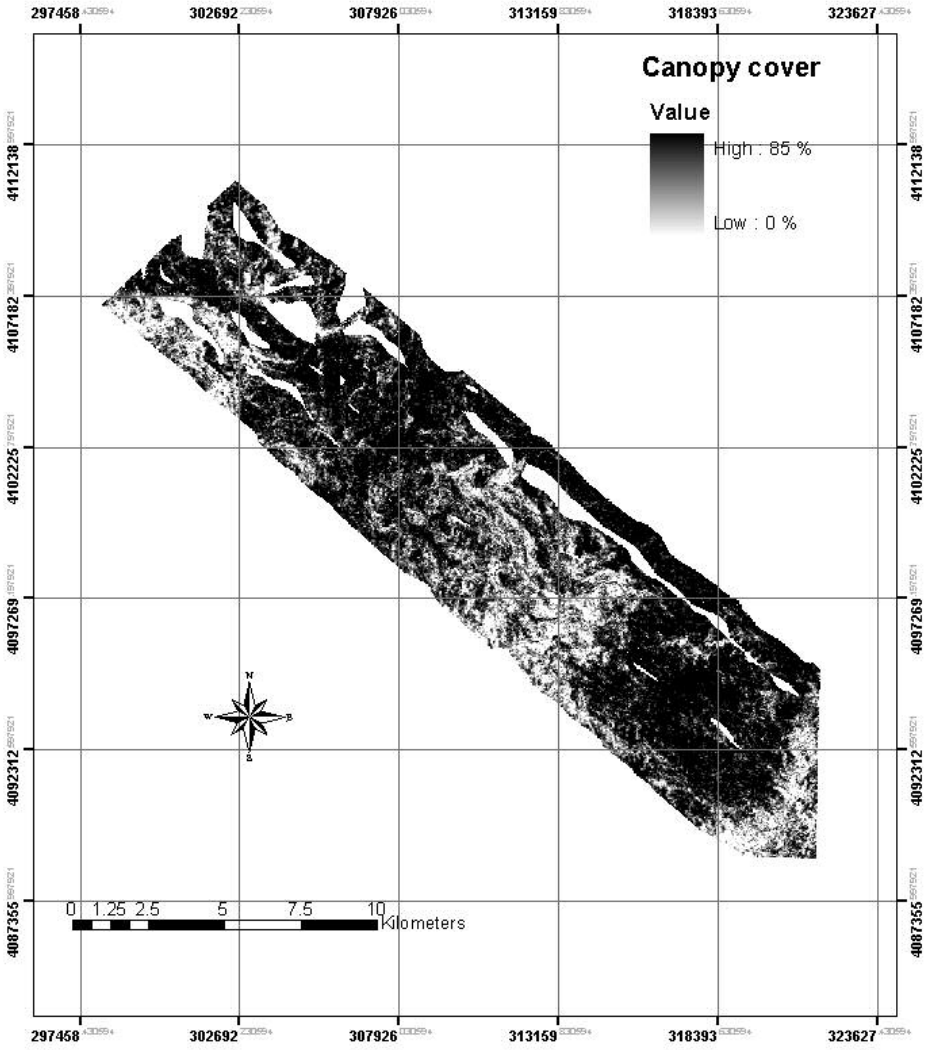

Figure 14. Biomass in Sierra National Forest.

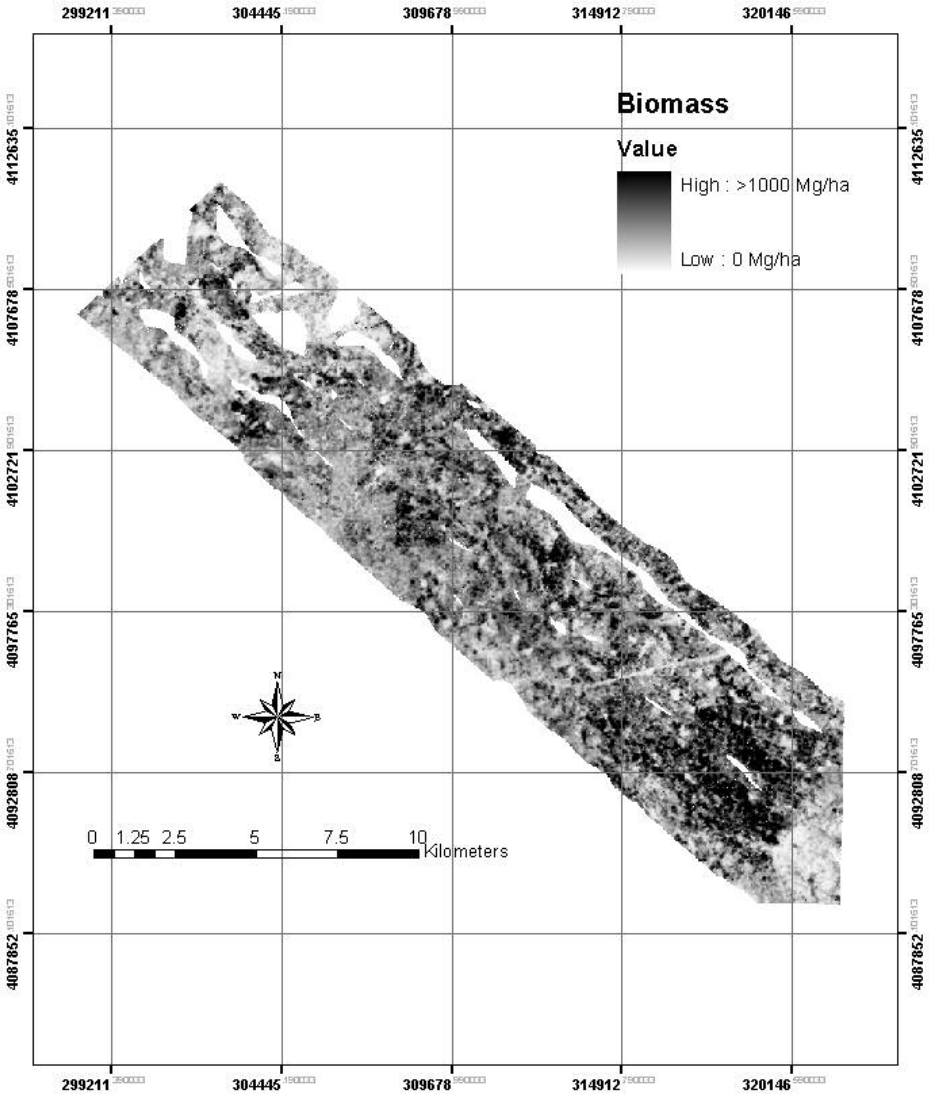

Conclusions

My results have shown the ability of LIDAR to characterize montane forest canopy structure – canopy height, canopy cover and biomass -- over the wide range of environmental conditions that occur over Sierra National forest, as a prerequisite for large area habitat mapping. From a LIDAR remote sensing perspective, the Sierra Nevada is difficult terrain, i.e., it contains steep slopes, highly variable cover, highly variable backgrounds and a mixture of natural (fire) and anthropogenic (selective logging) disturbance regimes.

LIDAR cannot provide all the indicators required for habitat mapping and indeed, canopy height, canopy cover, and biomass may not necessarily even be the best ones. However, they are nonetheless important metrics that have been exceptionally difficult to estimate over large areas using other field or remote sensing methods, such as passive optical or RaDAR. My ability to now map these provides an opportunity to test and assess their ecological importance in new ways.

There is additional structural information present in the LIDAR waveform that can be exploited for habitat characterization. For example, ecological theory suggests that the vertical distribution of canopy structural elements is the most important structural attribute for many forest-dwelling species, particularly avifauna (Trzcinski et al. 1999). Such vertical distributions, though not studied here, are straightforward to derive from LIDAR (e.g. canopy height (leaf and branch) profiles), and should prove useful.

Lastly, developing strategies for fusion of LIDAR with other remotely sensed data will be important for habitat mapping. Multi-spectral, hyperspectral, multi-angle

and radar methods all provide data that should be highly complementary with the structural information derivable from LIDAR. For example species-level information might be derived from hyperspectral observations. The creation of such fusion methods will require further research, but could lead to even more powerful approaches to habitat mapping.

Chapter 3: Retrieval of landscape scale forest structure through multi-sensor (LIDAR, IFSAR, ETM+, Quickbird) fusion

Introduction

Measurements of forest structure are critical for many applications, including wildlife management, fire modeling, and carbon stock estimation. Canopy height and associated metrics of vertical heterogeneity (North et al. 1999), when considered together with site characteristics, are indicators of old-growth forest conditions and thus are of interest to researchers studying old-growth endemics. Canopy height is an important input for ecosystem and fire models and is highly correlated with biomass. Biomass is a key component of the carbon cycle, as forests represent large carbon sources and sinks (Skole and Tucker 1993), and is also a surrogate for fuel loading estimation (Finney 1998). Large trees, in particular, may provide essential habitat for California spotted owls (North et al. 1999) and are an important component of aboveground biomass.

Traditionally, these attributes have been measured in the field using hand-held equipment. Field-based methods can be highly accurate but are time-consuming and thus are typically limited in scope to either mapping at fine scales or sampling at the landscape scale. Multi-spectral (Hyppa et al. 1998) and hyper-spectral remote sensing (Pu and Gong 2004) have been used to map structural metrics at moderate resolution and broad scales. However, passive optical sensors have difficulty penetrating beyond upper canopy layers (Weishampel et al. 2000) and are better suited for mapping horizontal structure, e.g., land cover type. Interferometric

synthetic aperture radar (InSAR) can provide measures of vertical structure at landscape scales at varying degrees of accuracy; however, at the present time these are best suited for structurally homogeneous forest types (Treuhaft and Cloude 1999, Treuhaft and Siqueira 2000). Full waveform-digitizing, large footprint LiDAR provides highly accurate measurements of forest structure at the footprint level of observation (Nelson et al. 1984, Nelson et al. 1988, Nilsson 1996, Lefsky et al. 1999a, Drake et al. 2002, Hyde et al. 2005); however, they are not capable of imaging entire landscapes. Due to the high cost of flight time, the need to limit scanning to near nadir in order to prevent ranging errors, and the presence of coverage gaps due to aircraft pitch and roll, a typical large footprint LiDAR mission acquires samples (albeit at a high frequency) instead of the wall-to-wall coverage provided by other, such as RaDAR or passive optical sensors.

The optimal strategy for mapping forest structure would include the finely-detailed measurements of the vertical dimension that field sampling provides as well as the broad spatial coverage of satellite (and aircraft) remote sensing. Although no single technology is currently capable of providing this level of forest structural information, advancements in InSAR and LiDAR will likely lead to broad-scale mapping of vertical structure in the near future. In the meantime, it is possible to map forest structure at intermediate scales by statistically combining or fusing information from multiple sensors to take advantage of the highly detailed vertical measurements provided by full waveform-digitizing LiDAR, the broad scale mapping capabilities of passive optical sensors, and the coarse sensitivity to horizontal and vertical structure afforded by InSAR. Combining information from multiple sensors, or data fusion,

has yielded promising results for the estimation of forest structural characteristics (Wulder, et al 2004). Hudak et al (2003) combined regression and co-kriging models from LiDAR and multi-spectral data; the results were more accurate than either data set alone. Wulder and Seeman (2003) used texture metrics from Landsat TM images to improve LiDAR estimates of canopy height (from 61% to 67% variability explained). Moghaddam et al (2002) found that combining Landsat TM and several RaDARs was more accurate in predicting ground-based measurements of forest structure than any single sensor alone. Slatton et al. (2001) combined LiDAR data with interferometric RaDAR to improve the estimates of vegetation heights.

Objectives

In the previous chapter, I established that LIDAR could be used to map forest structure at the footprint level of observation. Although LIDAR was also accurate at measuring canopy height and biomass at the stand (1 ha) level of observation, LIDAR is only sampling and not mapping at this scale. Therefore, it remains to be seen whether improvements could be made at the landscape scale by incorporating other sensors.

For this chapter, only large diameter (> 76 cm dbh) trees will be considered because at the stand level only stems in this size class were measured during our field validation effort. Furthermore, a comparison at the footprint level of observation is highly problematic due to the inconsistent geolocation accuracy and resolution of the various sensors used in this study.

The primary objective of this chapter is to quantify and compare the predictive power of individual remote sensing data sets to estimate large tree canopy height and

biomass at the landscape scale. The secondary objective is to fuse large footprint, waveform LiDAR data with other remote sensing data sets to determine if there is either synergy or redundancy in predictive power when combining other remote sensing data sets and large footprint, waveform LiDAR data. The tertiary objective is to ascertain the optimal sampling regime for large footprint, waveform LiDAR, i.e., to determine how sparsely large footprint, waveform LiDAR can be sampled (and fused with other remote sensing data sets) and still achieve a reasonable degree of predictive power.

This chapter is organized as follows. First, I describe collection of field plot data and provide details of the remote sensing (LVIS, SAR/InSAR, ETM+, Quickbird, DEM) data acquisition, which took place over the Sierra Nevada. This is followed by a presentation of the methods used in the processing and analysis of both remote sensing and field data, including the estimation of canopy height and biomass. I then present the results of statistical comparisons between field-derived and remote sensing-derived forest structural attributes and the results of multi-sensor fusion. Finally, I discuss the significance of results relative to the retrieval of forests structure at the landscape scale.

Data Collection

The data included in this chapter include in situ observations, LIDAR data sets (Figures 12 and 14), and other remote sensing data sets (Figure 15).

Figure 15. Other remote sensing data sets in the Sierra Nevada used in this study.

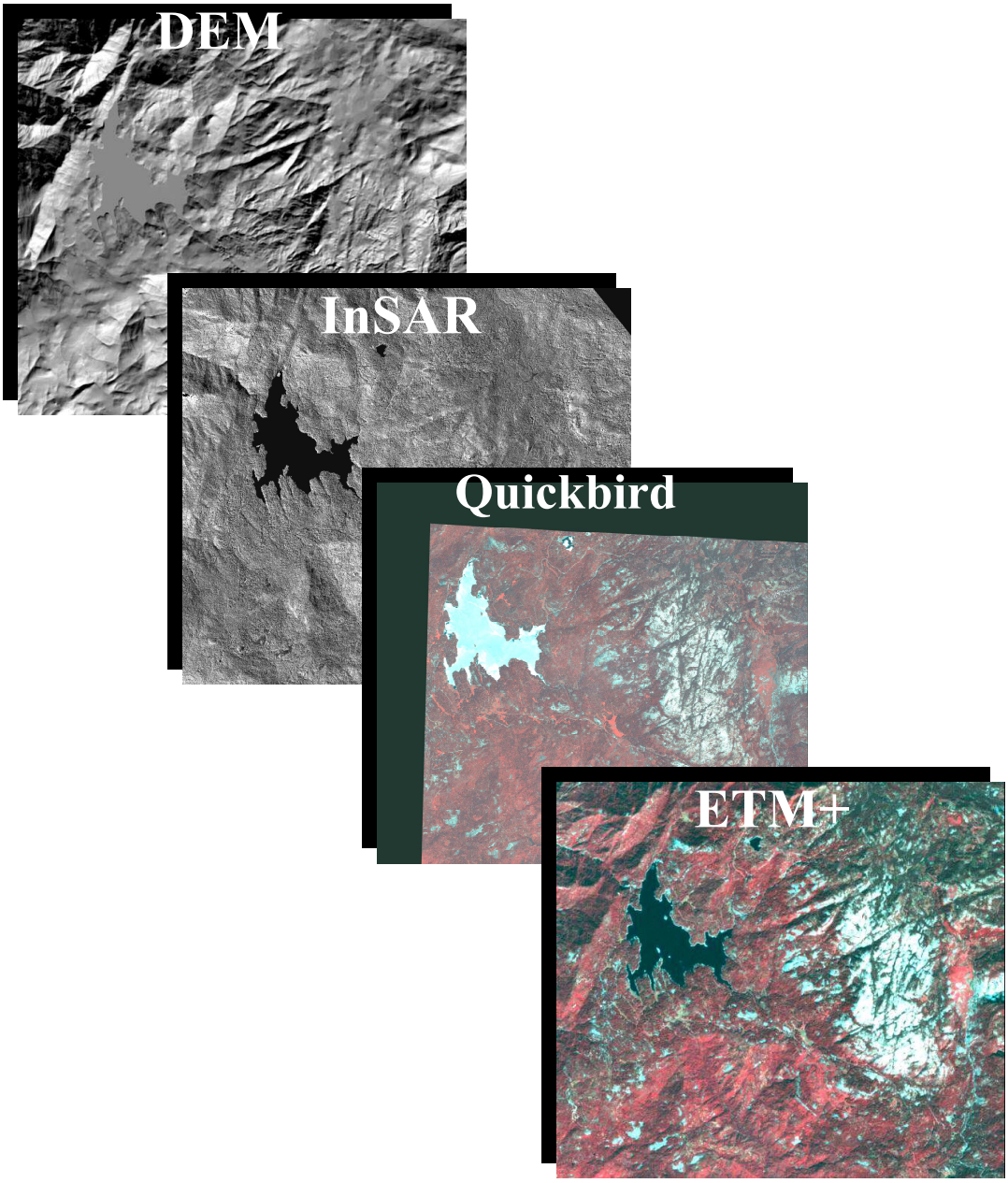

Digital Elevation Model (DEM) data

A 30 m resolution Digital Elevation Model was acquired from the U.S. Geological Survey. This data set consists of "bald earth" elevation, or the elevation of the earth's surface devoid of vegetation or anthropogenic features. The vertical resolution is +/- 7 m.

LiDAR data

See Chapter 2.

SAR/InSAR Data

An X-band (3 cm wavelength, HV polarization) single-baseline RaDAR data set was selected for this study because the interferometric scattering phase center of X-band occurs relatively near to the top of the forest canopy. The RaDAR data set was generated by the STAR-3*i* system from Intermap Technologies (Englewood, CO). The STAR-3i instrument was flown aboard a Learjet in August 1999 and acquired a 3500 sq km swath as well as a second overflight to minimize shadows and layover areas. Both a SAR backscatter intensity image and an InSAR "terrain model", that represents the elevation of the top (or near the top) of the canopy, were provided. The nominal spatial resolution of the data sets is 2.5 m and 10 m for the backscatter intensity image and the DEM, respectively. The reported accuracy for these products is 2.5 m RMSE horizontal and 3.0 m RMSE vertical. The intensity images are filtered to remove speckle.

ETM+ data

Two Landsat ETM+ scenes from October of 1999 covering Sierra National Forest and Sequoia National Park were acquired from USGS Eros Data Center. Each scene consists of six visible and short-wave infrared bands with a nominal spatial resolution of 30 m (thermal and panchromatic bands were not used). A second pair of ETM+ images for a second date (July 2000) was acquired from the University of Maryland Global Land Cover Facility. Both images were acquired during leaf-on conditions.

Quickbird data

Quickbird imagery was acquired from Satellite Imaging Corp (Houston, TX). Quickbird imagery consists of four spectral bands (3 visible, 1 near infra-red) with a nominal spatial resolution of 2 m. Images were acquired in June 2002 and May 2003 in leaf-on conditions.

Field data

One hundred twenty plots were distributed through the northern part the study area (Sierra National Forest) using a modified stratified random sampling scheme. Although the plots were centered on laser footprints, the actual waveforms were not examined before the stratification (to prevent bias). Hence, no attempt was made to retain only waveforms that showed a strong ground return. The number of plots placed within each land cover type was proportional to their actual distribution within Sierra National Forest, with the exception of the red fir class; this vegetation type was oversampled because of its importance as remnant old-growth. Concentric circular plots were established, with an inner plot of 0.07 ha (15 m radius) and an outer plot of

1 ha (56.4 m radius). The 0.07 ha "footprint" plots were designed to allow direct comparison of field measurements and individual LiDAR footprint measurements; the plot size was slightly larger than the nominal footprint to compensate for possible geolocation errors. The 1 ha "stand" plots were designed to be commensurate with existing USDA Forest Service Forest Inventory and Analysis plots.

Field plot data were collected during the summers of 2000 and 2001 and error-checked in 2002. Within the 0.07 ha plots, all live stems with a diameter at breast height (dbh) >= 10 cm were inventoried and species type was recorded. The dbh of each stem was measured with a fiberglass tape. The height of the stem, the height of the full crown, and the height of the partial crown (if present) were measured with an Impulse LR laser range finder (Laser Technology Inc., Englewood, CO). The sweep of the partial crown, if present, was estimated to the nearest 30 degrees. The shape of the crown was characterized as either elliptical, umbrella-shaped, conical, or cylindrical. Four crown radii (two each along and across slope) were measured with a fiberglass tape. The azimuth of each stem with respect to the plot center was measured with a flux gate digital compass (Laser Technology Inc., Englewood, CO) and the distance of each stem to the plot center was measured with the laser range finder.

Data Analysis

The focus of this study is the estimation of two structural metrics: canopy height and aboveground biomass. Canopy height is directly retrieved from waveform data using algorithms described below. It requires identification of a ground return in the

waveform, and associated with this, the identification of the canopy portion of the waveform. Biomass is not directly measured by LVIS; rather, metrics derived from LiDAR waveforms, such as canopy height, and height of median energy, are correlated with canopy structure to compute biomass estimates.

Past studies, e.g. Lefsky (1997), have relied mainly on manual methods for identifying ground returns, especially where the returns are weak relative to the background noise level. While appropriate for validation studies with small numbers of waveforms, manual methods are impossible for the large number of LVIS waveforms being used here (ca. one million). Because canopy height is determined relative to the ground, accurately retrieving ground elevation is critical. Thus, an automated algorithm (described in Hyde et al. 2005) for finding both ground and canopy height was employed.

While LVIS does not measure biomass directly, metrics derived from LiDAR have proven effective in estimating forest biomass (Nelson et al. 1984, Nelson et al. 1988, Nilsson 1996, Lefsky 1997, Lefsky et al. 1999a, Lefsky et al. 1999b, Drake 2001, Lefsky et al. 2001). Canopy height by itself is sufficient for accurate biomass prediction in some, more structurally simple, biomes as canopy height and biomass tend to be highly correlated (Lefsky et al. 1999b). In more structurally complex biomes, such as tropical and old-growth Western coniferous forests, some indication of the depth of the canopy is also useful for predicting biomass (Lefsky et al 1999a, Drake et al 2002). The metrics used in this study to estimate biomass include maximum canopy height, canopy height squared, canopy cover, canopy reflectance, and height of the median energy return (HOME) (Table 8).

Table 8. Metrics derived from LiDAR waveforms

Metric	Description
MINMAXHT	Minimum height of the top of the canopy within a 1 ha plot (m)
MAXMAXHT	Maximum height of the top of the canopy within a 1 ha plot (m)
MEANMAXHT	Mean height of the top of the canopy within a 1 ha plot (m)
STDEVMAXHT	Standard deviation of the height of the top of the canopy within a 1 ha plot (m)
MINMAXHT2	Minimum height squared of the top of the canopy within a 1 ha plot (m2)
MAXMAXHT2	Maximum height squared of the top of the canopy within a 1 ha plot (m2)
MEANMAXHT2	Mean height squared of the top of the canopy within a 1 ha plot (m2)
STDEVMAXHT2	Standard deviation of the height of the top of the canopy within a 1 ha plot squared (m2)
MINCOV	Minimum canopy cover within a 1 ha plot (%)
MAXCOV	Maximum canopy cover within a 1 ha plot (%)
MEANCOV	Mean canopy cover within a 1 ha plot (%)
STDEVCOV	Standard deviation of canopy cover within a 1 ha plot (%)
MINCANREF	Minimum canopy reflectance within a 1 ha plot (dn)
MAXCANREF	Maximum canopy reflectance within a 1 ha plot (dn)
MEANCANREF	Mean canopy reflectance within a 1 ha plot (dn)
STDEVCANREF	Standard deviation of canopy reflectance within a 1 ha plot (dn)
MINHOME	Minimum height of the median energy of the waveforms within a 1 ha plot (m)
MAXHOME	Maximum height of the median energy of the waveforms within a 1 ha plot (m)
MEANHOME	Mean height of the median energy of the waveforms within a 1 ha plot (m)
STDEVHOME	Standard deviation of the height of the median energy of the waveforms within a 1 ha plot (m)

SAR/InSAR data

Elevation from the USGS DEM, which represents the “bare earth” elevation or height of the ground beneath a forest canopy, was subtracted from the InSAR DEM, which represents the “first return” elevation, which includes the height of the canopy, to produce difference image reflecting the height of the InSAR scattering phase center, which will always be less than the observed canopy height, to produce a canopy

height model. Summary statistics (minimum, maximum, mean, median, standard deviation) of this metric, as well as SAR backscatter intensity, were calculated from all pixels whose majority was within the 1 ha plots (Table 9).

Table 9. Metrics derived from SAR/InSAR

Metric	Description
MIN.SARBS	Minimum SAR backscatter intensity for all pixels whose majority lies within a 1 ha plot (dn)
MAX.SARBS	Maximum SAR backscatter intensity for all pixels whose majority lies within a 1 ha plot (dn)
MEAN.SARBS	Mean SAR backscatter intensity for all pixels whose majority lies within a 1 ha plot (dn)
STDEV.SARBS	Standard deviation of SAR backscatter intensity for all pixels whose majority lies within a 1 ha plot (dn)
MIN.SARHT	Minimum InSAR height for all pixels whose majority lies within a 1 ha plot (m)
MAX.SARHT	Maximum InSAR height for all pixels whose majority lies within a 1 ha plot (m)
MEAN.SARHT	Mean InSAR height for all pixels whose majority lies within a 1 ha plot (m)
STDEV.SARHT	Standard deviation of InSAR height for all pixels whose majority lies within a 1 ha plot (m)

ETM+ data

A USGS DEM was used to orthorectify the ETM+ images. Digital numbers (DN) were converted to at-sensor radiances (L) using published ETM+ calibration constants (ETM+ Data Users Guide) and the following equation:

$L = a_0 + a_1 * DN$

Where a_0 and a_1 refer to the sensor gain and bias, respectively.

Atmospheric and topographic correction

Radiance was converted to reflectance using top-of-atmosphere irradiance derived using the MODTRAN atmospheric correction model (Berk et al. 1989). A cosine correction was used to correct for the influence of topography on the amount of

incident solar radiation. None of the field plots were obstructed by terrain, i.e. all field plots received direct and diffuse illumination at the time of image acquisition.

Metrics

Principle components and NDVI (NIR – red / NIR + red) were calculated for each image. Summary statistics (minimum, maximum, mean, median, standard deviation) of these metrics were calculated from all pixels whose majority was within the 1 ha plots (Tables 10 and 11).

Table 10. Metrics derived from ETM+ 1 (October 1999). All values are unitless.

Metric	Description
MIN.NDVI.1	Minimum NDVI for all pixels in ETM+ 1 whose majority lies within a 1 ha plot
MAX.NDVI.1	Maximum NDVI for all pixels in ETM+ 1 whose majority lies within a 1 ha plot
MEAN.NDVI.1	Mean NDVI for all pixels in ETM+ 1 whose majority lies within a 1 ha plot
STDEV.NDVI.1	Standard deviation of NDVI for all pixels in ETM+ 1 whose majority lies within a 1 ha plot
MIN.PCA1.1	Minimum first principle component for all pixels in ETM+ 1 whose majority lies within a 1 ha plot
MAX.PCA1.1	Maximum first principle component for all pixels in ETM+ 1 whose majority lies within a 1 ha plot
MEAN.PCA1.1	Mean first principle component for all pixels in ETM+ 1 whose majority lies within a 1 ha plot
STDEV.PCA1.1	Standard deviation first principle component for all pixels in ETM+ 1 whose majority lies within a 1 ha plot
MIN.PCA2.1	Minimum second principle component for all pixels in ETM+ 1 whose majority lies within a 1 ha plot
MAX.PCA2.1	Maximum second principle component for all pixels in ETM+ 1 whose majority lies within a 1 ha plot
MEAN.PCA2.1	Mean second principle component for all pixels in ETM+ 1 whose majority lies within a 1 ha plot
STDEV.PCA2.1	Standard deviation second principle component for all pixels in ETM+ 1 whose majority lies within a 1 ha plot
MIN.PCA3.1	Minimum first principle component for all pixels in ETM+ 1 whose majority lies within a 1 ha plot
MAX.PCA3.1	Maximum third principle component for all pixels in ETM+ 1 whose majority lies within a 1 ha plot
MEAN.PCA3.1	Mean third principle component for all pixels in ETM+ 1 whose majority lies within a 1 ha plot
STDEV.PCA3.1	Standard deviation third principle component for all pixels in ETM+ 1 whose majority lies within a 1 ha plot
MIN.PCA4.1	Minimum fourth principle component for all pixels in ETM+ 1 whose majority lies within a 1 ha plot
MAX.PCA4.1	Maximum fourth principle component for all pixels in ETM+ 1 whose majority lies within a 1 ha plot
MEAN.PCA4.1	Mean fourth principle component for all pixels in ETM+ 1 whose majority lies within a 1 ha plot
STDEV.PCA4.1	Standard deviation fourth principle component for all pixels in ETM+ 1 whose majority lies within a 1 ha plot
MIN.PCA5.1	Minimum fifth principle component for all pixels in ETM+ 1 whose majority lies within a 1 ha plot
MAX.PCA5.1	Maximum fifth principle component for all pixels in ETM+ 1 whose majority lies within a 1 ha plot
MEAN.PCA5.1	Mean fifth principle component for all pixels in ETM+ 1 whose majority lies within a 1 ha plot
STDEV.PCA5.1	Standard deviation fifth principle component for all pixels in ETM+ 1 whose majority lies within a 1 ha plot
MIN.PCA6.1	Minimum sixth principle component for all pixels in ETM+ 1 whose majority lies within a 1 ha plot
MAX.PCA6.1	Maximum sixth principle component for all pixels in ETM+ 1 whose majority lies within a 1 ha plot
MEAN.PCA6.1	Mean sixth principle component for all pixels in ETM+ 1 whose majority lies within a 1 ha plot
STDEV.PCA6.1	Standard deviation sixth principle component for all pixels in ETM+ 1 whose majority lies within a 1 ha plot

Table 11. Metrics derived from ETM+ 2 (July 2000). All values are unitless.

Metric	Description
MIN.NDVI.2	Minimum NDVI for all pixels in ETM+ 2 whose majority lies within a 1 ha plot
MAX.NDVI.2	Maximum NDVI for all pixels in ETM+ 2 whose majority lies within a 1 ha plot
MEAN.NDVI.2	Mean NDVI for all pixels in ETM+ 2 whose majority lies within a 1 ha plot
STDEV.NDVI.2	Standard deviation of NDVI for all pixels in ETM+ 2 whose majority lies within a 1 ha plot
MIN.PCA1.2	Minimum first principle component for all pixels in ETM+ 2 whose majority lies within a 1 ha plot
MAX.PCA1.2	Maximum first principle component for all pixels in ETM+ 2 whose majority lies within a 1 ha plot
MEAN.PCA1.2	Mean first principle component for all pixels in ETM+ 2 whose majority lies within a 1 ha plot
STDEV.PCA1.2	Standard deviation first principle component for all pixels in ETM+ 2 whose majority lies within a 1 ha plot
MIN.PCA2.2	Minimum second principle component for all pixels in ETM+ 2 whose majority lies within a 1 ha plot
MAX.PCA2.2	Maximum second principle component for all pixels in ETM+ 2 whose majority lies within a 1 ha plot
MEAN.PCA2.2	Mean second principle component for all pixels in ETM+ 2 whose majority lies within a 1 ha plot
STDEV.PCA2.2	Standard deviation second principle component for all pixels in ETM+ 2 whose majority lies within a 1 ha plot
MIN.PCA3.2	Minimum first principle component for all pixels in ETM+ 2 whose majority lies within a 1 ha plot
MAX.PCA3.2	Maximum third principle component for all pixels in ETM+ 2 whose majority lies within a 1 ha plot
MEAN.PCA3.2	Mean third principle component for all pixels in ETM2 whose majority lies within a 1 ha plot
STDEV.PCA3.2	Standard deviation third principle component for all pixels in ETM+ 2 whose majority lies within a 1 ha plot
MIN.PCA4.2	Minimum fourth principle component for all pixels in ETM+ 2 whose majority lies within a 1 ha plot
MAX.PCA4.2	Maximum fourth principle component for all pixels in ETM+ 2 whose majority lies within a 1 ha plot
MEAN.PCA4.2	Mean fourth principle component for all pixels in ETM+ 2 whose majority lies within a 1 ha plot
STDEV.PCA4.2	Standard deviation fourth principle component for all pixels in ETM+ 2 whose majority lies within a 1 ha plot
MIN.PCA5.2	Minimum fifth principle component for all pixels in ETM+ 2 whose majority lies within a 1 ha plot
MAX.PCA5.2	Maximum fifth principle component for all pixels in ETM+ 2 whose majority lies within a 1 ha plot
MEAN.PCA5.2	Mean fifth principle component for all pixels in ETM+ 2 whose majority lies within a 1 ha plot
STDEV.PCA5.2	Standard deviation fifth principle component for all pixels in ETM+ 2 whose majority lies within a 1 ha plot
MIN.PCA6.2	Minimum sixth principle component for all pixels in ETM+ 2 whose majority lies within a 1 ha plot
MAX.PCA6.2	Maximum sixth principle component for all pixels in ETM+ 2 whose majority lies within a 1 ha plot
MEAN.PCA6.2	Mean sixth principle component for all pixels in ETM+ 2 whose majority lies within a 1 ha plot
STDEV.PCA6.2	Standard deviation sixth principle component for all pixels in ETM+ 2 whose majority lies within a 1 ha plot

Quickbird data

A USGS DEM was used to orthorectify the images. Digital numbers (DN) were converted to at-sensor radiances (L) using published calibration constants (Satellite Imaging Corp., Houston, TX).

Atmospheric and topographic correction

Radiance was converted to reflectance using top-of-atmosphere irradiance derived using the MODTRAN atmospheric correction model (Berk et al 1989). A cosine correction was used to correct for the influence of topography on amount of incident solar radiation. None of the field plots were obstructed by terrain, i.e. all field plots received direct and diffuse illumination at the time of image acquisition.

Metrics

Principle components and NDVI (NIR – red / NIR + red) were calculated at the footprint level. Summary statistics (minimum, maximum, mean, median, standard deviation) of these metrics were also calculated from all pixels whose majority was within the 1 ha plots (Table 12).

Table 12. Metrics derived from Quickbird. All values are unitless.

Metric	Description
MIN.QBNDVI	Minimum NDVI for all pixels in Quickbird whose majority lies within a 1 ha plot
MAX.QBNDVI	Maximum NDVI for all pixels in Quickbird whose majority lies within a 1 ha plot
MEAN.QBNDVI	Mean NDVI for all pixels in Quickbird whose majority lies within a 1 ha plot
STDEV.QBNDVI	Standard deviation of NDVI for all pixels in Quickbird whose majority lies within a 1 ha plot
MIN.QBPCA1	Minimum first principle component for all pixels in Quickbird whose majority lies within a 1 ha plot
MAX.QBPCA1	Maximum first principle component for all pixels in Quickbird whose majority lies within a 1 ha plot
MEAN.QBPCA1	Mean first principle component for all pixels in Quickbird whose majority lies within a 1 ha plot
STDEV.QBPCA1	Standard deviation first principle component for all pixels in Quickbird whose majority lies within a 1 ha plot
MIN.QBPCA2	Minimum second principle component for all pixels in Quickbird whose majority lies within a 1 ha plot
MAX.QBPCA2	Maximum second principle component for all pixels in Quickbird whose majority lies within a 1 ha plot
MEAN.QBPCA2	Mean second principle component for all pixels in Quickbird whose majority lies within a 1 ha plot
STDEV.QBPCA2	Standard deviation second principle component for all pixels in Quickbird whose majority lies within a 1 ha plot
MIN.QBPCA3	Minimum first principle component for all pixels in Quickbird whose majority lies within a 1 ha plot
MAX.QBPCA3	Maximum third principle component for all pixels in Quickbird whose majority lies within a 1 ha plot
MEAN.QBPCA3	Mean third principle component for all pixels in Quickbird whose majority lies within a 1 ha plot
STDEV.QBPCA3	Standard deviation third principle component for all pixels in Quickbird whose majority lies within a 1 ha plot
MIN.QBPCA4	Minimum fourth principle component for all pixels in Quickbird whose majority lies within a 1 ha plot
MAX.QBPCA4	Maximum fourth principle component for all pixels in Quickbird whose majority lies within a 1 ha plot
MEAN.QBPCA4	Mean fourth principle component for all pixels in Quickbird whose majority lies within a 1 ha plot

Field plot data

Field measurements at the footprint and stand levels include maximum canopy height, i.e., the height of the tallest stem within each plot. Allometric equations relating stem biomass to height and dbh were obtained from the USDA Forest Service (Waddell and Hiserote 2003). These equations were applied to the field data to calculate total

standing (aboveground) biomass for each stem (>= 76 cm dbh); the biomass of all stems within each plot was added to provide stand level totals.

Methods

Stand (1 ha) level

Stepwise multiple linear regression was used to compare the remote sensing data sets to field data. The number of predictors in each model was limited to 10 to prevent overfitting. All regression models were cross-validated using the "Leave One Out" method. First, ETM+, Quickbird, LiDAR, and SAR/InSAR data sets were compared separately. Next, ETM+, Quickbird, and SAR/InSAR data sets were compared, in various combinations, to field data to produce models of canopy height and biomass. The combinations include: 1) LiDAR and Quickbird, 2) LiDAR and SAR/InSAR, 3) LiDAR and ETM+ scene 1 (October 1999), 4) LiDAR and ETM+ scene 2 (July 2000), 5) Quickbird, SAR/INSAR, ETM+ scene 1 (October 1999), and ETM+ scene 2 (July 2000), and, 6) LiDAR, Quickbird, SAR/INSAR, ETM+ scene 1 (October 1999), and ETM+ scene 2 (July 2000).

Landscape level

LiDAR data were randomly sampled at a variety of frequencies, corresponding to the following percentages of the total LiDAR data set: 1, 2, 5, 10, 20, 30, 40, 50, 60, 70, 80, 90, and 100 to simulate sparse LiDAR data availability. Where LiDAR data were present, canopy height and biomass maps at each sample interval were produced by applying the field-validated models to resampled 1 ha pixels. Where LiDAR data were not present, only the other remote sensing data sets (and their corresponding field-validated model) were used. The result was a series of images at each sample

interval that used LiDAR where present; the gaps where LiDAR was not present were "filled in" with the other remote sensing data sets. The mean canopy height and biomass of each image was then calculated.

Results

Stand (1 ha) level

For the single sensor models of canopy height (Tables 13 and 14), LiDAR ($r^2 = 0.76$, RMSE = 8.8 m) was more accurate than Quickbird ($r^2 = 0.66$, RMSE = 11.6 m), SAR/InSAR ($r^2 = 0.69$, RMSE = 9.9 m), ETM+ scene 1 ($r^2 = 0.73$, RMSE = 9.4 m), and ETM+ scene 2 ($r^2 = 0.70$, RMSE = 10.0 m). Cross-validation demonstrated that models produced by SAR/InSAR were far less robust ($r^2 = 0.53$, RMSE = 12.0 m) than LiDAR ($r^2 = 0.72$, RMSE = 9.4 m), as was the ETM+ scene 2 ($r^2 = 0.61$, RMSE = 11.07 m). The addition of any single sensor to the LiDAR results did not result in much improvement relative to LiDAR alone. The combination of all sensors (LiDAR, both ETM+ images, SAR/InSAR, and Quickbird) was more accurate ($r^2 = 0.84$, RMSE = 7.3 m) than LiDAR alone ($r^2 = 0.76$, RMSE = 8.8 m).

Table 13. Canopy height regression results.

Sensor(s)	Coefficient of determination (r2)	Root mean square error (m)	Cross-validated r2	Cross-validated RMSE (m)	n	p
LiDAR	0.76	8.8	0.72	9.4	111	< 0.00001
QB	0.66	10.5	0.61	11.6	111	< 0.00001
LiDAR + QB	0.79	8.2	0.76	8.7	111	< 0.00001
InSAR	0.69	9.9	0.53	12.0	111	< 0.00001
LiDAR + InSAR	0.76	8.8	0.73	9.1	111	< 0.00001
ETM1	0.73	9.4	0.69	9.9	111	< 0.00001
LiDAR + ETM1	0.82	7.8	0.78	8.2	111	< 0.00001
ETM2	0.70	10.0	0.61	11.07	111	< 0.00001
LiDAR + ETM2	0.81	8.0	0.76	8.6	111	< 0.00001
ETM1+ ETM2+ QB + InSAR	0.74	9.3	0.70	9.6	111	< 0.00001
LiDAR + ETM1 + ETM2 + QB+ InSAR	0.84	7.3	0.81	7.7	111	< 0.00001

Table 14. Canopy height models

Sensor(s)	Model
LiDAR	-4.01 + (0.7 * MEANMAXHT) + (0.72 * MAXMAXHT) +(-0.63 *MEANHOME)
QB	-262.2 + (45.7 * MEAN.QBNDVI) + (176.7 * STDEV.QBNDVI) + (-0.1* MIN.QBPC1) + (0.2 * STDEV.QBPC1) + (-0.2* STDEV.QBPC2) + (0.4* MEAN.QBPC3)
LiDAR + QB	1.23+ (1.52*MEANMAXHT)+(0.71*MEDIANMAXHT)+ (1.25*SDMAXHT) +(31.25*MAX.QBNDVI)+(-0.06 MIN.QBPCA1)
InSAR	-15.2 + (1.1 * MAX.SARHT) + (1.1* STDEV.SARHT)
LiDAR + InSAR	-4.01 + (0.7 * MEANMAXHT) + (0.72 * MAXMAXHT) + (-0.63 *MEANHOME)
ETM1	-83.7 + (-322.6 * MIN.NDVI.1) + (-192.4 * MAX.NDVI.1) + (0.3 * STDEV.PCA1.1) + (0.7 * MEAN.PCA2.1) + (-0.5* MAX.PCA4.1)
LiDAR + ETM1	-32.8+(0.6*MAXMAXHT)+(-301.4*MEAN.NDVI.1)+(0.4*MEAN.PCA2.1) (-0.4*MAX.PCA4.1)+(4*MAX.PCA6.1)+(-4*MEAN.PCA6.1)
ETM2	1453.0 + (4610.7 * MEAN.NDVI.2) + (32.3 * MAX.PCA2.2) + (-82.7 * MEAN.PCA2.2) + (-81.3 * STDEV.PCA2) + (92.4* MEAN.PCA3.2) + (84.2 * STDEV.PCA4.2) + (136.8 * MIN.PCA5.2) + (463.1 * STDEV.PCA5.2) + (2514.3* MIN.PCA6.2)
LiDAR + ETM2	835.9 +(0.7*MAXMAXHT)+(1855.5*MEAN.NDVI.2)+(35.1*MAX.PCA2.2) + (-60.3*MEAN.PCA2.2)+(-64.3*STDEV.PCA2)+(37.6*MEAN.PCA3.)+ (93.6*MIN.PCA5.2) +(377.3*STDEV.PCA5.2)
ETM1+ETM2+ QB + InSAR	-50.8 + (2.5 * STDEV.SARHT) + (-0.6 * MIN.PCA4.1) + (-1.1 * MEAN.PCA5.1) + (-1228.8 * MEAN.NDVI.2) + (-5.1* MEAN.PCA1.2) + (14.9* MAX.PCA2.2)
LiDAR+ETM1+ ETM2+QB+SAR	1109.1 + (0.7 * MAXMAXHT) + (-0.3 * MIN.SARBS) + (0.4 * MEAN.PCA2.1) + (12.3 * MAX.PCA2.2) + (26.4 * MEAN.PCA3.2) + (-78.6* MEAN.PCA4.2)

For the single sensor models of biomass (Tables 15 and 16), LiDAR (r^2 = 0.78, RMSE = 73.0 Mg/ha) was more accurate than Quickbird (r^2 = 0.46, RMSE = 114.6 Mg/ha), SAR/InSAR (r^2 = 0.69, RMSE = 86.6 Mg/ha), ETM+ scene 1 (r^2 = 0.57, RMSE = 104.8 Mg/ha), and ETM+ scene 2 (r^2 = 0.67, RMSE = 92.5 Mg/ha). Cross-validation demonstrated that models produced by SAR/InSAR were far less robust (r^2 = 0.46, RMSE = 112.7 Mg/ha) than LiDAR (r^2 = 0.72, RMSE = 81.4 Mg/ha), as was the ETM+ scene 1 (r^2 = 0.47, RMSE = 113.9 Mg/ha). The addition of any single sensor to the LiDAR results did not result in much improvement relative to LiDAR alone. The combination of all sensors (LiDAR, both ETM+ images, SAR/InSAR, and Quickbird) was more accurate (r^2 = 0.82, RMSE = 69.4 Mg/ha) than LiDAR alone (r^2 = 0.78, RMSE = 73.0 Mg/ha), but was not as robust; cross-validated LiDAR was more accurate (r^2 = 0.72, RMSE = 81.4 Mg/ha) than all sensors combined (r^2 = 0.71, RMSE = 83.3 Mg/ha).

Table 15. Biomass regression results.

sensor(s)	Coefficient of determination (r2)	Root mean-square error (Mg/ha)	Cross-validated r2	Cross-validated RMSE	n	p
LiDAR	0.78	73.0	0.72	81.4	111	< 0.00001
QB	0.46	114.6	0.41	118.3	111	< 0.00001
LiDAR & QB	0.82	68.5	0.77	74.0	111	< 0.00001
InSAR	0.69	86.6	0.46	112.7	111	< 0.00001
LiDAR & SAR	0.80	71.3	0.71	82.4	111	< 0.00001
ETM1	0.57	104.8	0.47	113.9	111	< 0.00001
LiDAR + ETM1	0.84	65.9	0.78	71.8	111	< 0.00001
ETM2	0.67	92.5	0.60	98.2	111	< 0.00001
LiDAR + ETM2	0.83	54.7	0.73	80.4	111	< 0.00001
ETM1+ETM2 +QB +InSAR	0.76	78.0	0.72	81.4	111	< 0.00001
LiDAR+ETM1 +ETM2 + QB+ InSAR	0.82	69.4	0.71	83.3	111	< 0.00001

Table 16. Biomass models

Sensor(s)	Model
LiDAR	-44.94 + (5.43* MEANMAXHT)+(-4.95 * MINMAXHT) + (27.55 * MEANHOME) + (-9.94 * MEDIANHOME) + (-3.24 * MEANCOVER) + (3.78 * SDCOVER)
QB	-3970.2 + (-2.4 * MIN.QBPC3) + (6.4* MEAN.QBPC3) + (4.1* MAX.QBPC4)
LiDAR + QB	-564.9 + (5.6 * MEANMAXHT) +(-4 * MINMAXHT) + (29.4 * MEANHOME) + (9.9 * MEDIANHOME)+ (-2.6 * MEANCOVER)+(3.9 * SDCOVER) + (699.2 * MEAN.QBNDVI) +(0.9 * MEAN.QBPC2) + (-0.7 * MIN.QBPC3)
InSAR	-419.5 + (-5.1* MIN.SARHT) + (19.0* MEAN.SARHT)
LiDAR + SAR	14.4 + (5.2 * MEANMAXHT) + (-4.8 * MINMAXHT) + (29.0 * MEANHOME) + (-10.2 * MEDIANHOME) + (-3.1* MEANCOVER) + (4.0 * SDCOVER) + (-0.7 * MAX.SARBS)
ETM1	-6226.1 + (-10570.8 * MEAN.NDVI.1) + (2.8 * MEAN.PCA1.1) + (12.1 * MEAN.PCA2.1) + (8.2 * MAX.PCA3.1) + (-19.4 * STDEV.PCA3.1) + (32.8 * MIN.PCA5.1) + (-30.8 * MAX.PCA5.1) + (89.0* STDEV.PCA5.1)
LiDAR + ETM1	116.8+(3.2 * MEANMAXHT) + (-3.4 * MINMAXHT) + (32.3 * MEANHOME) + (-13.3 * MEDIANHOME) + (-1.8 * MEDIANCOVER) + (2.6 * SDCOVER) + (-1339.5 * MAX.NDVI1) + (MAX.PCA5.1)
ETM2	-100326.0 + (-19766.8 * MAX.NDVI.2) + (-258441.1 * MEAN.NDVI.2) + (-341.1* MEAN.PCA1.2)+ (289.7 * MAX.PCA2.2) + (3161.3 * MEAN.PCA2.2) + (-286.4 * MIN.PCA3.2) +(-3818.3 * MEAN.PCA3.) + (-695.1* MEAN.PCA4.2) + (1659.6* MEAN.PCA5.2)
LiDAR + ETM2	13126 + (3.6 * MEDIANMAXHT) + (32 * MEANHOME) + (-15 * MEDIANHOME) + (-1.93 * MEDIANCOVER) + (2.22 * SDCOVER) + (-3943 * MAX.NDVI2) + (-18 * MEAN.PCA1.2) + (204*STDEV.PCA3) + (-383 * MEAN.PCA4.2)
ETM1+ETM2 QB+ InSAR	-3693.0 + (-381.2 * MIN.QBNDVI) + (9.5 * MIN.SARHT) + (18.1 * STDEV.SARHT) + (-2828.3 * MEAN.NDVI.1) + (4.3 * MAX.PCA3.1) + (-9.7 * STDEV.PCA3.1) + (1028.0* MEAN.PCA5.2)
LiDAR+ETM1+ ETM2+ QB+ InSAR	-62598.7 + (2.5* MAXMAXHT) + (9.8 * MEANHOME) + (8.7 * SDHOME) + (3.7 * MIN.SARHT)+ (-1070.1 * MAX.NDVI.1) + (-205370.9 * MEAN.NDVI.2) + (-245.8* MEAN.PCA1.2)+ (2475.6* MEAN.PCA2.2) + (-3160.0 * MEAN.PCA3.) + (-630.8* MEAN.PCA4.2)

Landscape scale

Mean canopy height and biomass over the entire landscape were calculated using the 1, 2, 5, 10, 20, 30, 40, 50, 60, 70, 80, 90, and 100 % LiDAR samples; the results are plotted in Figure 16. Mean canopy height remained relatively stable as LiDAR sample size increased (Figure 16a), declining only about 1.5 m as the sample size approached 100%. Biomass (Figure 16b) increased fairly substantially, from about 155 to 175 Mg/ha.

Figure 16. Landscape scale canopy height and biomass as a function of LiDAR sample size

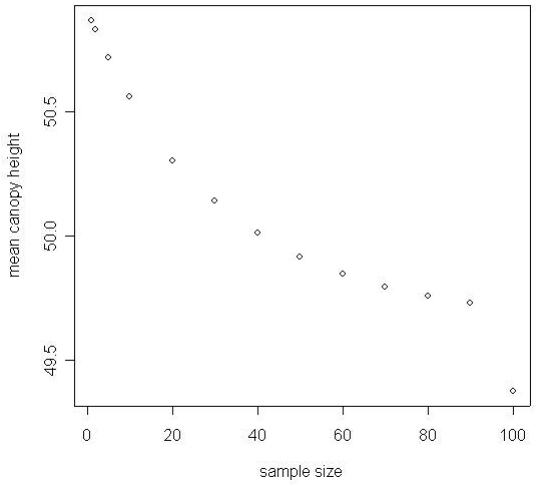

A

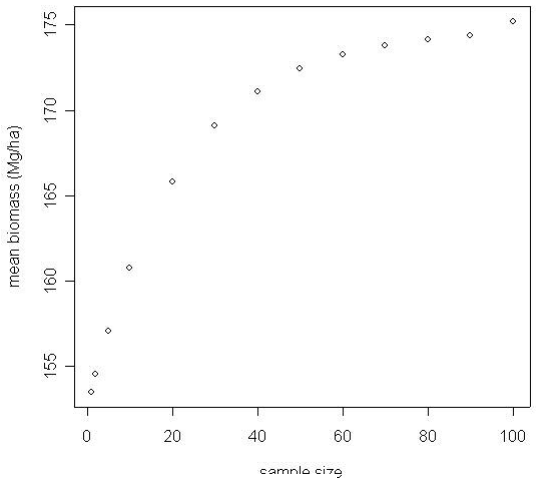

B

Discussion

LiDAR has been shown to be effective in estimating forest structure. One unique aspect of this study is that LiDAR was shown to be effective in measuring height and biomass of large trees, which are important components of wildlife habitat and represent a key carbon reservoir. Other sensors did not perform as well, particularly with respect to biomass. This is not surprising given that only LiDAR has the ability to provide an accurate return from both the top and bottom of the canopy and provide a volumetric response (via HOME). While the backscatter from other, longer wavelengths RaDARs (e.g., C, L and P) are sensitive to canopy volume, the X band wavelength used in this study is much less so. The InSAR height metric was less accurate at predicting height and biomass than LiDAR height, possibly because the X band penetrated further into the top of the canopy, causing a foreshortening of the height measurement. It is also probable that at least some of the elevation values from the DEM were corrupted by the canopy; LiDAR ground elevation values are likely more reliable since we are confident that the last return is actually coming from the ground. However, other sensors did have significant utility in aiding LiDAR in the prediction of canopy height. In contrast, the other sensors did not contribute as much to the accuracy of the biomass predictions.

At the landscape scale, as LiDAR sample size increases, the estimate of the height of big trees stays about the same. If the image containing the 100% LiDAR sample is used as a baseline of height "truth", then the fused canopy height images are reasonably accurate regardless of the size of the LiDAR sample. In other words, the gaps in LiDAR coverage are measured fairly accurately with the other sensors,

providing a reasonable approximation of canopy height. However, this is not true of biomass; gaps in LiDAR coverage are not measured as accurately with the other remote sensing data sets and the net result is over a 10% reduction in total estimated biomass for the entire landscape.

Recall that the ultimate goal of this effort is to provide spatially continuous maps of forest structure at the landscape scale as a prerequisite for habitat suitability studies. Using the statistical relationship developed between field and LiDAR plus other remote sensing data sets for canopy height and biomass, I created maps of each of these over the domain of the data sets (Figures 17 & 18). It is this mapping of forest structural characteristics at the landscape scale which we believe will be of great benefit to future habitat studies.

Conclusion

LiDAR provides accurate estimates of stand level canopy height and biomass at the stand (1 ha) level even though it is sampling, not mapping at this scale. Some improvements were achieved by adding some or all additional remote sensing data sets. However, these improvements come at some cost, including 1) cost of data acquisition, 2) cost of data processing, and 3) statistical certainty. The cost of acquiring and processing ETM+ is relatively minimal; the cost of acquiring (Quickbird) or processing (InSAR) is not. Atmospheric and topographic correction of passive optical data is also not trivial, requiring computing power, time, and expertise.

It is not clear at this point whether or not estimates of big tree height and biomass at the stand (1 ha) scale have more utility for habitat modeling than do

samples taken at the footprint scale. It is possible that these maps do not provide any additional predictive power for a given application, but there is no way to know this *a priori*.

.

Figure 17. Canopy height map from LIDAR and other remote sensing data sets. The units are in meters.

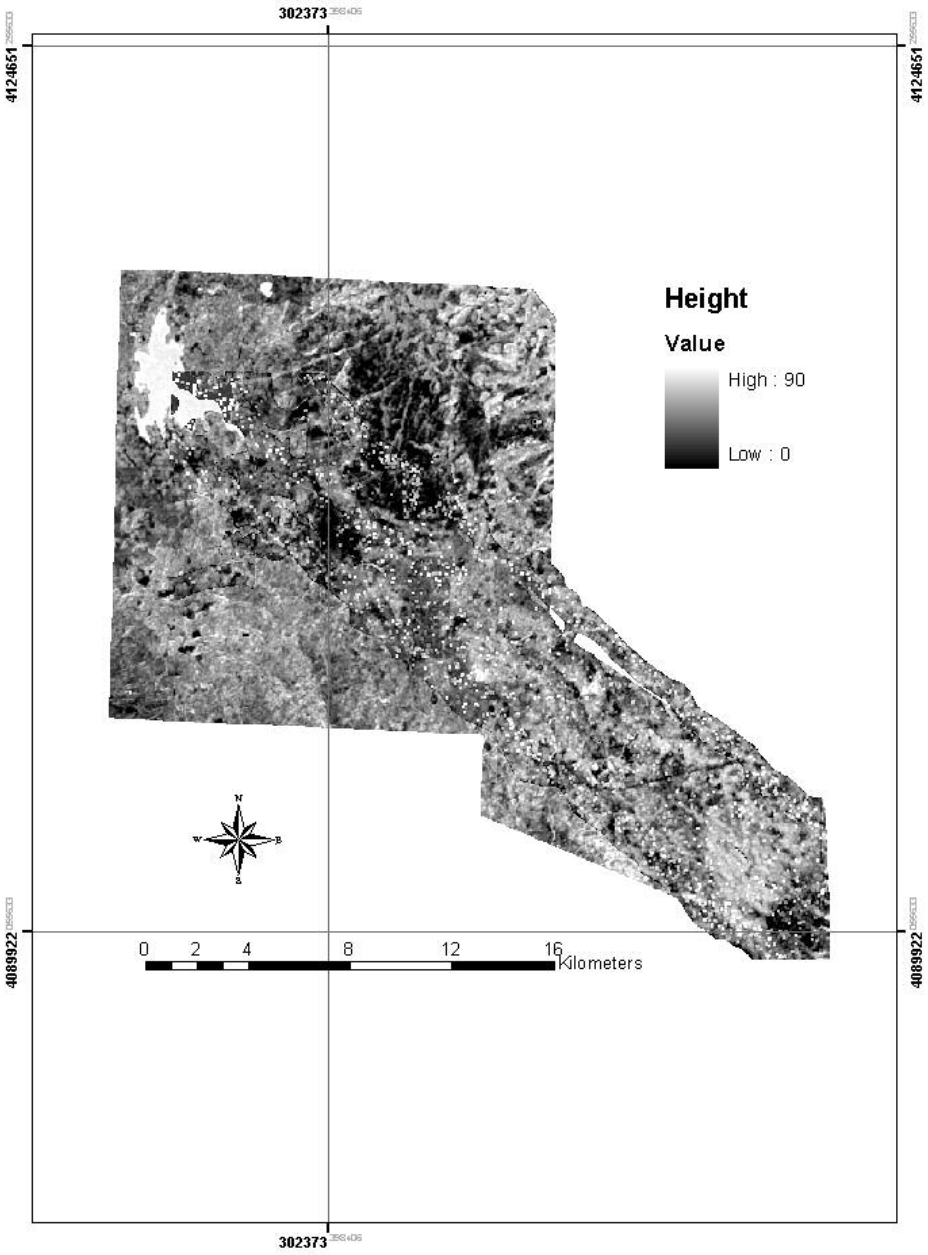

Figure 18. Biomass map from LIDAR and other remote sensing data sets. The units are in Mg/ha.

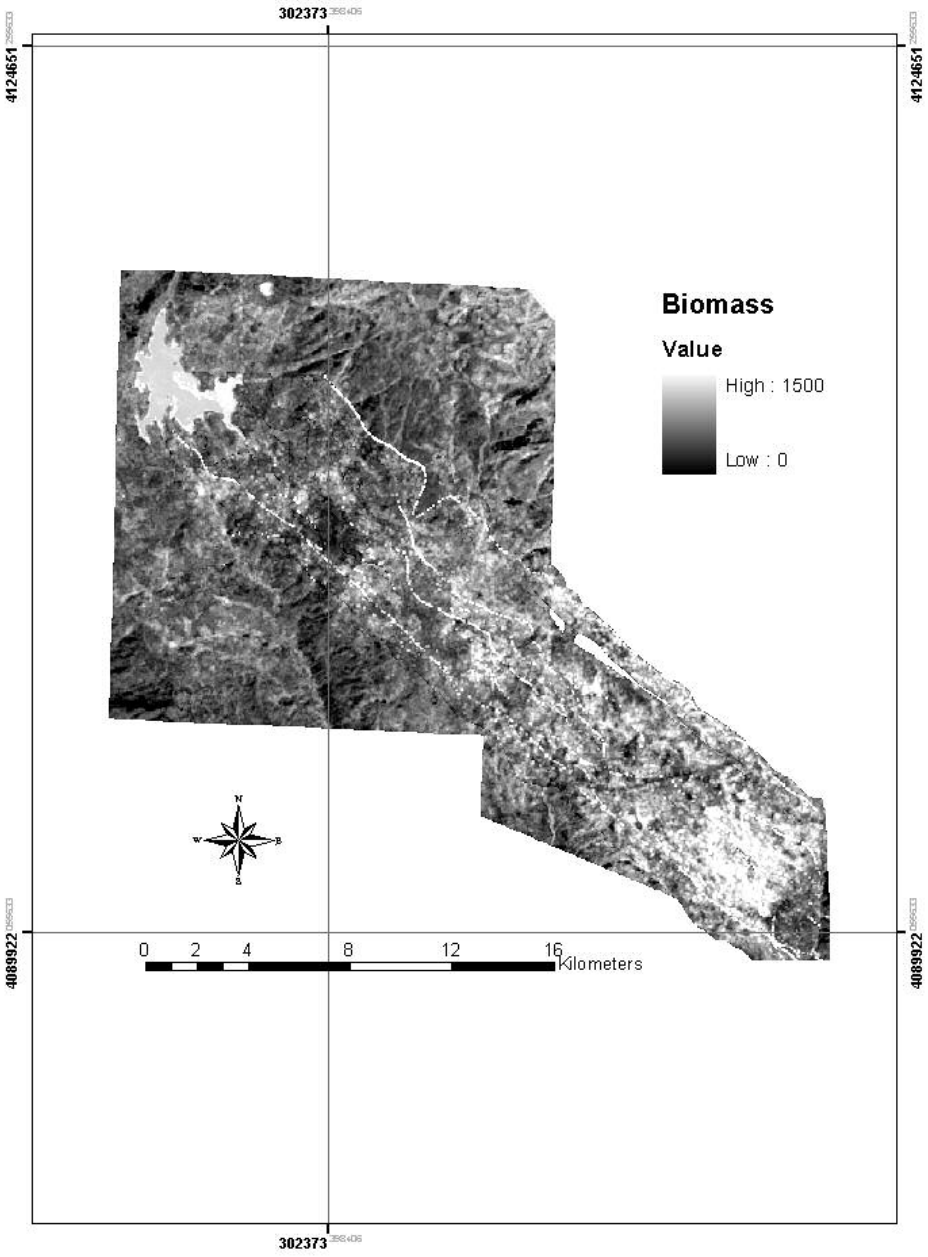

Chapter 4: Mapping California spotted owl habitat using forest structural characteristics derived from remote sensing

Introduction

One of the most critical challenges for natural resources management is balancing the needs of multiple, often competing, uses. This is particularly true in the National Forests, where the USDA Forest Service is responsible for fire management as well as maintaining water quality and biological diversity. For example, Sierra National Forest must conduct prescribed burns while maintaining critical habitat for California spotted owls, *Strix occidentalis*. There remains a great deal of uncertainty regarding how much habitat alteration spotted owl populations can tolerate (Lee and Irwin 2005), which aspects of forest structure that are being modified are important, and how best to measure forest structure within spotted owl habitat (Hunsaker et al 2002).

A variety of forest structural attributes have been used as indicators of habitat quality for spotted owls. (North et al. 1999) found that canopy height and canopy height variability was associated with spotted owl foraging activity. (Blakesley et al. 1992) found that variability of canopy height and canopy cover provides a multitude of perches and areas in the forest open enough to allow diving flights for prey capture. Spotted owls are likely to nest in areas with greater canopy cover (>=70%) or basal area of snags, medium-, and old-growth trees although the California subspecies may tolerate lower amounts of cover, ca. 50% (Hunsaker et al. 2002). The size of the dominant or co-dominant canopy-forming trees is correlated with owl foraging intensity, suggesting that "large" trees are critical elements of owl habitat (North et al 1999).

Current USDA Forest Service protocol for assessing spotted owl habitat includes field measurements of canopy cover using a moosehorn densitometer. Tree heights are sometimes collected, typically using an inclinometer- although hand-held laser rangefinders are now being used with increasing frequency. Biomass estimates are not being made but can be calculated from height measurements if the species is identified and diameter at breast height (DBH) measurements are also made in the field. These measurements are collected at the plot (< 1 ha) level are not available at the landscape scale. Canopy cover classes (0-19%, 20-39%, 40-49%, 50-69% and 70-100%) are estimated at the landscape scale using airphoto interpretation and satellite image classification (Hunsaker et al 2002). However, this is a more or less ordinal measurement and reflects the difficulty in separating tree and shrub cover.

Remote sensing methods, primarily multi-spectral (Hyppa et al. 1998) and more recently hyperspectral (Pu and Gong 2004) have been explored as cost effective means of measuring forest structural characteristics in a spatially and temporally continuous manner. However, these techniques are poorly suited for measuring vertical forest canopy structure (Weishampel et al. 2000). Radar methods, such as interferometric synthetic aperture radar (InSAR) are better at recovering structure in forests, especially those that are structurally simple or have open canopies (Treuhaft and Cloude 1999, Treuhaft and Siqueira 2000), but as is the case with multi-spectral methods, these are primarily by correlation.

In contrast, LiDAR remote sensing directly measures important vertical and spatial forest structure. Numerous studies using both small footprint (< 0.5 m radius) and large footprint, waveform digitization airborne LiDAR, have demonstrated its

ability to recover structure such as canopy height, canopy cover, canopy height profile, canopy volume, biomass and basal area at unprecedented accuracies (Nelson et al. 1984, Nelson et al. 1988, Nilsson 1996, Lefsky 1997, Lefsky et al 1999a, Lefsky et al 1999b, Lefsky et al 2001, Dubayah and Drake 2000, Drake et al 2002). However, LiDAR data sets are expensive (Table 1) and not available everywhere. It is, however, possible to leverage the high information content of LiDAR with the lower lost, more widely available multi-spectral and RaDAR data sets through data fusion (Chapter 3).

Objectives

The objective of this chapter is to assess the use field-validated, landscape scales maps of canopy height, canopy cover, and biomass to as indicators of CASPO habitat and habitat quality. These maps are twofold: footprint level (0.07 ha) structure maps of canopy height, canopy cover, and biomass derived from LiDAR observations (Hyde et al. 2005) and stand level (1 ha) maps of the height and biomass of large (> than 76 cm, following USDA Forest Service field protocols) trees derived from LiDAR, RaDAR, and passive optical sensors (Chapter 3).

The remainder of this chapter is organized as follows. First I describe my collection of field plot data, and give details of the data acquisition over the Sierra Nevada. Next I present our methods for data processing and analysis of spotted owl, LiDAR and remote sensing data, including the derivation of canopy height, canopy cover and biomass. I then give the results of statistical comparisons between remote sensing metrics and owl demographic data. Finally, I discuss the significance of my

results relative to the retrieval of forests characteristics from remote sensing, and the implications of these for mapping spotted owl habitat.

Study area and data sets

The study area is located in the Sierra Nevada mountains of California (Figure 19). This site is approximately 60,000 ha, with elevation ranging from 853 to 2,743 m. Vegetation types include white fir (*Abies concolor*), red fir (*Abies magnifica*), Sierran mixed-conifer, ponderosa pine (*Pinus ponderosa*), and montane hardwood-conifer (for a complete description, see Hunsaker et al (2002) and Chapter 2).

Figure 19. Sierra National Forest is located in the Sierra Nevada range of California. This ca. 60,600 ha area is primarily comprised of montane hard-wood conifer, ponderosa pine, Sierran mixed-conifer, white fir, and red fir. The box on the right side of the image marks the approximate location of the study area within Sierra National Forest

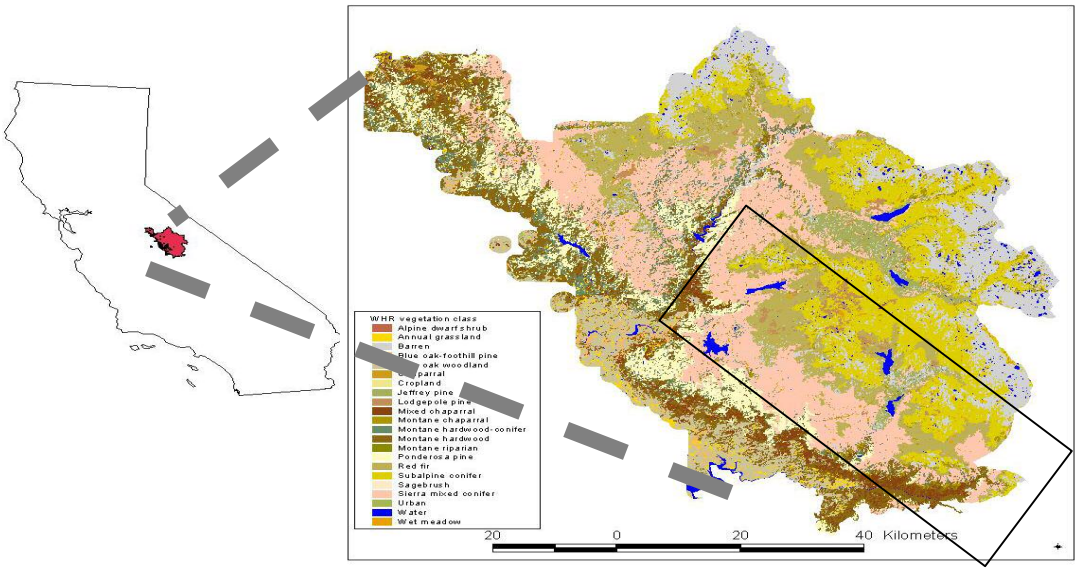

Owl data were provided by the USDA Forest Service and described in Hunsaker et al (2002). Radio collar telemetry was used to locate points within Sierra National Forest where spotted owls were found. Minimum convex polygons were applied to the telemetry data to delineate the home ranges of each nesting pair as a function of the 50, 70, and 90% probabilities of occupancy. The home range estimates were then

averaged across all nesting pairs to produce "owl analysis areas" (OAA), or the area surrounding nest sites likely used by owls (Figure 20).

Figure 20. California spotted owl nest locations in relation to the study area. All nest sites are shown here. The upper left and lower right corner coordinates for the image are given in UTM eastings and northings.

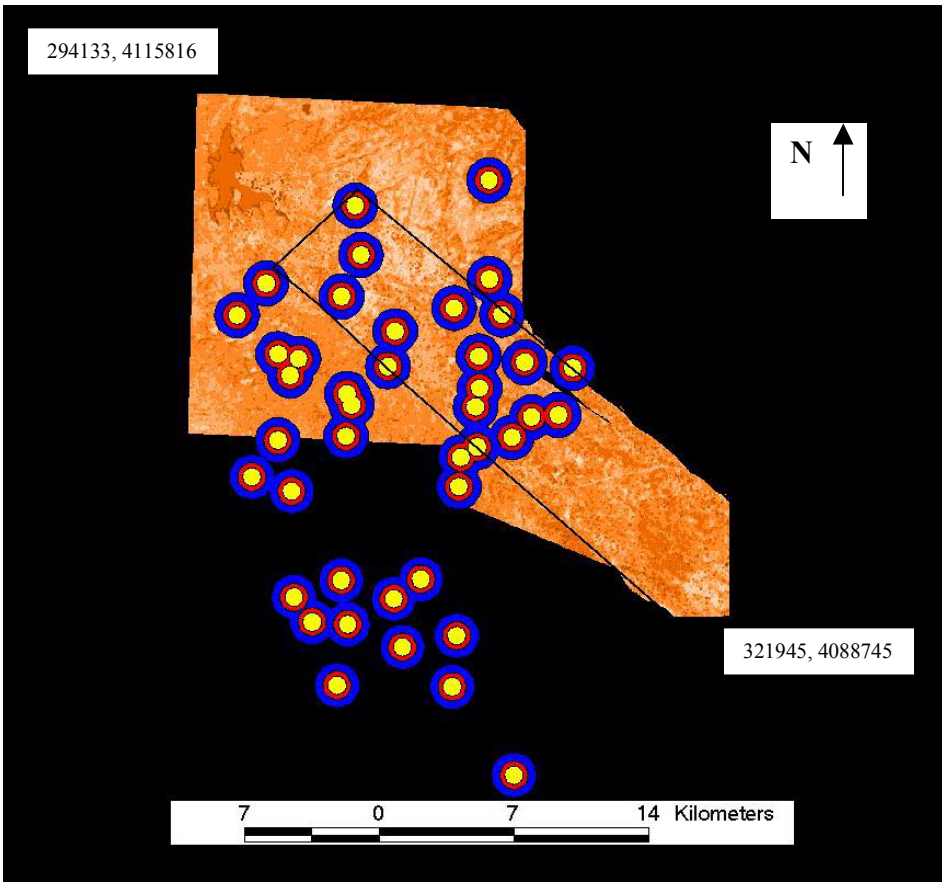

The area of each OAA is 72 ha, 168 ha, and 430 ha, representing the 50, 70, and 90% probability of occupancy, respectively. From 1991 to 1999, 43 sites were visited; the UTM coordinates of the nest or main roost was recorded as well as the number of fledglings. For each nesting pair a productivity index score was calculated by normalizing the number of fledglings per year by the average number of fledglings produced by all nests in any given year (Hunsaker et al 2002).

Remote sensing data

Maps of forest structure, i.e., canopy height, canopy cover, and biomass were created by applying models relating *in situ* observations to LiDAR footprints, creating landscape-scale maps with a resolution of 25 m (Hyde et al. 2005). Maps of large tree canopy height and biomass were created by applying models relating *in situ* observations to LiDAR, RaDAR, and passive optical sensors, creating maps with a resolution of 1 ha (Chapter 3).

Methods

Owl Data

The UTM coordinates for each nest or main roost site were averaged across all observations to account for small shifts in movement. The resulting point locations representing the centers of owl analysis areas were buffered to create polygons equivalent to 72 ha, 168 ha, and 430 ha owl analysis areas (Hunsaker et al 2002). Two sets of control sites, corresponding to the LiDAR only and fused structure maps, were selected and buffered to match the size of the 72 ha, 168 ha, and 430 ha OAAs (Figure 21). Each control site was located as closely as possible to OAA while minimizing overlap; large tracts of land cover types, such as water, barren, urban/built, and grasslands, not present in OAA were also avoided.

Figure 21. CASPO nest sites and controls within the study area. The grey areas are the actual owl sites; the multi-colored areas are the controls. The upper left and lower right corner coordinates for the image are given in UTM eastings and northings.

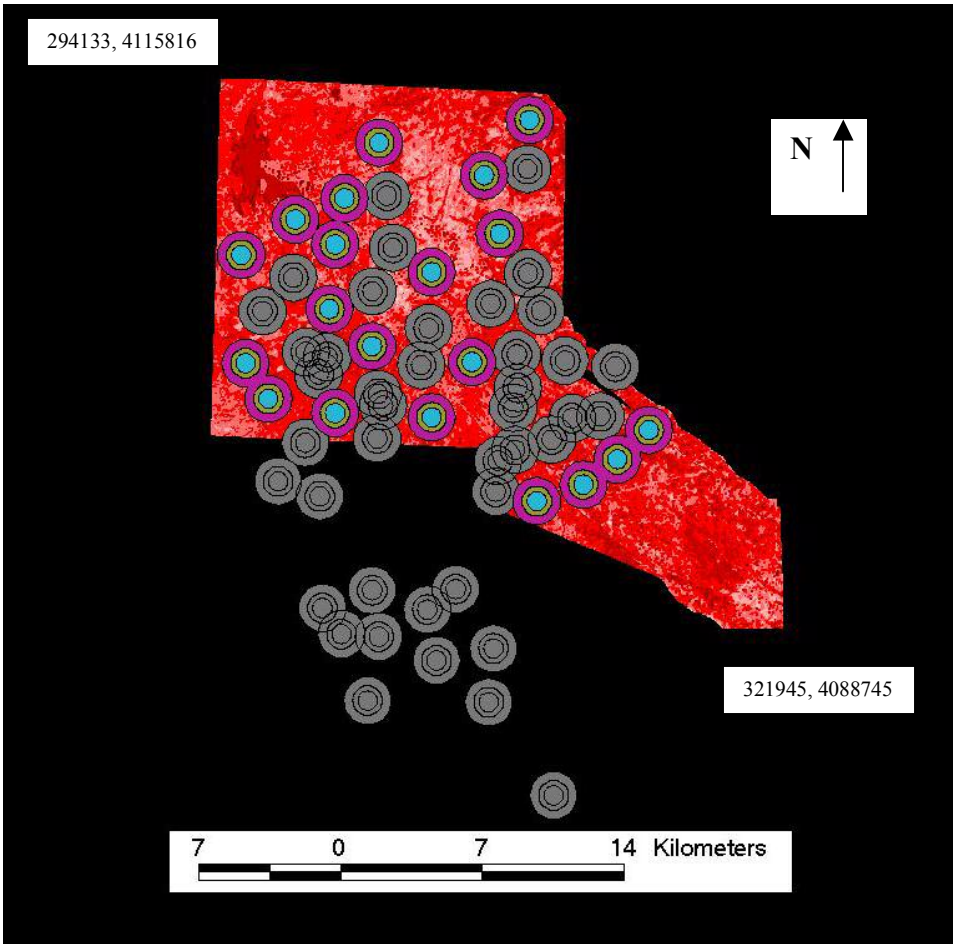

Remote sensing data

Mean and standard deviation canopy height, canopy cover, and biomass of all stems for each owl analysis area were calculated from the LIDAR-derived maps of structure at the footprint level (Hyde et al. 2005) (Table 17).

Table 17. Canopy structure metrics derived from LiDAR 25 m footprint observations

Metric	Description
Meanht72	Mean canopy height for all 72 ha OAAs (m)
Stdevht72	Standard deviation of canopy height for all 72 ha OAAs (m)
Meanht168	Mean canopy height for all 168 ha OAAs (m)
Stdevht168	Standard deviation of canopy height for all 168 ha (m)
Meanht430	Mean canopy height for all 430 ha OAAs (m)
Stdevht430	Standard deviation of canopy height for all 430 ha OAAs (m)
Meancv72	Mean canopy cover for all 72 ha OAAs (%)
Stdevcv72	Standard deviation of canopy cover for all 72 ha OAAs (%)
Meancv168	Mean canopy cover for all 168 ha OAAs (%)
Stdevcv168	Standard deviation of canopy cover for all 168 ha (%)
Meancv430	Mean canopy cover for all 430 ha OAAs (%)
Stdevcv430	Standard deviation of canopy height for all 430 ha OAAs (%)
Meanbm72	Mean biomass for all 72 ha OAAs (Mg/ha)
Stdevbm72	Standard deviation of biomass for all 72 ha OAAs (Mg/ha)
Meanbm168	Mean biomass for all 168 ha OAAs (Mg/ha)
Stdevbm168	Standard deviation of biomass for all 168 ha (Mg/ha)
Meanbm430	Mean canopy biomass for all 430 ha OAAs (Mg/ha)
Stdevbm430	Standard deviation of biomass for all 430 ha OAAs (Mg/ha)

Mean and standard deviation canopy height and biomass of large trees was calculated for each owl analysis area using structure maps derived from data fusion (Chapter 3) (Table 18).

Table 18. Canopy structure metrics derived from LiDAR, RadAR and passive optical sensors (1 ha resolution)

Metric	Description
Meanht72f	Mean canopy height for all 72 ha OAAs (m)
Stdevht72f	Standard deviation of canopy height for all 72 ha OAAs (m)
Meanht168f	Mean canopy height for all 168 ha OAAs (m)
Stdevht168f	Standard deviation of canopy height for all 168 ha (m)
Meanht430f	Mean canopy height for all 430 ha OAAs (m)
Stdevht430f	Standard deviation of canopy height for all 430 ha OAAs (m)
Stdevcv430	Standard deviation of canopy height for all 430 ha OAAs (%)
Meanbm72f	Mean biomass for all 72 ha OAAs (Mg/ha)
Stdevbm72f	Standard deviation of biomass for all 72 ha OAAs (Mg/ha)
Meanbm168f	Mean biomass for all 168 ha OAAs (Mg/ha)
Stdevbm168f	Standard deviation of biomass for all 168 ha (Mg/ha)
Meanbm430f	Mean canopy biomass for all 430 ha OAAs (Mg/ha)
Stdevbm430f	Standard deviation of biomass for all 430 ha OAAs (Mg/ha)

Statistical methods

Analysis of variance (ANOVA) was used to test for significant differences between canopy structure metrics in OAAs and the controls sites. Canopy height, canopy cover, and biomass were examined at the footprint (25 m resolution) level; canopy height and biomass were examined at the stand (1 ha resolution) level. Linear

regression and stepwise multiple linear regression was used to relate structure metrics and indices of owl nest productivity.

Results

There is a significant difference between the mean canopy height of 72 ha OAA and controls ($p = 0.004$, $df = 1, 18$); the difference is less significant for 168 ha OAA and controls ($p = 0.014$, $df = 1, 18$) and not significant for 430 ha OAA and controls (Figure 22).

Figure 22. Mean canopy height in owl analysis and control areas, derived from LIDAR at the footprint level.

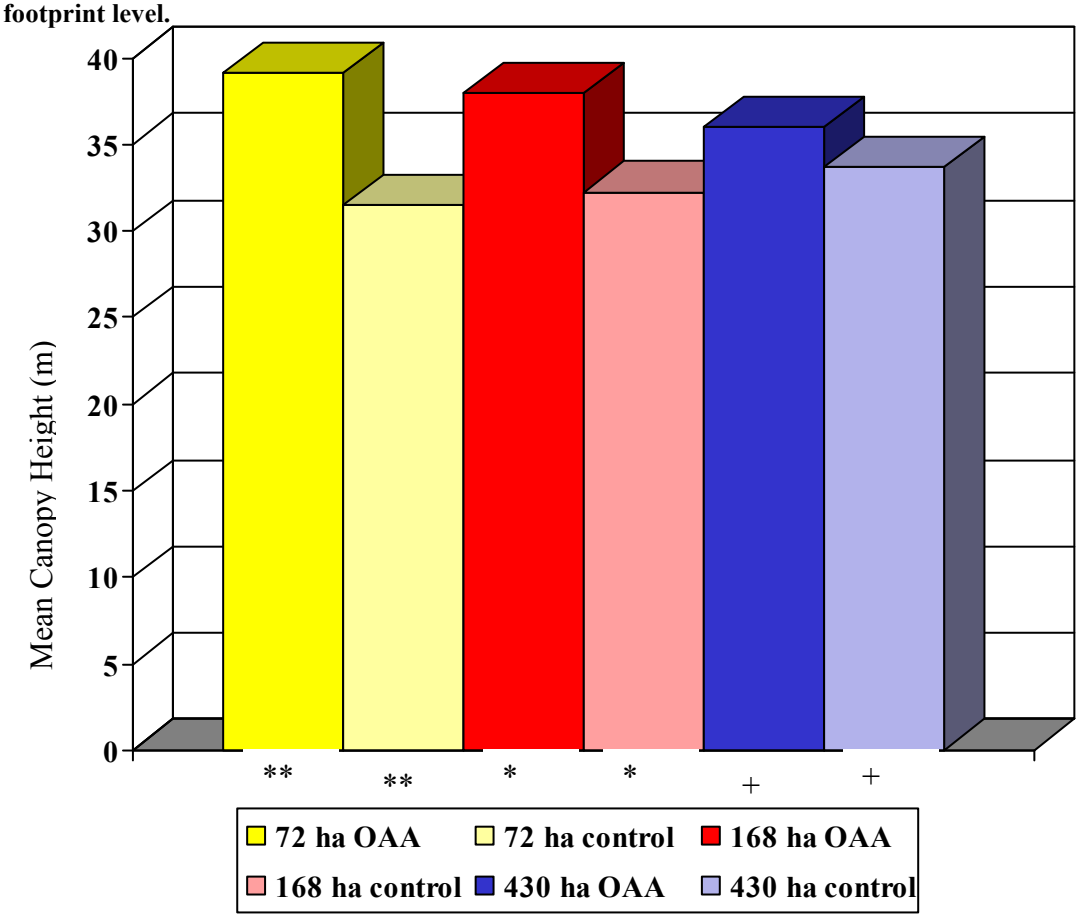

* significant at the 0.05 level
** significant at the 0.01 level
*** significant at the 0.001 level
\+ not significant

There are no significant differences between the standard deviation of canopy height between 72, 168, and 430 ha OAA and controls (Figure 23).

Figure 23. Standard deviation canopy height in owl analysis and control areas, derived from LIDAR at the footprint level.

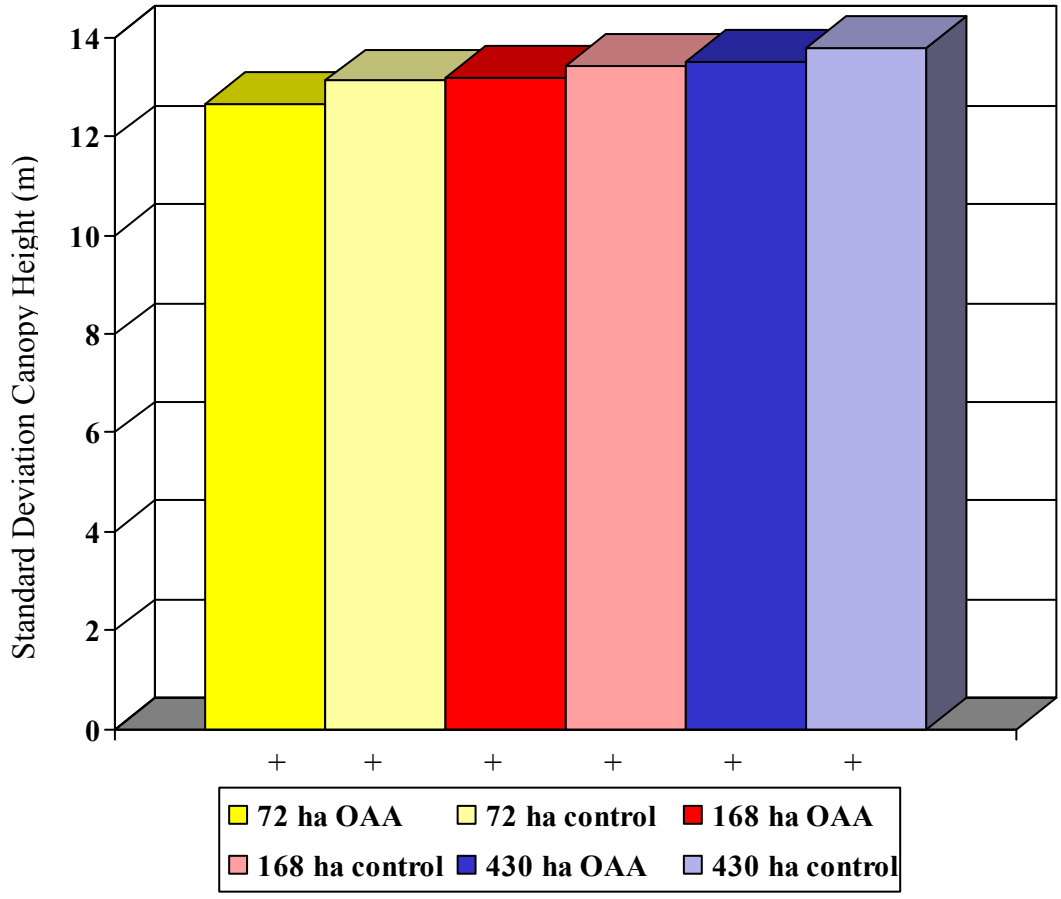

*	significant at the 0.05 level
**	significant at the 0.01 level
***	significant at the 0.001 level
+	not significant

There are significant differences between the mean canopy cover of 72 ha OAA and controls ($p = 0.013$, $df = 1, 18$) and between 168 ha OAA and controls ($p = 0.048$, $df = 1, 18$); the difference between 430 ha OAA and controls is not significant (Figure 24).

Figure 24. Mean canopy cover in owl and control areas, derived from LIDAR at the footprint level

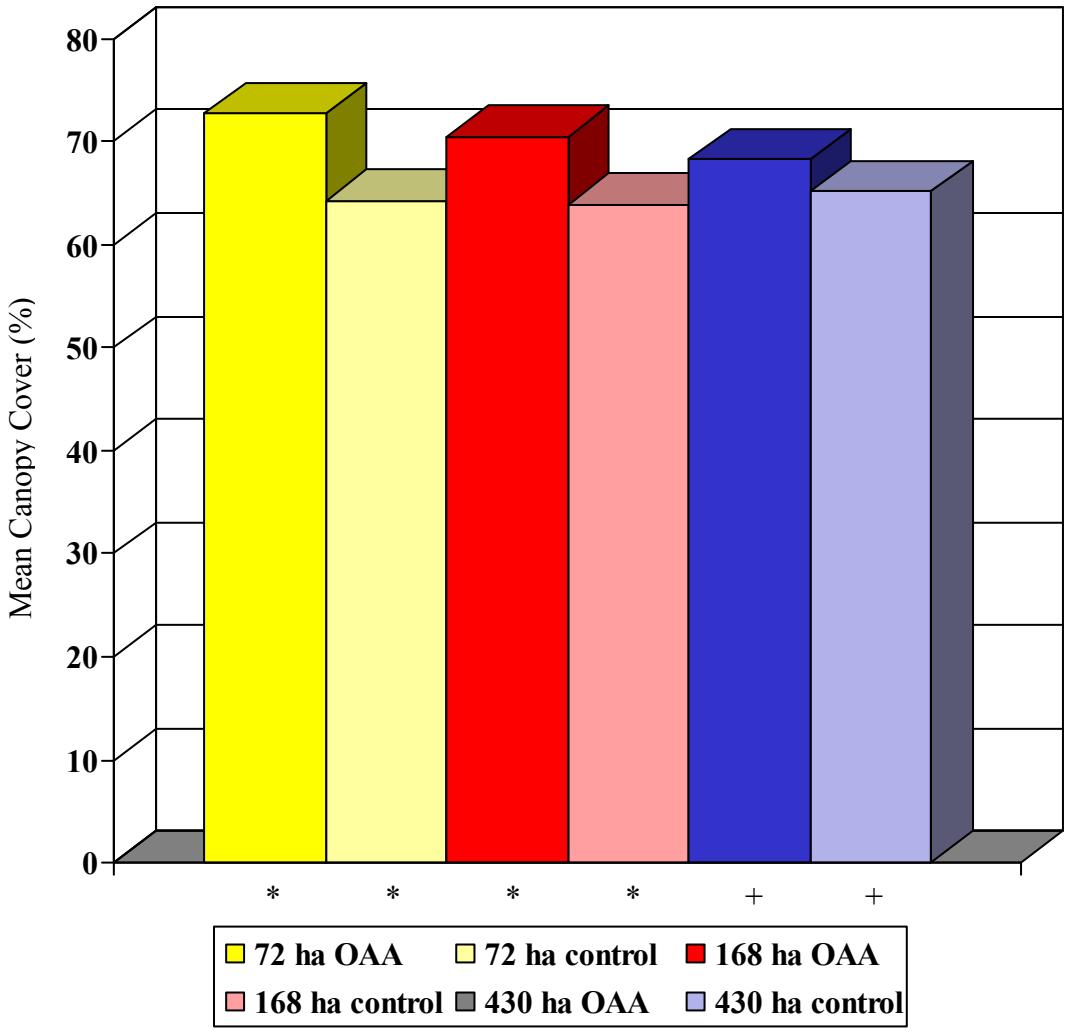

* significant at the 0.05 level
** significant at the 0.01 level
*** significant at the 0.001 level
\+ not significant

There are significant difference between the standard deviation canopy cover of 72 ha OAA and controls ($p = 0.080$, $df = 1, 18$) and between 168 ha OAA and controls ($p =$

0.090, df = 1, 18); the difference between 430 ha OAA and controls is not significant (Figure 25).

Figure 25. Standard deviation canopy cover in owl and control areas, derived from LIDAR at the footprint level

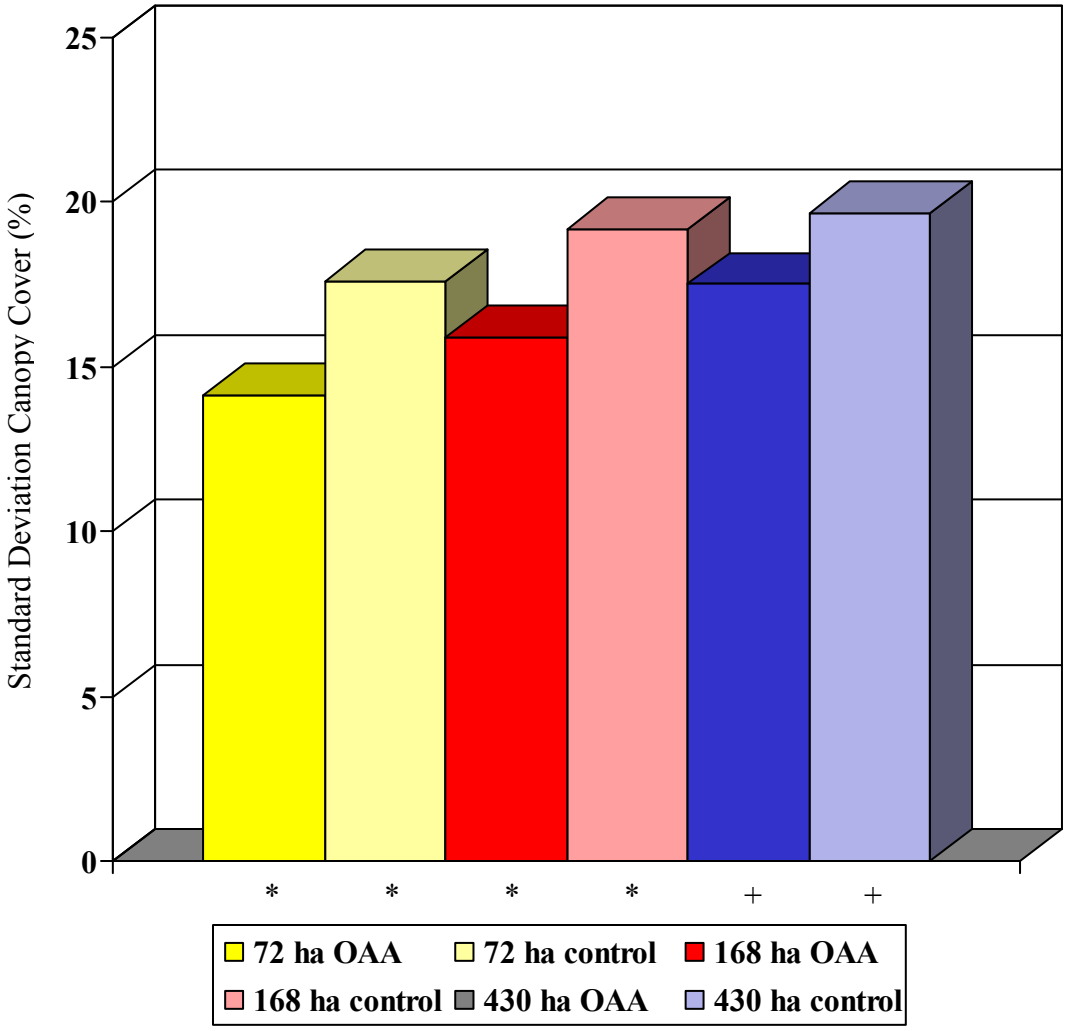

* significant at the 0.05 level
** significant at the 0.01 level
*** significant at the 0.001 level
\+ not significant

There is a significant difference between the mean biomass of 72 ha OAA and controls ($p < 0.001$, df = 1, 18); the difference is less significant between 168 ha OAA

and controls (p = 0.007, df = 1, 18) and not significant between 430 ha OAA and controls (Figure 26).

Figure 26. Mean biomass in owl analysis and control areas, derived from LIDAR at the footprint level

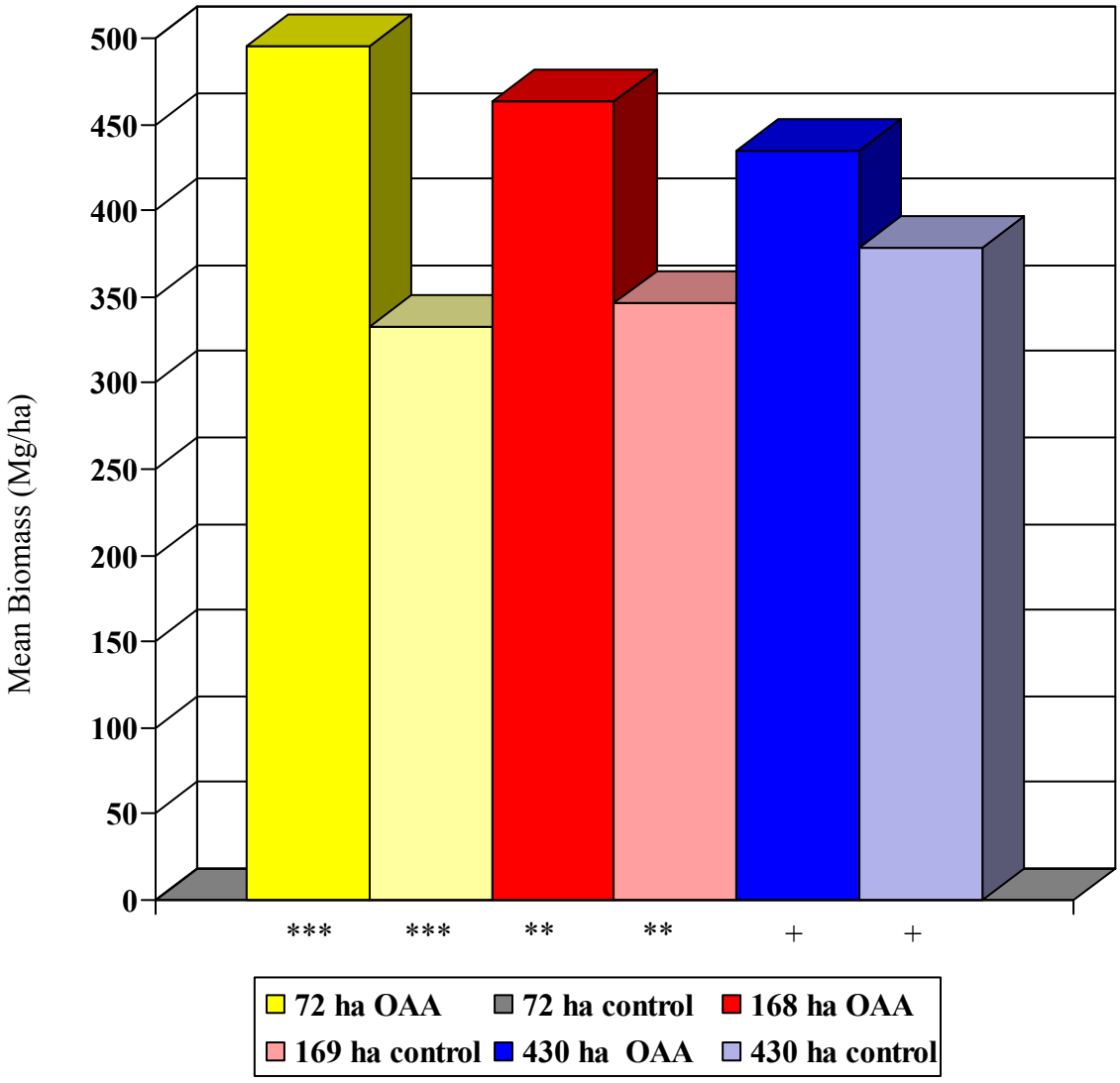

* significant at the 0.05 level
** significant at the 0.01 level
*** significant at the 0.001 level
\+ not significant

There are significant differences between the standard deviation of biomass of 72 ha OAA and controls ($p < 0.001$, $df = 1, 18$) and between 168 ha OAA and controls ($p = 0.007$, $df = 1, 18$); the difference between 430 ha OAA and controls are not significant (Figure 27).

Figure 27. Standard deviation biomass in owl analysis and control areas, derived from LIDAR at the footprint level

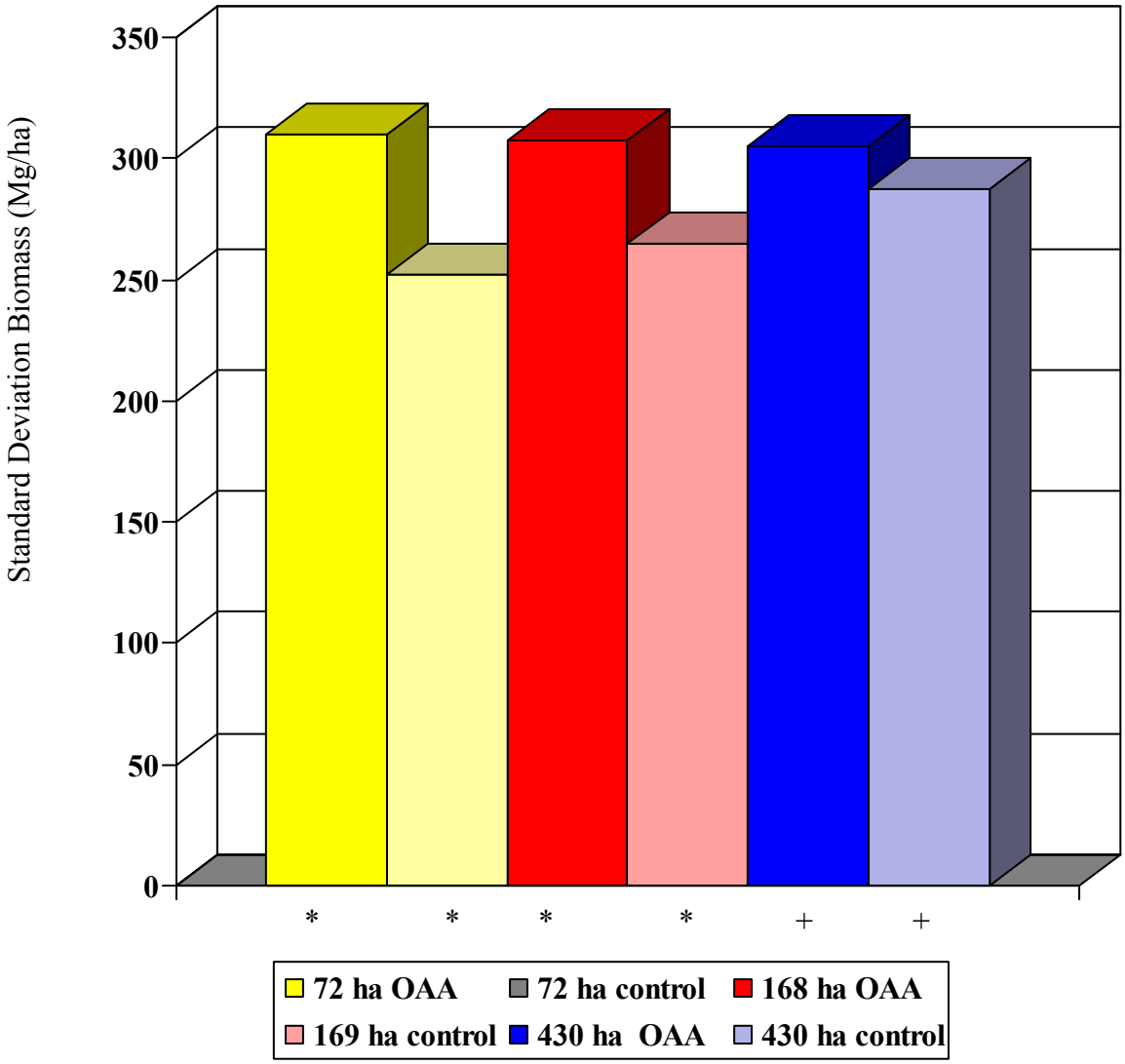

* significant at the 0.05 level
** significant at the 0.01 level
*** significant at the 0.001 level
\+ not significant

There are significant differences between mean canopy height of large trees between 72 ha OAA and controls ($p < 0.001$, $df = 1, 44$); the difference between 168 ha OAA and controls ($p = 0.003$, $df = 1, 44$) and between 430 ha OAA and controls ($p = 0.032$, $df = 1, 44$) are less significant (Figure 28).

Figure 28. Mean large tree height in owl analysis and control areas, derived from remote sensing at the stand level.

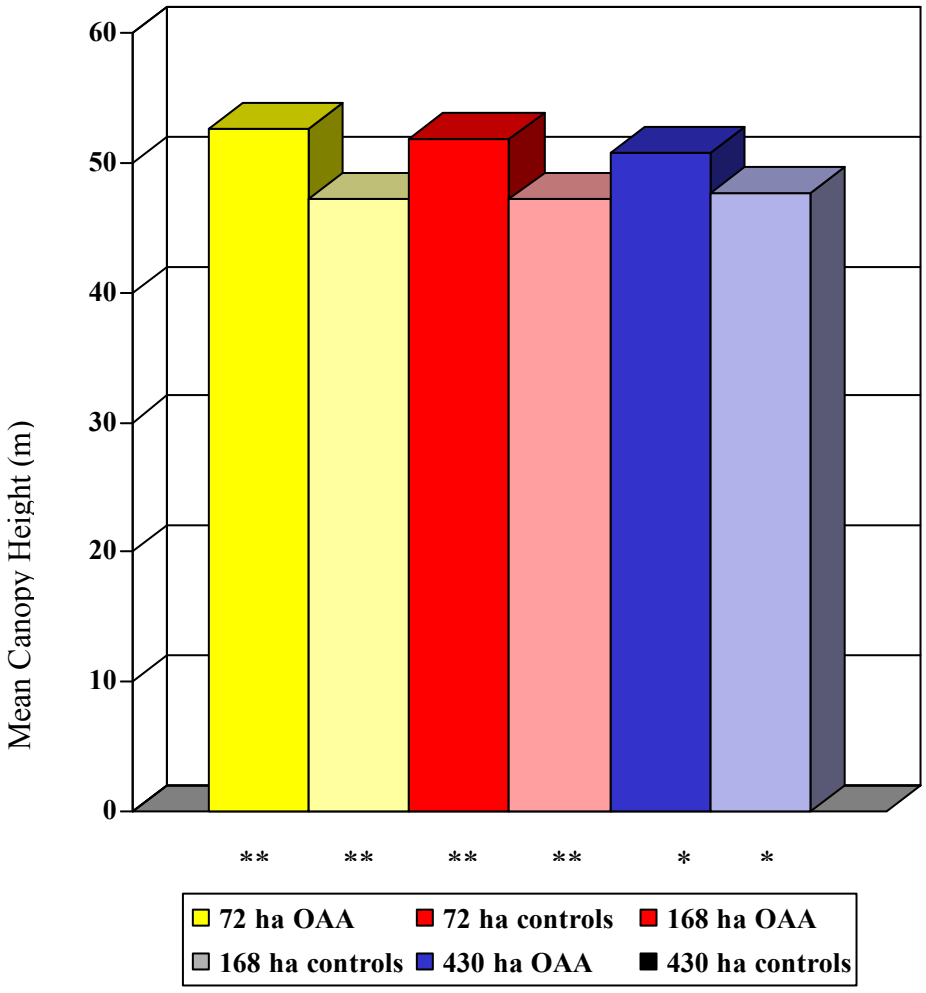

* significant at the 0.05 level
** significant at the 0.01 level
*** significant at the 0.001 level
\+ not significant

There are no significant differences between the standard deviation of canopy height between 72, 168, and 430 ha OAA and controls (Figure 29)

Figure 29. Standard deviation large tree height in owl analysis and control areas, derived from remote sensing at the stand level.

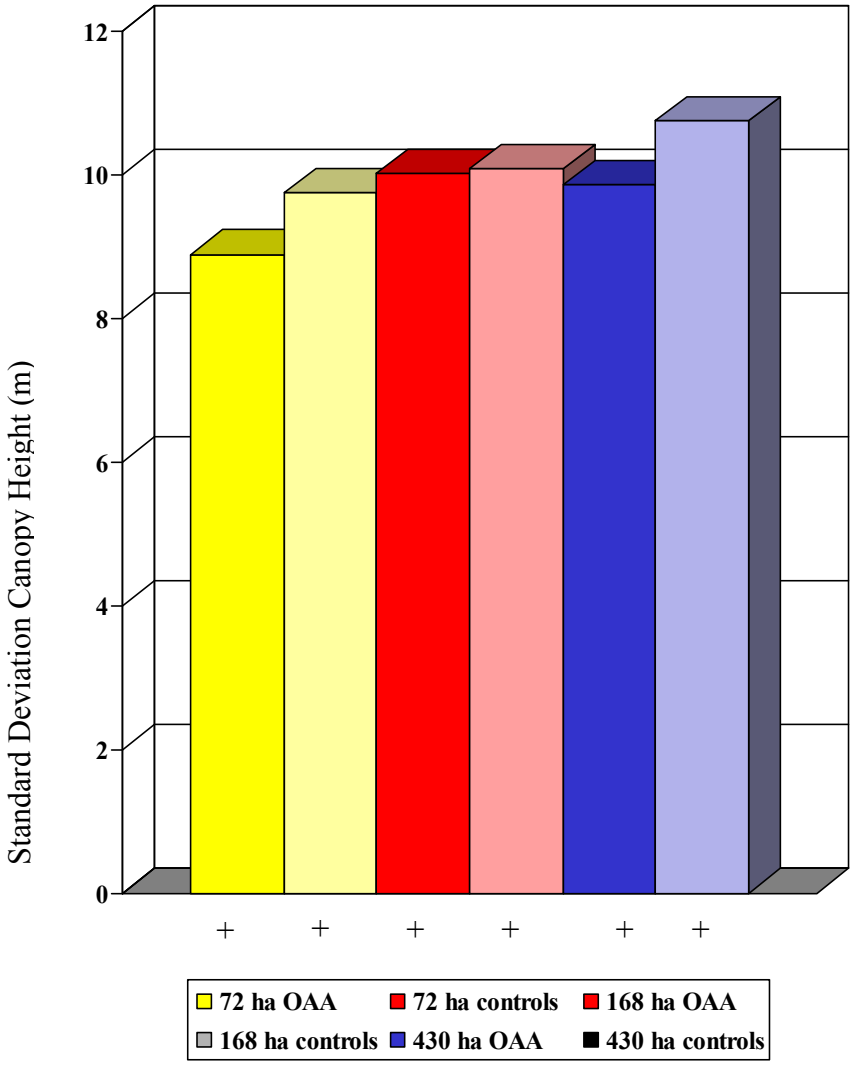

* significant at the 0.05 level
** significant at the 0.01 level
*** significant at the 0.001 level
\+ not significant

There are significant differences between mean large tree biomass between 72 ha OAA and controls ($p < 0.002$, $df = 1, 44$), 168 ha OAA and controls ($p < 0.004$, $df = 1, 44$) and 430 ha OAA and controls ($p < 0.037$, $df = 1, 44$) (Figure 30).

Figure 30. Mean large tree biomass in owl analysis areas, derived from remote sensing at the stand level

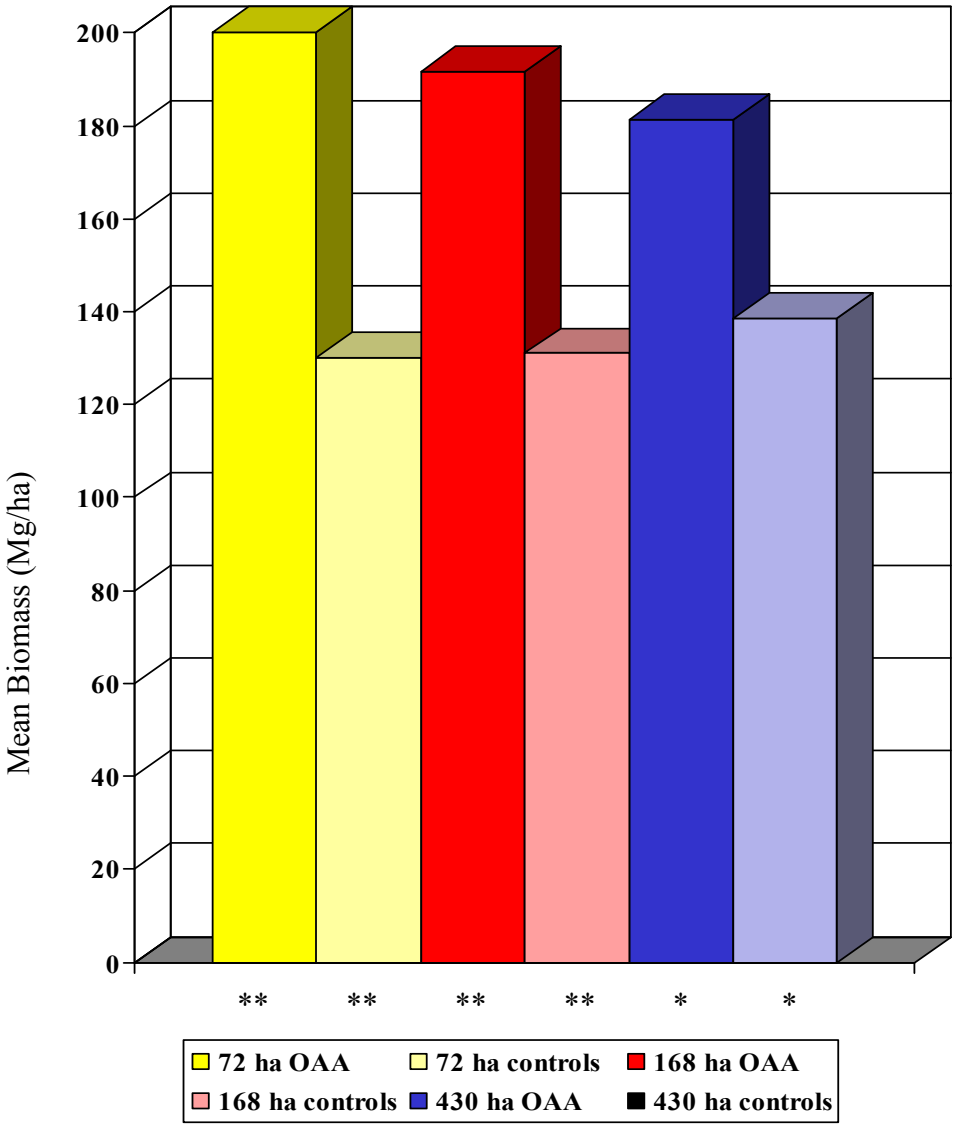

* significant at the 0.05 level
** significant at the 0.01 level
*** significant at the 0.001 level
\+ not significant

There are significant differences between the standard deviation of large tree biomass between 72 ha OAA and controls ($p < 0.027$, $df = 1, 44$), 168 ha OAA and controls ($p < 0.025$, $df = 1, 44$) and 430 ha OAA and controls ($p < 0.031$, $df = 1, 44$) (Figure 31).

Figure 31. Standard deviation large tree biomass in owl analysis areas, derived from remote sensing at the stand level

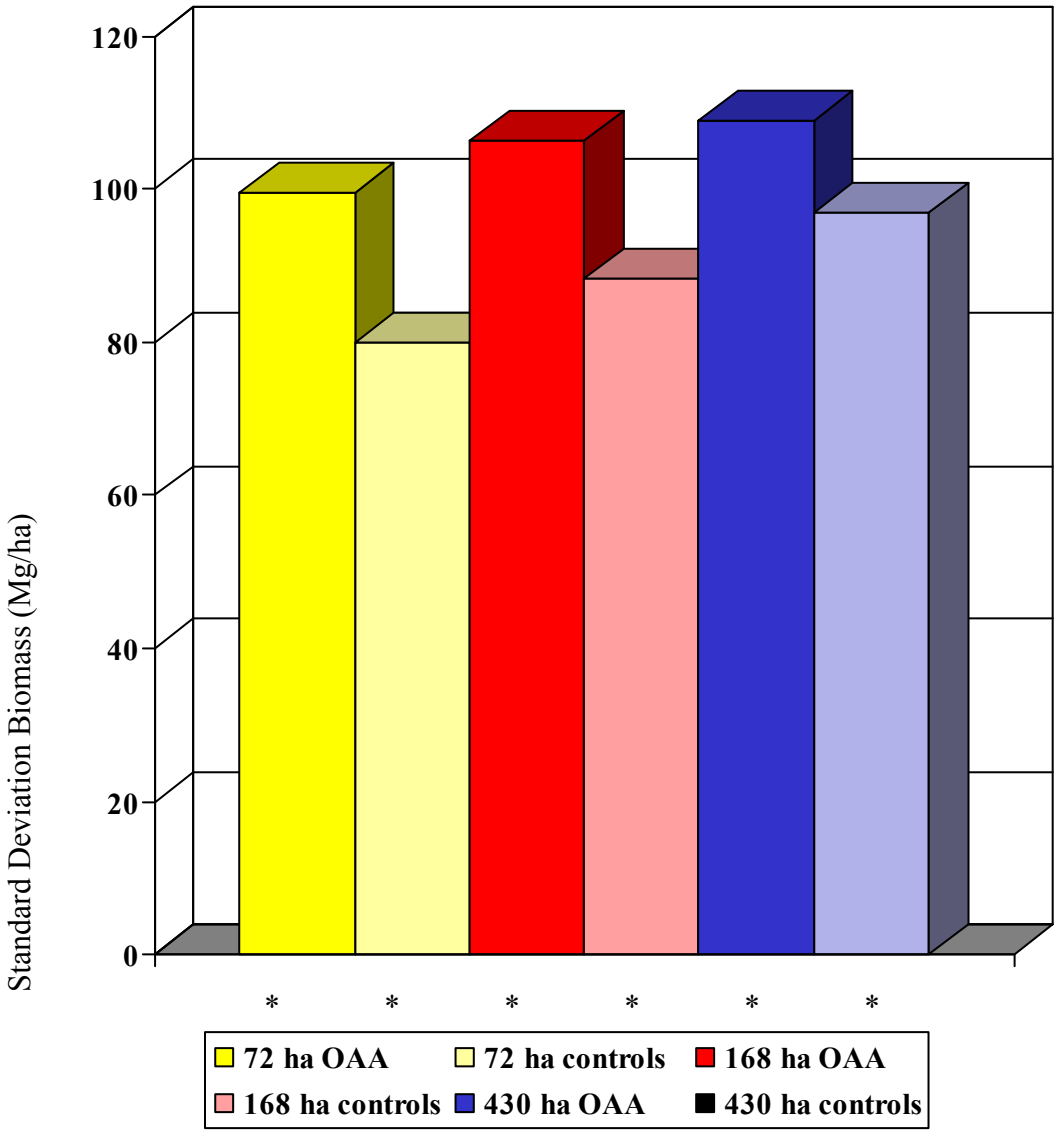

* significant at the 0.05 level
** significant at the 0.01 level
*** significant at the 0.001 level
\+ not significant

At the footprint level (Table 18, Figure 32) , nest productivity was correlated with mean canopy height of 430 OAA (r^2 = 0.315, n = 14, SE = 0.04), mean canopy cover of 72 ha OAA (r^2 = 0.289, n = 14, SE = 0.04), stand deviation of canopy cover of 168 ha OAA (r^2 = 0.245, n = 14, SE = 0.04), and mean canopy cover of 430 ha OAA (r^2 = 0.254, n = 14, SE = 0.04). At the stand level (Table 18), nest productivity was correlated with standard deviation of canopy height of 430 ha OAA (r^2 = 0.121, n = 27, SE = 0.078) and mean biomass of 430 ha OAA (r^2 = 0.483, n = 27, SE = 0.06). Stepwise multiple linear regression of all possible combinations did not produce significant results at either the footprint or the stand level of analysis.

Table 19. Regression results and models from analysis of footprint and stand level metrics and an owl reproductive index.

Metric	Coefficient of determination (r^2)	P	n	Standard error	Model
meanht430	0.315	0.037	14	0.040	0.290 + (0.005 * meanht430)
meancv72	0.289	0.048	14	0.040	0.174 + (0.004 * meancv72)
stdevcov168	0.245	0.072	14	0.040	0.572 + (-0.006 * stdevcov168)
meancv430	0.254	0.066	14	0.043	0.264 + (0.003 * meancv430)
stdevht430f	0.121	0.081	27	0.078	0.317 + (0.012 * stdevht430f)
meanbm430f	0.483	8.072e-05	27	0.060	0.305 + (0.001 * meanbm430f)

Figure 32. Results of step-wise multiple linear regression models between remote sensing metrics and a spotted owl reproductive index. The best single variable model (large tree biomass from 430 ha OAA) is shown here.

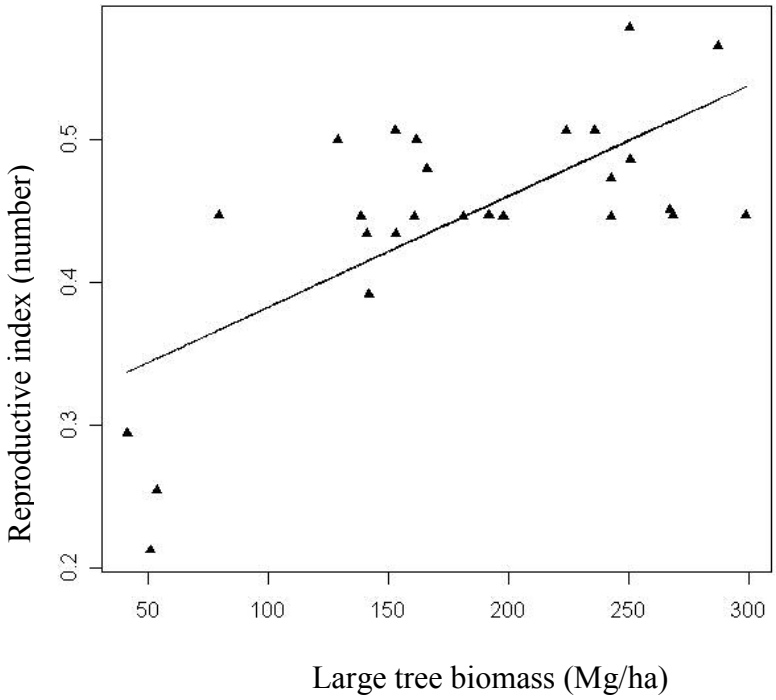

Discussion

As expected, I found statistically significant differences in structure between areas inhabited by owls and areas not currently occupied. I am not suggesting that spotted owls perceive structure the same way, or at the same scale, as does LiDAR or any other sensor; however, there is some correlation between the two. Individual owls undoubtedly search for a suite of characteristics that include something that humans perceive and have labeled "owl-growth"-- and remote sensing can quantify characteristics that correlate with these conditions. I do not suggest that LIDAR or any other sensor can perceive spotted owl prey items, nest or roost sites. Rather,

remote sensing can record the "signature" of a particular structural type that correlates with conditions that owls can perceive.

In many cases, the statistical significance between metrics was strongest when comparing 72 ha OAA with controls, and the significance declined or disappeared entirely as the area around the nest site increased. This suggests that there is a core activity area around owl nest sites where old-growth conditions are more important and that this area is ringed by another where structure is intermediate between the core and the surrounding matrix of non-habitat. This is not surprising in that it is unlikely that one would find abrupt discontinuities in nature outside of heavily disturbed areas This argues for maintaining buffer zones around known owl locations, separating them from other land use practices, such as recreation and timber harvest.

I also found weak to moderate correlations between structure metrics and owl nest productivity. This suggests that canopy structure plays a role in habitat quality beyond simple presence or absence. This is important because no organism occupies the entire range of conditions in which it can tolerate; niches are seldom, if ever, saturated in that sense for a variety of reasons not related directly to structure. I am not claiming that areas outside of OAAs are unsuitable for owls or that unoccupied areas are so because of structure only. However, spotted owls obviously do not occupy the landscape at random and some structural signature perceptible by remote sensing indicates a higher probability of occupancy than do other signatures. Two caveats are in order: First, the relationship between large tree biomass and owl productivity could be curvilinear. A logarithmic function fit to the data produced a

higher coefficient of variation ($r^2 = 0.630$) than did a linear model. Second, there are three outlying points where both nest productivity and biomass are low; if these points are removed, the relationship weakens considerably ($r^2 = 0.116$). Further analysis should reveal whether these sites are unusual structurally or if there is a problem with the data. It is possible that these sites are low quality and are occupied by juveniles attempting to establish new territories.

I was somewhat surprised by the weak results regarding canopy cover given the results of previous efforts; Hunsaker (et al 2002) found a correlation ($r = 0.37$) and between canopy cover and owl productivity. It is interesting that biomass, particularly biomass of large trees, was so significant (although see the caveats above). I believe that this is could be because of how LiDAR "sees" biomass, i.e., as a composite of canopy height and canopy cover. I would expect, then, that there are other metrics relating to the vertical dimension that would be as or more useful than biomass, which is a coarse surrogate for structural complexity.

Conclusion

There are many other metrics that LIDAR and other remote sensing data sets could provide. We selected only those that were reasonably easy to calculate and compare with existing field data. Additional information regarding the vertical structure of habitat exist in LIDAR waveforms, while measurements like canopy cover and HOME are just simple correlates to a much richer, more complex signature. Some index of heterogeneity could be developed; for example, standard deviation or variance (or even semivariance) in waveform energy. Additionally, other sensors

besides the ones used here can provide structural information, including hyperspectral or multi-angle passive optical sensors and longer wavelength RaDARs.

We were not able to use the full owl data set because we lacked the spatial coverage with LiDAR to do so. In fact, additional flight days were planned that would have accomplished this, but mechanical problems with the aircraft carrying LVIS prevented us from doing so. It would be advantageous for future studies to have adequate resources to map broader areas with large footprint LiDAR; at the present time, only one such instrument exists and it is supported as an experimental, not an operational, system. Management of forests of the size of National Forests requires a far richer data set than we were able to provide in this pilot project. Small footprint LiDAR is another alternative method, although I suspect that there are elements of vertical complexity that only a full waveform-digitizing system can capture. It would be useful to compare structure metrics derived from small footprint systems with our results to confirm or deny our suspicions. This also limited our ability to use randomly selected locations for control plots; there simply is not enough coverage to generate non-overlapping random control plots.

I only had large tree data at the 1 ha level as the field protocol was selected to match previous U.S. Forest Service surveys; large trees are reasonably sparse at this scale. Recall that I had highly detailed information about very small stems (10+cm dbh) at the footprint level in order to perform a calibration/validation experiment. If I was able to conduct a similar wildlife habitat analysis project in the future, I would design the field protocol differently; we would likely increase the minimum dbh

threshold and map a smaller area, perhaps measuring stems > 30 cm dbh and reducing the plot size to 0.5 ha.

I was only able to examine the demography data for a single, albeit highly important, species. There are many other species of interest, including Northern goshawks and fishers, within Sierra National Forest that almost certainly are found only or preferentially in areas with a structural signature discernable by LiDAR and other sensors. It would also be interesting to look at indices of overall diversity and examine their relationships with forest structure. I also recognize that the structure maps that we created are not limited to wildlife habitat analysis; forest structure is an important component of fuel loads and fire propagation modeling, as well as carbon sequestration and hydrologic modeling. LVIS also captured the elevation of the ground under the canopy, which is notoriously difficult to acquire.

Using our results, I created maps of *potential* spotted owl habitat using the LiDAR structure maps and fused remote sensing maps; these areas include the structural signatures of locations of OAA as defined in our results. The map created from LiDAR only (Figure 33) represents all pixels that where the structural metric is above the mean value: height > 22.7 m, cover > 42.8%, biomass > 275 mg/ha. The map derived from LIDAR and the other remote sensing data sets (Figure 34) was created with the following criteria: height > 49 m, biomass > 172 mg/ha. Not surprisingly, the map derived from big tree data at the landscape scale (from all remote sensing data sets) tracks the structure maps created from just LIDAR. In both potential habitat maps, an area known to be old-growth (the Teakettle Experimental Area) is clearly identified. The thresholds I chose are arbitrary and do not reflect a

known critical threshold below which owls cannot survive; they are merely intended to demonstrate their utility, i.e., that maps of this sort could be highly useful to the U.S. Forest Service for management and planning of the Sierra National Forest.

Figure 33. Potential habitat for CASPO, based on canopy height, cover, and biomass criteria (height > 22.7 m, cover > 42.8%, biomass > 275 mg/ha). The numbers in the legend correspond to the number of criteria met, 0-3. This map is based on footprint level LIDAR data only. The upper left and lower right corner coordinates for the image are given in UTM eastings and northings.

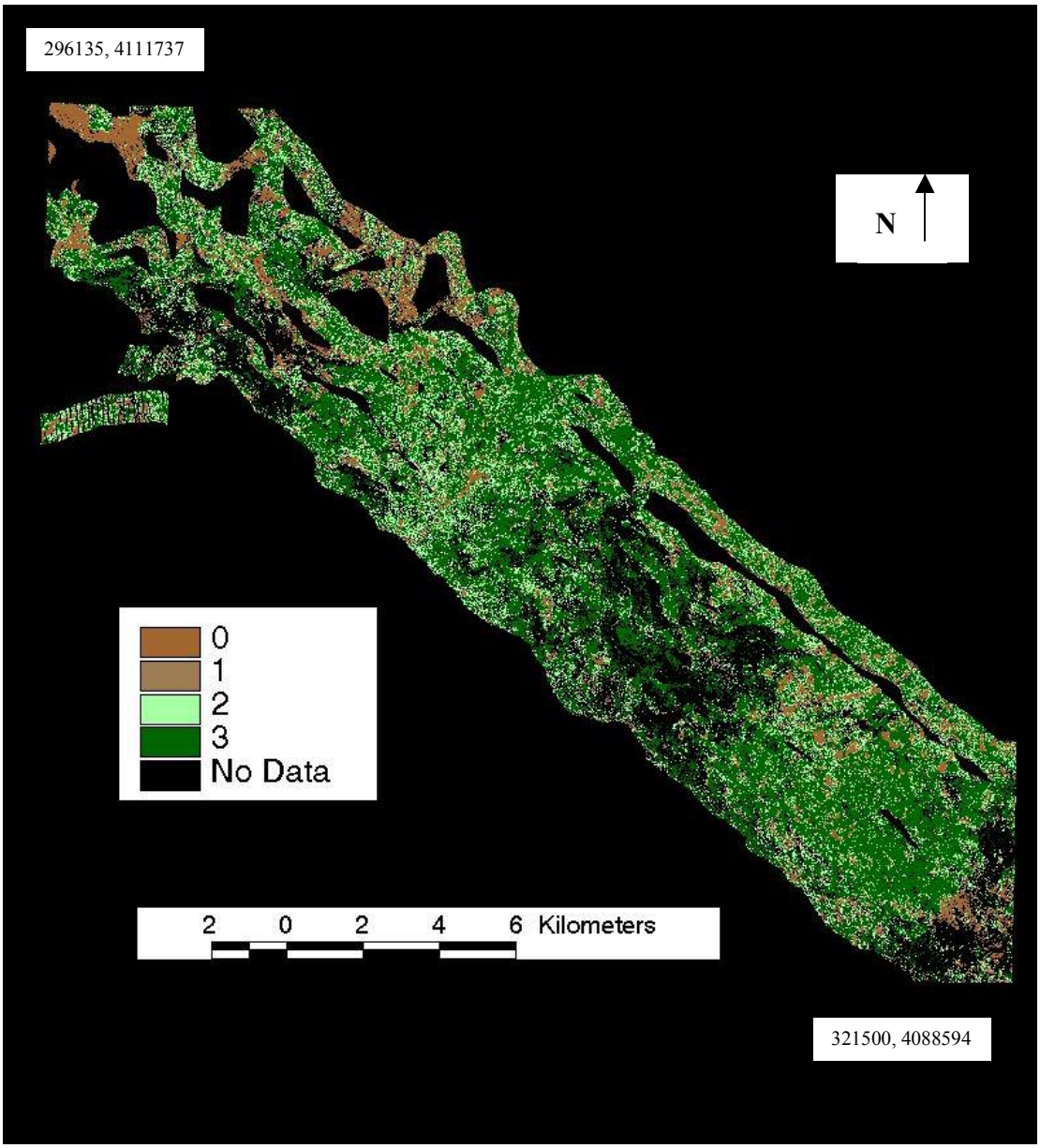

Figure 34. Potential habitat for spotted owls, based on big tree canopy height and biomass criteria (height > 49 m, biomass > 172 mg/ha). The numbers in the legend correspond to the number of criteria met, 0-2. This map is based on fusion of LIDAR and other remote sensing data. The upper left and lower right corner coordinates for the image are given in UTM eastings and northings.

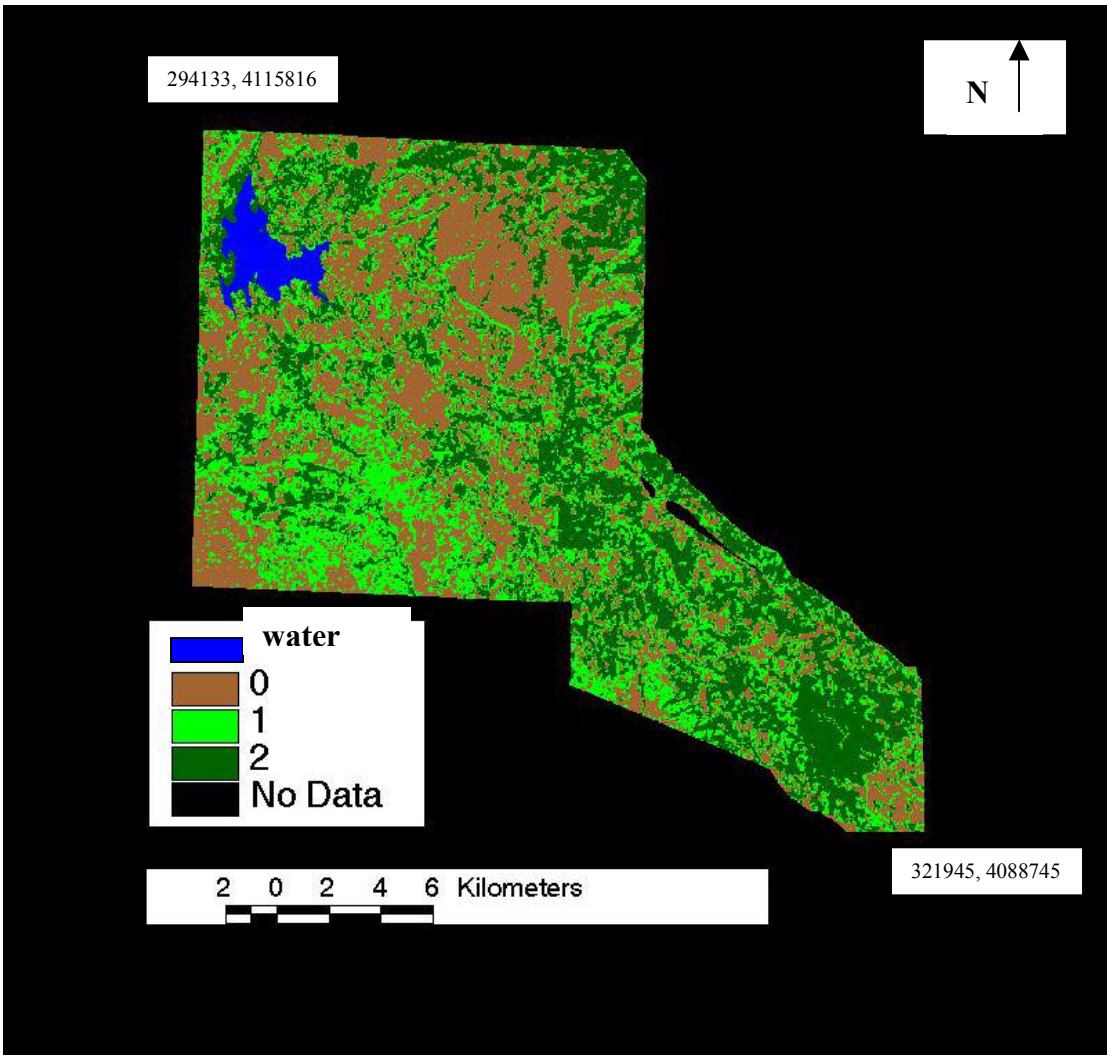

Chapter 5: Discussion and Conclusion

Discussion

I demonstrated that LIDAR can recover measurements of forest structure with high degree of accuracy relative to field measurements. Previously, it was assumed by many in the LIDAR community that LIDAR would not perform adequately in steep, mountainous terrain because of slope effects. The reason for this is that heights are determined relative to the mean ground elevation within a footprint, so that a stem which is upslope of the footprint center will appear taller and one which is down slope will appear shorter than the actual height. Also, low-lying vegetation could be convolved with the ground return, making ground determination inaccurate.

While slope undoubtedly does have an effect, it is masked by more important considerations. The largest factor determining canopy height retrieval is the spatial arrangement of canopy materials. Height retrieval accuracy is highest when the tallest stem is at the center of a LIDAR footprint. There is an energy drop-off at the outer edge of LIDAR footprints. While this phenomenon was known, the magnitude had never been quantified with field observations. One reason for this is that (to my knowledge) no other calibration/validation study had carefully geolocated individual stems to test this effect. This result applies to habitat mapping in that the effective pixel or grid size for LiDAR-derived maps are much smaller than previously anticipated. This is easy to correct in terms of map creation, but the resulting grids will have more coverage gaps.

Canopy cover was also retrieved with the same level of accuracy as previous studies. I found that some of the assumptions used by previous researchers did not

apply in my study area; canopy cover did not require a correction for light extinction and the reflectivity difference between ground and vegetation was smaller than previously reported; both of these assumptions were violated and if these factors were applied to the data collected in the Sierras, my results would have been significantly worse. This is not especially surprising given that most of the original calibration/validation work was done in deciduous forest, which have quite a different gap structure than the conifers of the Sierras, as well as different lifeforms (broadleaves vs. conifers). However, Lefsky (1999a) did extend his assumptions (canopy reflectance ratios and light extinction effects) to conifers in the Pacific Northwest (with good results) and his assumptions were widely accepted.

At the stand level, I found that the amount of the plot that was mapped was the largest determinant of accuracy. This suggested that using other sensors could fill in some of the gaps in LIDAR coverage. In the earliest SLICER and LVIS missions, the sensor acquired swaths (ca. 1 km wide). However, there were gaps within the tracks due to pilot error, as well as pitch and roll of the aircraft. So, LIDAR was not exactly mapping the landscape; rather, it was sampling with a high degree of frequency in some areas, while completely missing others. This led me to investigate the use of other data sets to fill in these gaps.

I did find that some additional predictive power vis-à-vis big tree biomass, (and to a lesser extent, big tree canopy height) can be achieved by using information from multiple remote sensing data sets. However, the cost of acquiring and processing the additional data sets is considerable. Recall that the field data was limited, therefore I was only able to validate sparse LIDAR and other remote sensing

data using stand (1 ha) level data. It is possible that other remote sensing data sets can more accurately map canopy height and biomass of all stems rather than just big trees. Because of incongruities of scale and geolocation, I could not compare the footprint level stem maps to Landsat data, for example. This would require inventorying all stems at the 1 ha level, which was not practical given logistical constraints.

I have shown that maps of forest structure derived from LIDAR and remote sensing can be used to map (California spotted owl) CASPO habitat. Ecological theory (and particularly the subdiscipline of landscape ecology) suggests that a strong relationship exists between environmental structure and biological processes. While there is nothing about CASPO that suggests that it perceives structure in the same way as a do LIDAR footprints or satellite pixels, there is undoubtedly some correlation between the two. Individual owls undoubtedly search for a suite of characteristics that correspond roughly to what humans perceive and have labeled "owl-growth"-- and remote sensing can quantify characteristics that correlate with these conditions. I do not suggest that LIDAR or any other sensor can perceive CASPO prey items or roost sites. Rather, remote sensing can record a "signature" of a forest type that correlates with conditions that owls can perceive.

This signature was used to create maps of *potential* CASPO habitat. At any given time, these may be unoccupied. Instead of targeting these areas for preservation, it might be useful to flip the argument around. What is about the environment that makes it unsuitable habitat for CASPO? It is likely that these areas include sites that were logged. They also include rock outcrops, wet meadows, and

other naturally-occurring gaps in the forest. These areas could be targeted for more intensive development, since one could argue that if they were not used by CASPO over the last 10 years or so, they are not likely to be used if enough suitable habitat is available. If it is determined that CASPO populations have insufficient numbers, these areas could be targeted for reforestation efforts. Future LIDAR missions (or the results of this effort) can be used to monitor the CASPO habitat.

Conclusion

LIDAR is a highly effective tool than can used to map forest structure, from which a signature can be extracted that indicates potential CASPO habitat. While other remote sensing data sets can provide some additional structure information, multi-sensor fusion has some benefit in mapping habitat; a larger portion of the landscape can be mapped, but at a high cost of production (Table 2). An alternative would be to simply acquire more LiDAR data; this could include a blend of large and small footprint systems given the limited availability of the former.

It should be noted that configuration of LVIS for this mission was intended to provide a testbed for a satellite LIDAR system (VCL). Current and future LVIS missions will be flown with a smaller footprint size and less gaps in coverage. LVIS is becoming more of an imaging system rather than effectively a high intensity sampling instrument, as it had been in the past. Therefore, some of the calibration/validation issues elucidated here will simply evaporate as LVIS evolves.

However, future space-based missions will result in sparse LiDAR samples because no future satellite-based LiDAR system ever proposed will image the entire planet; fusing LiDAR and the other remote sensing data sets that provide wall-to-wall

coverage (RaDAR and passive optical sensors) would be highly useful. Co-kriging would seem to be a highly useful tool. Forest structure is spatially autocorrelated, so using kriging to fill in coverage gaps would be ideal. However, Sierra forests are highly variable because of disturbance, so there are locations that would have had a different structure had they been undisturbed. Using ancillary data sets to "inform" a kriging model would account for these discontinuities in structure that are aspatial in nature.

Future fusion efforts will be far more sophisticated. Here, I used fusion in the statistical sense. An improved fusion method could include physical models or mechanisms that seek to better understand the interaction between electromagnetic energy and the target (forest canopies). Instead, this effort was highly focused on one particular application, mapping owl habitat. For those purposes, simple correlations between remote sensing variables and *in situ* observations of structure known to be diagnostic of owl habitat were suitable.

CASPO are by no means the only species that depends on old-growth forests. Other species, too, have their own habitat requirements, some of which will correlate to an environmental "signature" that remote sensing can measure. A comprehensive evaluation of habitat would include the requirements of many species, not just CASPO. Because of its status as a management indicator species, CASPO data are available. Because CASPO is a "charismatic megafauna", there is a great deal of interest in its preservation. Future efforts should include consideration of the needs of all forest organisms, not just the ones we like.

LIDAR can supplant some field measurements. Aside from a few calibration/validation plots to insure that the sensor is working properly, there is not a huge need to conduct detailed inventorying of forests—if the only structural measurements needed are canopy height, canopy cover, and biomass. LIDAR sensors have performed well enough in all types of terrain and ecosystems to warrant a great deal of confidence in these measurements. If it turns out that something like foliar height diversity structure is more important for some species, then future field efforts should concentrate here. Other aspects of waveforms at the landscape scale should be exploited. For example, one could quantify patchiness or fragmentation in vertical structure.

It should also be noted that the forest structure that was measured here was done so with wildlife habitat analysis as the ultimate goal. However, these structural attributes are highly informative for many other purposes, including ecosystem dynamics, carbon flux modeling, wildfire modeling, hydrologic modeling, and many others.

Glossary

CE- Canopy energy; the canopy portion of a LIDAR waveform

DBH- Diameter at Breast Height; a measure of a tree's girth

DEM – Digital Elevation Model; a 3-D representation of a topographic surface

ETM+ - Enhanced Thematic Mapper (Landsat 7); a multi-spectral satellite platform

GE- Ground energy; the ground portion of a LIDAR waveform

HOME – Height of the median energy return; the height of the midpoint of the cumulative energy return.

IFSAR – Interferometric Synthetic Aperture Radar; an advanced radar system that can map canopy height

LHT – Laser height; the height of the canopy as detected by LIDAR

LiDAR – Light detecting and ranging; laser altimetry or the near-infrared equivalent to RADAR

LVIS – Laser Vegetation Imaging Sensor; a large footprint, airborne LIDAR platform

NDVI – Normalized Difference Vegetation Index; a measure of vegetative "greenness"

NIR- Near Infra-red; the portion of the electromagnetic spectrum in which LVIS operates ca. 1064 nanometers

QB- Quickbird; a high spatial resolution, multi-spectral satellite platform

RaDAR – radio detecting and ranging

SAR - Synthetic aperture radar; a RADAR sensor used in ecological studies

USFS- United States Forest Service; government organization within the Department of Agriculture charged with managing the National Forests

USGS – United States Geologic Survey; government organization within the Department of Interior charged with studying and mapping natural resources within the United Sates

VCL- Vegetation Canopy LIDAR; a proposed spaceborne LIDAR platform

VDIS- Vertical distribution of intercepted surfaces;

VIS- Visible portion of the spectrum (red, green, blue)

Bibliography

Aber, J.D. (1979). Foliage-height profiles and succession in Northern hardwood forests. *Ecology* 60: 18-23.

August, P.V., 1983. The role of habitat complexity and heterogeneity in structuring tropical mammal communities. Ecology, 64(6): 1495-1507.

Bassow, S.L. and Bazzaz, F.A., 1997. Intra- and inter-specific variation in canopy photosynthesis in a mixed deciduous forest. Oecologia, 109: 507-515.

Bebi, P., Kienast, F. and Schonenberger, W., 2001. Assessing structures in mountain forests as a basis for investigating the forests' dynamics and protective function. Forest Ecology and Management, 145: 3-14.

Beier, P. and Drennan, J.E., 1997. Forest structure and prey abundance in foraging areas of Northern Goshawks. Ecological Applications, 7(2): 564-571.

Berk, A., Bernstein, L. and Robertson, D., 1989. MODTRAN: A moderate resolution model for LOWTRAN7. GL-TR-89-0122, U.S. Air Force Geophysics Laboratory, Bedford, MA.

Bias, M.A. and Gutierrez, R.J., 1992. Habitat associations of California spotted owls in the central Sierra Neveda. Journal of Wildlife Management, 56(3): 584-595.

Blair, J.B., Rabine, D.L. and Hofton, M.A., 1999. The laser vegetation imaging sensor: a medium-altitude, digitisation-only, airborne laser altimeter for mapping vegetation and topography. ISPRS Journal of Photogrammetry and Remote Sensing, 54: 115-122.

Blakesley, J.A., Franklin, A.B. and Gutierrez, R.J., 1992. Spotted owl roost and nest site selection in northwestern California. Journal of Wildlife Management, 56(2): 388-392.

Call, D.R. and Gutierrez, R.J., 1992. Foraging habitat and home-range characteristics of California spotted owls in the Sierra Nevada. The Condor, 94: 880-888.

Castel, T., Caraglio, Y., Beaudoin, A. and Borne, F., 2001. Using SIR-C SAR data and the AMAP model for forest attributes retrieval and 3-D stand simulation. Remote Sensing of Environment, 75(2): 279-290.

Cohen, W.B. and Spies, T.A., 1992. Estimating structural attributes of douglas-fir Western hemlock forest stands from Landsat and SPOT imagery. Remote Sensing of Environment, 41(1): 1-17.

Cohen, W.B., Spies, T.A., Alig, R.J., Oetter, D.R., Maiersperger, T.K. and Fiorella, M., 2002. Characterizing 23 years (1972-95) of stand replacement disturbance in western Oregon forests with Landsat imagery. 5(2): 122-137.

Danson, F.M. and Curran, P.J., 1993. Factors affecting the remotely sensed response of coniferous forest plantations. Remote Sensing of Environment, 43(1): 55-65.

DeGraaf, R.M., Hestbeck, J.B. and Yamasaki, M., 1998. Associations between breeding bird abundance and stand structure in the White Mountains, New Hampshire and Maine, USA. Forest Ecology and Management, 103(2-3): 217-233.

Diner, David J., Gregory P. Asner, Roger Davies, Yuri Knyazikhin, Jan-Peter Muller, Anne W. Nolin, Bernard Pinty, Crystal B. Schaaf, and Julienne Stroeve. (1999), New directions in Earth Observing: Scientific applications of multi-angle remote sensing, *Bull. Am. Meteorol. Soc.*, **80**(11), 2209-2228.

Dobson, M.C., Ulaby, F.T., Pierce, L.E., Sharik, T.L., Bergen, K.M., Kellndorfer, J., Kendra, J.R., Li, E., Lin, Y.C., Nashashibi, A., Sarabandi, K. and Siqueira, P., 1995. Estimation of Forest Biophysical Characteristics in Northern Michigan with Sir-C/X-Sar. Ieee Transactions on Geoscience and Remote Sensing, 33(4): 877-895.

Downes, B.J., Lake, P.S., Schreiber, E.S.G. and Glaister, A., 1998. Habitat structure and regulation of local species diversity in a stony, upland stream. Ecological Monographs, 68(2): 237-257.

Drake, J., 2001. Estimation of tropical forest biomass. Dissertation Thesis, University of Maryland, College Park, MD.

Drake, J., Dubayah, R., Knox, R., Clark, D. and Blair, J.B., 2002. Sensitivity of large-footprint lidar to canopy structure and biomass in a neotropical rainforest. Remote Sensing of Environment, 81(2-3): 378 - 392.

Dubayah, R., Blair, J.B., Bufton, J.L., Clark, D.B., JaJa, J., Knox, R.G., Luthcke, S.B., Prince, S. and Weishampel, J., 1997. The vegetation canopy lidar mission, Land Satellite Information for the Next Decade II. American Society for Photogrammetry and Remote Sensing, pp. 100-112.

Dubayah, R. and Drake, J., 2000. Lidar remote sensing for forestry. Journal of Forestry, 98(6): 44-46.

Fahrig, L. and Merriam, G., 1985. Habitat patch connectivity and population survival. Ecology, 66: 1762-1768.

Finney, M.A., 1998. FARSITE: Fire Area Simulator - Model development and evaluation. (RP-4): 1-+.

Fukushima, Y., Hiura, T. and Tanabe, S., 1998. Accuracy of the MacArthur-Horn method for estimating a foliage profile. Agricultural and Forest Meteorology, 92(4): 203-210.

Hofton, M.A., Blair, J.B., Minster, J.-B., Ridgway, J.R., Williams, N.P., Bufton, J.L. and Rabine, D.L., 2000. An airborne scanning laser altimetry survey of Long Valley, California. International Journal of Remote Sensing, 21(12): 2413-2437.

Hofton M., Rocchio L., Blair J.B., Dubayah R. (2002). Validation of Vegetation Canopy Lidar sub-canopy topography measurements for a dense tropical forest. Journal Of Geodynamics 34 (3-4): 491-502

Hudak, A.T., Lefsky, M.A., Cohen, W.B. and Berterretche, M., 2002. Integration of lidar and Landsat ETM plus data for estimating and mapping forest canopy height. Remote Sensing of Environment, 82(2-3): 397-416.

Hunsaker, C.T., Boroski, B.B. and Steger, G.N., 2002. Relations between canopy cover and occurrence and productivity of California spotted owls, Predicting Species Occurences, Issues of Accuracy and Scale. Island Press, Covelo, CA.

Hutchison, B.A., Matt, D.R., McMillen, R.T., Gross, L.J., Tajchman, S.J. and Norman, J.M., 1986. The architecture of a deciduous forest canopy in Eastern Tennessee, USA. Journal of Ecology, 74(3): 635-646.

Hyde, P., Dubayah, R., Peterson, B., Blair, J.B., Hofton, M., Hunsaker, C., Knox, R. and Walker, W., 2005. Mapping forest structure for wildlife habitat analysis using waveform lidar: Validation of montane ecosystems. Remote Sensing of Environment, 96(3-4): 427-437.

Hyppa, J., Huppa, H., Inkinen, M. and Engdahl, M., 1998. Verification of the potential of various remote sensing devices for forest inventory, Proceedings of IEEE Geosciences and Remote Sensing Society. California Institute of Electrical and Electronics Engineers, Pasadena, CA, pp. 1812-1814.

Kasischke, E.S., Melack, J.M. and Dobson, M.C., 1997. The use of imaging radars for ecological applications- a review. Remote Sensing of Environment, 59: 141-156.

Kimes, D.S., Holben, B.N., Nickeson, J.E. and McKee, W.A., 1996. Extracting forest age in a Pacific Northwest Forest from thematic mapper and topographic data. Remote Sensing of Environment, 56(2): 133-140.

Kimes, D.S., Nelson, R.F., Salas, W.A. and Skole, D.L., 1999. Mapping secondary tropical forest and forest age from SPOT HRV data. International Journal of Remote Sensing, 20(18): 3625-3640.

King, D.I. and DeGraaf, R.M., 2000. Bird species diversity and nesting success in mature, clearcut and shelterwood forest in northern New Hampshire, USA. Forest Ecology and Management, 129(1-3): 227-235.

Koike, F., 1985. Reconstruction of two-dimensional tree and forest canopy profiles using photographs. Journal of Applied Ecology, 22(3): 921-929.

Koike, F. and Syahbuddin, 1993. Canopy structure of a tropical rain-forest and the nature of an unstratified upper layer. Functional Ecology, 7(2): 230-235.

Lee, D. and L. Irwin. 2005. Assessing risks to spotted owls from forest thinning in fire-adapted forests of the western United States. Forest Ecology and Management, 211: 191–209

Lefsky, M.A., 1997. Application of lidar remote sensing to the estimation of forest canopy and stand structure. Dissertation Thesis, University of Virginia.

Lefsky, M.A., Cohen, W.B., Acker, S.A., Parker, G.G., Spies, T.A. and Harding, D., 1999a. Lidar remote sensing of the canopy structure and biophysical properties of douglas-fir western hemlock forests. Remote Sensing of Environment, 70: 339-361.

Lefsky, M.A., Harding, D., Cohen, W.B., Parker, G. and Shugart, H.H., 1999b. Surface lidar remote sensing of basal area and biomass in deciduous forests of eastern Maryland, USA. Remote Sensing of Environment, 67: 83-98.

Lefsky, M.A., Cohen, W.B. and Spies, T.A., 2001. An evaluation of alternate remote sensing products for forest inventory, monitoring, and mapping of Douglas-fir forests in Western Oregon. Canadian Journal of Forest Research, 31: 78-87.

MacArthur, R.H., 1958. Population ecology of some warblers of northeastern coniferous forests. Ecology, 39(4): 599-619.

MacArthur, R.H. and Horn, H.S., 1969. Foliage profile by vertical measurements. Ecology, 50(5): 802-804.

MacArthur, R.H. and MacArthur, J.W., 1961. On bird species diversity. Ecology, 41(3): 594-598.
Meyer, K. E. and W. F. Laudenslayer. 1988. A guide to wildlife habitats of California. 1988. Sacramento: California Dept. of Fish and Game.
Meir, P., Grace, J. and Miranda, A.C., 2000. Photographic method to measure the vertical distribution of leaf area density in forests. Agricultural and Forest Meteorology, 102(2-3): 105-111.
Moghaddam, M., Dungan, J.L. and Acker, S., 2002. Forest variable estimation from fusion of SAR and multispectral optical data. 40(10): 2176-2187.
Monsi, M., Uchijima, Z. and Oikawa, T., 1973. Structure of foliage canopies and photosynthesis. Annual Review of Ecology and Systematics, 4: 301-327.
Morrison, M.L., Marcot, B.G. and Mannan, R.W., 1998. Wildlife-habitat relationships. The University of Wisconsin Press, Madison, 458 pp.
Naesset, E., 1997. Determination of mean tree height of forest stands using airborne laser scanner data. ISPRS Journal of Photogrammetry and Remote Sensing, 52: 49-56.
Nelson, R., Krabill, W. and Maclean, G., 1984. Determining forest canopy characteristics using airborne laser data. Remote Sensing of Environment, 15: 201-212.
Nelson, R., Krabill, W. and Tonelli, J., 1988. Estimating forest biomass and volume using airborne laser data. Remote Sensing of Environment, 24: 247-267.
Nelson, R., Oderwald, R. and Gregoire, T.G., 1997. Separating the ground and airborne laser sampling phases to estimate tropical forest basal area, volume, and biomass. Remote Sensing of Environment, 60(3): 311-326.
Nilsson, M., 1996. Estimation of tree heights and stand volume using an airborne lidar system. Remote Sensing of Environment, 56: 1-7.
North, M.P., Franklin, J.F., Carey, A.B., Forsman, E.D. and Hamer, T., 1999. Forest stand structure of the northern spotted owl's foraging habitat. Forest Science, 45(4): 520-527.
Peterson, B.E., 2000. Recovery of forest canopy heights using large-footprint lidar. Master's Thesis, University of Maryland, College Park, 59 pp.
Pianka, E.R., 1966. Convexity, desert lizards, and spatial heterogeneity. Ecology, 47(6): 1055-1059.
Pu, R.L. and Gong, P., 2004. Wavelet transform applied to EO-1 hyperspectral data for forest LAI and crown closure mapping. Remote Sensing of Environment, 91(2): 212-224.
Ranson, K.J., Sun, G., Knox, R.G., Levine, E.R., Weishampel, J.F. and Fifer, S.T., 2001. Northern forest ecosystem dynamics using coupled models and remote sensing. Remote Sensing of Environment, 75: 291-302.
Recher, H.F., 1971. Bird species diversity: a review of the relation between species number and environment. Proceedings of the Ecological Society of Australia, 6: 135-152.
Rocchio, L., 2000. Lidar remote sensing of sub-canopy topography. Thesis, University of Maryland, College Park, 101 pp.
Rosenzweig, M.L. and Winakur, J., 1969. Population ecology of desert rodent communities: habitat and environmental complexity. Ecology, 50: 558-572.

Rotenberry, J.T. and Wiens, J.A., 1980. Habitat structure, patchiness, and avian communities in North American steppe vegetation: a multivariate analysis. Ecology, 61(5): 1228-1250.

Skole, D. and Tucker, C., 1993. Tropical deforestation and habitat fragmentation in the Amazon: Satellite data from 1978 to 1988. Science, 260: 1905-09.

Slatton, K.C., Crawford, M.M. and Evans, B.L., 2001. Fusing interferometric radar and laser altimeter data to estimate surface topography and vegetation heights. Ieee Transactions on Geoscience and Remote Sensing, 39(11): 2470-2482.

Steininger, M.K., 1996. Tropical Secondary Forest Regrowth in the Amazon: Age, Area and Change Estimation with Thematic Mapper Data. International Journal of Remote Sensing, 17: 9-27.

Tanaka, H. and Nakashizuka, T., 1997. Fifteen years of canopy dynamics analyzed by aerial photographs in a temperate deciduous forest, Japan. Ecology, 78(2): 612-620.

Tanaka, T., Yamaguchi, J. and Takeda, Y., 1998. Measurement of forest canopy structure with a laser plane range-finding method - development of a measurement system and applications to real forests. Agricultural and Forest Meteorology, 91(3-4): 149-160.

Treuhaft, R.N. and Cloude, S.R., 1999. The structure of oriented vegetation from polarimetric interferometry. Ieee Transactions on Geoscience and Remote Sensing, 37(5): 2620-2624.

Treuhaft, R.N. and Siqueira, P.R., 2000. Vertical structure of vegetated land surfaces from interferometric and polarimetric radar. Radio Science, 35(1): 141-177.

Trzcinski, M.K., Fahrig, L. and Merriam, G., 1999. Independent effects of forest cover and fragmentation on the distribution of forest breeding birds. Ecological Applications, 9(2): 586-593.

Waddell, K. and Hiserote, B., 2003. Technical documentation for the integrated database, version 1.0, USDA Forest Service Pacific Northwest Research Station.

Weishampel, J.F., Ranson, K.J. and Harding, D.J., 1996. Remote sensing of forest canopies. Selbayana, 17: 6-14.

Weishampel, J.F., Blair, J.B., Knox, R.G., Dubayah, R. and Clark, D.B., 2000. Volumetric lidar return patterns from an old-growth tropical rainforest canopy. International Journal of Remote Sensing, 21(2): 409-415.

Wilson, E.O., 1999. The Diversity of Life. W.W. Norton and Company, New York, NY, 424 pp.

Wilson, J.W., 1965. Stand structure and light penetration. I. Analysis by point quadrats. Journal of Applied Ecology, 2: 383-390.

Wulder, M. and Seeman, D., 2003. Forest inventory height update through the integration of lidar data with segmented Landsat imagery. Canadian Journal of Remote Sensing, 29(5): 536-543